Sheffield Hallam University

A Sheffield Hallam University thesis

Fines are charged at 50p per hou

~ 4 MAY

ProQuest Number: 10694099

![ProQuest](ProQuest logo)

ProQuest 10694099

Optical Packet Networking Using Optical Time Division Multiplexing

RUIXIN GAO

A thesis submitted in partial fulfilment of the requirements of Sheffield Hallam University for the degree of Doctor of Philosophy

Optical Communication Research Group
School of Engineering, Sheffield Hallam University
Sheffield, United Kingdom

September 2003

DECLARATION

No portion of the work referred to in this thesis has been submitted in support of an application for another degree or qualification to this or any other university, institute of learning or industrial organisation.

Ruixin Gao

September 2003

ACKNOWLEDGEMENTS

First, my sincere gratitude to my director of studies Professor Z Ghassemlooy and my supervisors Professor Peter Ball and Dr. Graham Swift for their certain guidance, constructive criticism and strong support during this research. Their contributions in both technical and personal matters have been fundamental in the development of this thesis.

I would like to thank all my colleagues in the Optical Communication Research and Electronics Research Groups, School of Engineering, Sheffield Hallam University for useful discussions.

Finally, I would also like to thank my parents, my sisters, my uncle George Sui, my aunt Jennifer Gao, my friends Hui Sun, Kai Zhao, and Shuhua Hong for their love, support and encouragement.

Ruixin Gao

Abstract

Growing demands for capacity have stimulated the development of high-speed optical shared media networks. At present, most research on optical networking has concentrated on wavelength-division multiplexing (WDM). Optical time-division multiplexing (OTDM), which offers advantages over WDM networks, is considered as an alternative to WDM for future networks proving a single stream data rates of 100 Gb/s using a single wavelength. In such systems all optical routers, which overcome the bottleneck of optoelectronic conversion, play an important role. This thesis concentrates on the modelling and simulation of a novel optical router, which uses two terahertz optical asymmetric demultiplexers (TOAD) as the routing element for OTDM systems.

In this work, the author has developed a mathematical model of an all optical router based on TOADs. The model architecture is based on a system, which has as its input an OTDM packet containing header and payload information. The model simulates extraction of header information, using one TOAD, from the data stream, which is subsequently used to make a routing decision. The payload information is routed through a second TOAD according to the information contained in the header. A comprehensive theoretical analysis supported by computer simulations has been carried out to study characteristics of crosstalk, noises, signal to noise ratio (SNR), Bit error rate (BER), and power penalty of the router. The results obtained, whenever possible, have been compared with the experimented data.

The performance analysis of the all optical router is shown by the simulation results. The proposed router is capable of routing packet containing data in excess of 250 Gb/s all in optical domain.

New models of all optical router with multi-input and outputs have been developed i.e. 1x4 router, 2x2 router, which are based on 1x2 TOAD routers. Results show that threshold switching energy is present at 0. 2 pJ. Higher values result in a decrease in crosstalk and lower values result in negligible switching. Also shown is crosstalk induced penalty depends on the crosstalk level of individual 1x2 switches as well as on the size and architecture of the switching fabric.

Finally, it has been shown that the proposed all-optical router has potentially useful characteristics as a component for high-speed optical TDM networks due to its ultrafast switching capability compared with existing devices. At this stage a simple 8 by 8 Banyan network is presented, however further work will enhance the model to a network with more inputs and outputs.

Contents

VIII

List of Figures

X

GLOSSARY OF ABBREVIATIONS

ASE	Amplified Spontaneous Emission
BER	Bit Error Rate
BPF	Band Pass Filter
CCW	Counter Clockwise
CW	Clockwise
EDFA	Erbium-doped Fibre Amplifier
FP-SLA	Fabry-Perot SLA
FWM	Four Wave Mixing
FWHM	Full Width Half Maximum
I/O	Input / Output
MZI	Mach-Zender Interferometer
NOLM	Nonlinear Optical Loop Mirror
NLWG	Nonlinear Waveguide Switch
NXT	Neighbour Channel Crosstalk
MEMS	Micro-Electro-Mechanical Systems
OTDM	Optical Time Division Multiplexing
RIN	Relative Intensity Noise
RMS	Root-Mean-Square
RXT	Residual Crosstalk
SLA	Semiconductor Laser Amplifier
SDH	Synchronous Digital Hierarchy
SONET	Synchronous Optical Network
TDM	Time Division Multiplexing
TOAD	Terahertz Optical Asymmetric Demultiplexer
TW-SLA	Travelling Wave SLA
UNI	Ultrafast Nonlinear Interferometer
WDM	Wavelength Division Multiplexing

GLOSSARY OF SYMBOLS

Symbol	Definition
a	Gain coefficient of an SLA
A_{eff}	Effective cross section area of an SLA
B	Electrical bandwidth
B_o	Optical bandwidth
c	Speed of light
c_d	Velocity of photons moving
CXT_{ROUTER}	Router channel crosstalk
d	Active area depth of SLA
E	Electric field
E_a	Energy gap between conduction bands
E_c	Control pulse energy
E_{CTRL}	Optimised control pulse energy for TOAD
E_{max}	Maximum signal energy for TOAD routing for avoiding the perturbation of the SLA properties
E_p	Photon energy
E_{sat}	Saturation energy of an SLA
E_{sp}	Spontaneous emission field
E_{tot}	Total energy within the segment
f	Frequency
$f_j(j)$	The discrete probability density function
F	Noise figure
F_{CCW}	Gain and phase function of TOAD in the CCW direction
F_{CW}	Gain and phase function of TOAD in the CW direction
g	Differential gain of an SLA
g_1 and g_2	The degeneracies of the two energy levels
g_p	Peak differential gain of the gain spectrum of an SLA
G_{CCW}	CCW gain of signal pulses in TOAD

G_{CW}	CW gain of signal pulses in TOAD
G_s	Single pass gain
G_{ss}	Small signal gian of an SLA
h	Planck's constant
i_a^2	Power spectral density of the electrical input noise current
I_o	Light intensity
I_b	Bias current
I_c	Electrical current
J	Bias current density
k	Boltzman constant
K	Field coupling factor
L	The half of the length of the fibre loop
L_f	Loss due to the optical filter
L_{opt}	Loss between amplifier and photodetector
L_{SLA}	Length of the SLA
M	Number of packets
M_{TDM}	Number of OTDM channels
n	Refractive index
n_0	Refractive index in the absence of an input signal
n_f	Refractive index of the fibre
n_{sp}	Population inversion parameter
N	Carrier density
N_o	Transparent carrier density
N_i	Carrier density without singal applied
N_{ph}	Number of photons per unit energy
N_{s-sp}	signal-spontaneous beat noise spectral density
N_{sp-sp}	spontaneous-spontaneous beat noise spectral density
N_{th}	Carrier density of lasing threshold
NXT_{ROUTER}	Router neighbour channel crosstalk

P	Optical power
P_{avg}	Averaged optical power for the signal
P_{in}	Optical power of the input signal
P_N	Noise power of an SLA
P_o	Peak optical power of a pulse
P_{sat}	Saturation power
P_{sig}	Signal power
P_{sp}	Spontaneous emitted power
$p_i(t)$	Probability function of Gaussian shape
$p(t)$	Input data packet power profile
q	Electron charge
r	Reflectivity of SLA
r_1	Reflectivity of the input facet of an SLA
r_2	Reflectivity of the output facet of an SLA
r_w	Extinction ratio of switching window
R	Responsivity of the photo-detector
R_B	Channel bit rate
R_G	Optimal gain ratio between CW and CCW pulses for maximum TOAD switching gain
R_L	Load resistance of the photo-detector
RIN_{DEMU}	Demultiplexer relative intensity noise
RIN_{ROUTER}	Router relative intensity noise
RMS_{jitter}	RMS timing jitter of signal pulses
RXT_{DEMU}	Demultiplexer residual crosstalk
RXT_{ROUTER}	Router residual crosstalk
T	Temperature in Kelvin
T_b	Bit duration of an OTDM time slot
T_D	Packet duration
T_w	Width of switching window
$T_x(t)$	Switching window profile of the router

V	Volume
V_g	Group velocity
V_{SLA}	Volume of the active medium of an SLA
$w(t)$	Output signal profile of the TOAD router
X_{ct}	Crosstalk of multi-ports router
XT_T	Total crosstalk
z	Longitudinal position of light propagation
ε_0	Vacuum permittivity
α	Loss coefficient
α_{SLA}	Photon loss coefficient of an SLA
α_{LEF}	Linewidth enhancement factor
σ^2_{s-sp}	Optical amplifier beat noise power density between signal and spontaneous emission
σ^2_{sp-sp}	Optical amplifier beat noise power density between spontaneous emission components
σ^2_{th}	Optical amplifier thermal noise power density
ω	Optical frequency
ρ	Energy density
Γ	Confinement factor
χ	Excess noise coefficient of SLA
γ	Excess loss of the coupler
$d\Omega$	Solid angle (blackbody radiation theory)
dn/dN	Refractive index differential coefficient
ΔT	Separation time between two pulses
λ	Optical wavelength
λ_0	Centre wavelength of input signal
λ_p	Wavelength of peak gain
λ_s	Signal wavelength
$\Delta\lambda_g$	Spectral width of the differential gain of an SLA
τ	Time reference (of a pulse / switching profile)

τ_c	Width of control pulse
τ_{sig}	Duration of the signal bit
τ_{sp}	Carrier spontaneous life-time
ϕ	Optical phase
ϕ_{CW}	Phase shift for CW component
ϕ_{CCW}	Phase shifts for CCW component
$\Delta\phi$	Phase difference between CW and CCW signal pulses
Φ_k	Random phase for each component of spontaneous emission
η	Photodiode quantum efficiency
η_{DEMUX}	Switching ratio of the target pulse energy
η_{in}	Input coupling efficiencies of the optical amplifier
η_{out}	Output coupling efficiencies of the optical amplifier

Chapter 1

Introduction

The growing demand for increased network capacity has generated interest in the development of ultrafast transparent optical networks (TONs). In these networks, the tardy opto-electrical (O/E) or electro-optical (E/O) conversions that are inherent in current fibre network systems are avoided. Consequently, there is a significant reduction in bandwidth bottlenecks resulting in superior quality of service (QoS). To date most research on optical networking has concentrated on wavelength division multiplexing (WDM) [1-4], which routes different packets according to the wavelength of the optical carrier. In WDM systems, which require high flat gain amplifiers, nonlinearity associated with fibre results in SNR degration as the number of channel increases, and cross phase modulation limits the number of the channels. Therefore, optical time-division multiplexing (OTDM) is considered as an alternative to WDM for future networks, which utilise a single wavelength for high (> 100 Gbit/s) data rates [4-6]. In OTDM networks many signals are interleaved before being transmitted using a single wavelength. Each signal from a lower bit-rate source is broken up into many segments (slots), each having very short duration, and are multiplexed in a rotating repeating sequence (i.e. round robin fashion) onto a high bit-rate transmission line. The use of short duration pulses (preferably soliton) allows information to be transmitted at very high bit rates (>100 Gb/s). An asset of OTDM is its flexibility, which allows for variation in the number of signals that can be transmitted over a single fibre, and the ability to adjust the time intervals to make optimum use of the available

1

bandwidth. It is therefore believed that OTDM networks are excellent candidates for meeting the future ultrafast network requirements [7-8]. It is not envisaged as a replacement but complementary to the WDM, where the major traffic at the backbone to be carried by OTDM.

Practical resolution of OTDM system is a challenge and costly task facing researchers and service providers. Many technologies have been proposed, including ultrashort optical pulse generation, time division multiplexing, optical repeaters, synchronisation, time domain demultiplexing and so on, which may be used to set up an all optical OTDM network. The key element for OTDM networks would be all-optical routers, which are capable of switching signal in the optical domain, thus overcoming the bottleneck of optoelectronic conversion process. Therefore, particular attention has to be paid to all optical routers. A few types of all optical routers have been developed by researchers [38-42]. Here we investigate all optical router based on the terahertz optical asymmetric demultiplexer (TOAD) by developing a mathematical model.

1.1 Organisation of Thesis

The thesis is divided into nine chapters. Following the introduction, a technical and historical review for optical communication systems is given in Chapter 2. This chapter begins by introducing optical communication history. And then goes on to describe TDM, WDM and OTDM systems. The challenges and trends of optical communication systems are discussed.

2

Chapter 3 presents a review of current technologies for the switching of signals in the optical domain. Switchers are characterised by the switching time, repetition rate, control pulse energy, and practicality. Summary of the key device criteria for the all–optical switches shows that the most likely candidate for an optical router is TOAD, which has been investigated in this work.

One of objectives of this project is to develop a model of an all optical router based on the terahertz optical asymmetric demultiplexer (TOAD). The operation of TOAD is based on the nonlinear properties of semiconductor laser amplifier (SLA). Thus the theoretical background of SLA is introduced in Chapter 4. This chapter presents SLAs with the accompanying equations that describe the characteristics of the device under continuous wave input. The concept of noise of SLA and how it originates from amplified spontaneous emission are described and its contribution to receiver generated noise is shown with the introduction of noise equations.

In Chapter 5, a new mathematical model for all optical router is presented. The model architecture is based on a system, which has as its input an OTDM packet containing header and payload information. The model numerically simulates the extraction of the header information from the incoming OTDM packet using a single TOAD, which is subsequently used to make a routing decision for the packet payload. The payload information is routed through a second TOAD according to the information contained in the header.

Based on this mathematical model, a comprehensive noise and crosstalk analysis of the all optical router is presented in Chapter 6. A new mathematical model for maximising the

3

amplitude of the switching transmission window together with the simulation performance namely the bit error rate (BER) is also presented in this chapter. After describing the origins of the noise and crosstalk associated with an all-optical router, the simulation results of the noise and crosstalk are presented and analysed.

Chapter 7 presents bit-error-rate performances of the router. This chapter begins by presenting the system model of the receiver and signal to noise ratio (SNR). All the noise courses including those related to the router such as: (i) The channel crosstalk originating from the leakage of non-target channels and (ii) the relative intensity noise induced by the timing jitter in router are discussed and expressed mathematically. A comprehensive expression for the BER is presented and results for the BER for different data rates with /without router compared with the base line are given. The compact of the crosstalk and the relative intensity noise of the router on the optical power penalty for 100 Gbps OTDM are also investigated.

Chapter 8 investigates novel all optical routers with multi-input and output, say 1x4, 2x2 routers. In this chapter, 1x4 router that uses TOADs as the routing element is described in detail by means of mathematical modelling. The mathematically model developed is used to investigate performance of the 1x4 router. The results presented are compared with 1x2 router. The chapter goes on to discuss the operation of the 2x2 routers based on TOADs with input and output buffers. Using the mathematical model developed for 1x2 router, the 2x2 router is simulated and results are shown at various stages. Finally the multiports router based on Banyan network is introduced, where the 2x2 switches could be based on TOAD. The OTDM packet address bit is modified to include "N" address bits. A novel N bit address recognition unit based on 3-stage TOAD is introduced. Mathematical expression

for the crosstalk for the series and parallel multiports router configuration is given. Results for a particular case study is presented.

Finally, conclusions and suggestions of further works are discussed in Chapter 9.

1.2 Aims and Objectives

The fundamental aim of the work presented in this thesis is to design and develop a novel all optical router based on TOAD for LANs/MANs and identify the system requirements and physical specifications for the proposed devices. In order to achieve these, a number of research objectives have been identified, as outlined below:

❖ Design and simulate a novel all optical router in high-speed communication systems.

❖ Develop model to investigate novel architectures for OTDM packet switching networks.

❖ Investigate characteristics of the all optical router against various system parameters such as: packet format, node size, bit-rate, type of switching network, node routing architecture, and choice of ultrafast demultiplexer.

❖ Identify the advantages and drawbacks of the proposed network model, compare it to the existing network models and further modify model.

1.3 Original Contributions

During the course of this work, the following original contributions have been made:

❖ Development of a new analytical model for calculating the width of all optical router switching window. (Section 5.2)

❖ Optimisation of the all-optical router parameters for maximising peak transmission of the all optical router switching window. (Section 5.3)

❖ Development of a new convolution approach for calculating the profile of all optical router switching window. (Section 5.3.3)

❖ Optimisation of the switching energy of all optical router for maximising the peak transmission of switching window. (Section 5.3.4)

❖ Analysis of relative intensity noise, residual crosstalk and neighbour channel crosstalk in all optical router. (Section 6.2)

❖ Bit-error-rate comparisons of with and without all optical router for 100 Gb/s bit rate. (Section 7.4)

❖ Optimisation of the device parameters for all optical router for minimising the power penalty at different bit rate (100 Gb/s -300Gb/s). (Section 7.4)

❖ Development of a new model of 1x4 and 2x2 all optical routers based on TOADs. (Sections 8.2 and 8.3)

❖ Analysis of relative intensity noise, residual crosstalk and neighbour channel crosstalk of all optical router in the Banyan network. (Section 8.5.3)

1.4 Publications

The work presented in this thesis has resulted in the following publications, which are listed in chronological order.

R. Gao, Z. Ghassemlooy, G. Swift, and P. Ball, "Simulation of all optical time division multiplexed router", *Proceedings of Photonics West 2001*, 4292, pp.214-223, Jan. 2001.

R. Gao, A. Als, Z. Ghassemlooy, G. Swift, and P. Ball, "Simulated Error Performance of An All Optical Time Division multiplexed system", *Proceedings of the Convergence of Telecommunications, Networking & Broadcasting 2001*, pp.171-176, Liverpool, UK, June 2001.

R. Gao, Z. Ghassemlooy, G. Swift, and P. Ball, "Performance analysis of all optical time division multiplexed router based on terahertz optical asymmetric demultiplexer", *Proceedings of SPIE Asia-Pacific Optical and Wireless Communications 2001*, 4582, pp.152-158, November 2001.

R. Gao, Z. Ghassemlooy, and P. Ball, "BER Analysis of Packet Based High-Speed OTDM System Employing All Optical Router ", *Proceedings of 7th European Conference on Networks & Optical Communications*, 4292, pp.214-223, June, 2002.

R. Gao, Z. Ghassemlooy, and P. Ball, "Crosstalks Analysis for All Optical Routers", *Proceedings of third international symposium on communication systems networks and digital signal Processing*, pp.173-176, UK, July, 2002.

R. Gao, Z. Ghassemlooy, and P. Ball, "BER Analysis of Packet Based High-Speed OTDM System Employing All Optical Router ", *accepted by the Microwave & Optical Technology Journal*, 2003.

R. Gao, A. Als, Z. Ghassemlooy, G. Swift, and P. Ball, "Performance analysis of all optical time division multiplexed router based on terahertz optical asymmetric demultiplexer", *submitted to the Optical Communication Journal*, 2003.

Chapter2

Literature Review and Survey: TDM, WDM and OTDM

2.1 Introduction to Optical Communications

Light has been used for communicating information since signal fires were used to send messages. Manually operated signal lanterns on ship and signal flares are other examples of early optical communication systems. A revolution in optical communication occurred in 1880 when Alexander Graham Bell reported the modulation of sunlight with the sound of a bell for speech transmission over a distance of 200 m [9]. From the late 1880's to the early 1960's low capacity short range links represented the state-of-the-art in optical communication. For atmospheric communication, light was really only practical for line of sight, short distance transmission, since scattering and weather conditions proved to be an obstacle for the optical signal. To overcome some of these problems, dielectric waveguiding which has a history dating back to 1910 Hondros [10] was used to confine the optical signal. In 1950 B. Brian Sr. at American Optical was developing optical fibre bundles for light transmission. Some significant milestones in optical communication include: the invention of the laser in the 1960's, the development of low loss optical fibre in the 1970's, a demonstration of long life semiconductor laser diodes in the 1980's, and the

8

development of practical amplifiers by the 1990's. Collectively these paved the way for a concerted effect into the development of practical optical communication systems.

In particular the development of low loss optical fibre allowed significant advances to be made in fibre communication with Kao [11] predicating that 20 dB/km loss was achievable in glass fibres by removing the impurities. At this level, optical fibre communication was becoming a viable alternative. Prior to this the losses were in the 1000 dB/km range (coaxial cables which guide electromagnetic waves exhibit losses between 5 and 10 dB/km). Research continued on optical fibres and by 1977 the fibre losses were reported to be as low as 0.5 dB/km for 1200 nm wavelengths.

Nowadays, optical fibre is a exceedingly low-loss propagation medium. Losses can approach 0.15 dB/km and, with modest amounts of optical amplification, multi-Gbps data streams can be transmitted over tens of thousands of kilometres without electronic regeneration. Conventional electronic systems only give an order of magnitude less transport capacity. In comparison, convention coaxial cables will lose half the electrical power in just a few hundred meters whilst a good quality optical fibre loses half of the optical power in the propagating field in 15-20 km. In addition to significantly lower loss, packaging and volume benefits are also a feature. Low-loss coaxial cables often have diameters of a centimetre or more. Consideration of the cross-section area is particularly significant when fibres are used in crowded conduits.

In parallel with the development of fibre systems, work continued on the various components needed to complete the optical communication system [12-15]. Semiconductors as optical sources included light emitting diodes (LED) and injection

9

lasers, which were compatible in size with the optical fibre system, were becoming widespread. LEDs operate at much lower current than injection lasers, but their mechanism of light generation is by spontaneous emission and consequently the optical output of an LED is of random phase with no coherence. The injection laser on the other hand uses stimulated emission in a resonant cavity providing a coherent light source. The spectral width of an LED is also much wider than the laser. For 800-850 nm wavelength operation GaAlAs devices have spectral widths in the range 30-60 nm and 1-2 nm for LEDs and lasers respectively. However the LED does offer certain advantages over the laser, e.g. lower cost, ease of manufacture, reliability, and it gives a linear light output current curve. The first semiconductor lasers were fabricated from alloys of gallium arsenide which emitted in the range 0.8-0.9 μm. The range of emission was extended to 1.1 to 1.5 μm, taking advantage of improved fibre characteristics. The laser and LED are now becoming well established with a lifetime improvement from a few hours up to 25 years for semiconductor lasers and 100 years for LED's.

The most common wavelengths used for optical communications fall between 0.83 and 1.55 microns. Other wavelengths can also be used but this range encompassed the most popular applications. A wavelength of 1 micron corresponds to a frequency of 300 THz (300,000 GHz), which is considerable higher than those associated with conventional radio, microwave, or millimetre-wave communication systems. A high centre frequency implies that extremely high modulation bandwidths should, in principle, be possible. A one-percent bandwidth is easily achieved for optical carriers, which is far greater modulation bandwidth than a microwave carrier can provide. Although wide bandwidth is important, it is not only the reason optical communication systems technology is causing such revolutionary

changes in communication. To gain a broader understanding, we need to examine the advantages light has in both guided and unguided modes of transmission.

Traditional communication techniques based on electronics are now being challenged by these new optical systems [16-20].

The research and development into fibre communication systems is driven by the promise of communication systems offering numerous advantages such as small physical size, low costs and high interference immunity. In the past several years, lightwave systems have been demonstrated with increasingly higher bit rates. Electrical TDM system has achieved a bit rate of 40 Gbit/s [21], whilst a wavelength-division-multiplexed system with sixteen different wavelength channels has been demonstrated operated at 640 Gbit/s [22]. Significantly an optical time division multiplexed system has been shown to have an aggregate rate of 250 Gbit/s at single wavelength [23]. Aggregate bit rates achieved for laboratory system for TDM, WDM and OTDM are shown in Figure 2.1.
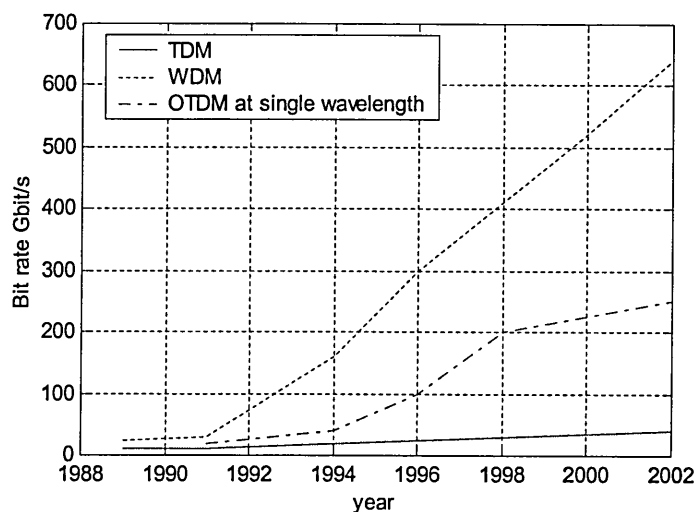
Figure 2.1 Demonstrated aggregate bit rates for TDM, WDM and OTDM laboratory lightwave systems

11

In respect of composite optical communication systems the point to point system is now well established, and is the most common configuration used for optical communications. It is now possible for such optical fibre systems to cross oceans and continents, while free-space systems provide high data-rate communication links between satellites at geosynchronous distance. Optical communications, in combination with microwave and wireless technologies, are enabling the construction of high-capacity networks with global connectivity.

In current optical communication systems, any processing of the signal is performed electronically following by an optical to electronic conversion, the electronic signal is then to be converted back to the optical domain. This creates a bottleneck for future networks proving date rates up to 100 Gbit/s. The bottleneck significantly reduces the speed of transmission in addition to the relatively slow electrical switching rates. The speed limitation of electronic switching is currently limited to about 10 Gbit/s [24]. To meet the requirement of future broadband multimedia services, which is likely to require speeds of the order of 100 Gbit/s [25], the all optical communication network is a solution, which can transmit information at very high bit rates (>100 Gbit/s).

A number of consortiums are actively working on areas of high-speed communications, e.g.

❖ The PHOTON project (Physical-Layer High-Speed Optoelectronics for Tomorrow's Optical Networks), funded by the Engineering and Physical Sciences Research Council (EPSRC), focuses on cost-effective technological solutions to enable the introduction of

the optical networking into the premises, access layer and metro layer of a network. This project is a collaboration between a large number of UK universities and industry.

❖ At the University of Cambridge hardware based research is being carried out so that current networking systems such as Gigabit Ethernet can progress to Terabit Ethernet [26, 27].

❖ Another project called OPSnet project researches optical packet switching, in particular building upon the results obtained from the earlier EPSRC project WASPNET, which demonstrated a prototype switch within a network environment. As many of the networking issues facing the development of an optical backbone layer have come into focus during the past year, a clearer idea of the functions and performance needed from optical packet switching are starting to emerge. For example new technologies and technical approaches are required to enable operation at 40 Gb/s, with scalability to >100 Gb/s. The networking issues associated with the integration of the optical backbone layer and the IP layer require effective solutions. In this project, fundamental asynchronous packet operation has been made, which have major impacts on the hardware solutions. The outcomes from the design and test of an all-optical packet switched node, enabled the major key issues for realistic packet networks to be understood; the OPSnet project seeks to answer a number of these. Expected outcomes are therefore concerned with understanding:

- ♦ The relative merits of asynchronous and synchronous packet operation, and the impact of asynchronous operation on switch and network performance.
- ♦ The impact of data traffic statistics on switch design.
- ♦ The design of an asynchronous optical packet switch for 40 Gb/s operation.

13

A network demonstrator supporting an end-to-end connection across the electronic and optical domains will support these activities.

❖ A study into the development of European network linking major centres in Europe is " COST 239: Ultra-High Capacity Optical Transmission Networks". The findings of this study in terms of data requirements of European cities are summarised in Table 2.1.

Table 2.1 Typical data requirements of European cities

Cities	Data rate (Gbit/s)
London-Paris	150
Paris-Madrid	120
Zurich-Milan	90
Milan-Rome	120
Prague-Berlin	90
Berlin-Moscow	90

2.2 Lightwave Systems

2.2.1 Time division multiplexing network

Time-division multiplexing (TDM) is a well-known technique that has been widely used for point-to-point digital telecommunication systems and networks. In a TDM based system

as shown in Figure 2.2, a number of nodes, say N, share a common broadcast channel (i.e., the transmission medium) in the round-robin fashion. Sharing is usually equal, i.e., when a node's turn comes up, it transmits for T units of time before relinquishing the channel. (However, unequal sharing can be affected by having node i transit for k_iT time units, where $i = 1,2,\ldots, N$, and the k_i are arbitrary integers that are known to all the nodes.)
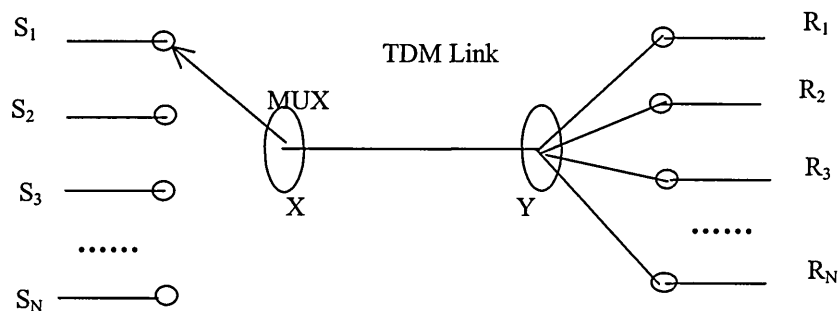
Figure 2.2 A TDM link and multiplexer

Nodes in a TDM system must also be perfectly synchronised, so that nodal transmissions do not collide with one another (as in a random, multiaccess communication network), and they do not "spill over" into their adjacent nodes' transmission windows. In a synchronous TDM system, a node gets its allotted time even if it is idle. Thus, time in such a synchronous TDM channel consists of a sequence of equal-sized, nonoverlapping frames, with each node getting exactly one turn to transmit a frame. (Such a frame is also referred to as a cycle, period, or a TDM frame in the literature.) Also, note that two consecutive transmission instants at any node are separated by exactly one frame length.

Frame synchronisation is implemented with the beginning of each frame being marked by a special bit pattern. Since all frames are of the same length, and each node's relative

transmission instant in a frame and its transmission duration are known to all nodes, a nodal transmitter need not identify itself explicitly—this information is implicit. For a point-to-point TDM link as shown in Figure 2.2, the TDM multiplexer provides this synchronisation information, while in a distributed, broadcast, multiaccess TDMA network, the synchronisation bits may be transmitted by any designated node, which is generally the one that is the first transmitted data in a frame.

An asynchronous TDM system, on the other hand, does not waste any time on idle nodes. Thus, while all nodes are still scanned in round-robin fashion, only the active nodes transmit on the channel, consequently, the frame lengths are not fixed any longer, and a nodal transmitting must also identify itself explicitly in its transmission, thereby increasing the amount of overhead information per frame.

Trade-offs to be considered when designing or comparing a synchronous to an asynchronous TDM system include simplicity of design or operation, channel utilisation (and, hence, access delay), and amount of overhead.

Network architectures have been proposed [12] that employ switches such that a TDM packet be routed all optically from one of the incoming fibre ports of a switch to its desired output port. There is generally no notion of a synchronous TDM frame on any link, so according to our above classification, this is an asynchronous TDM system. Frequently, such a network is referred to as a photo packet network in the literature.

2.2.2 Wavelength division multiplexing network

2.2.2.1 WDM network
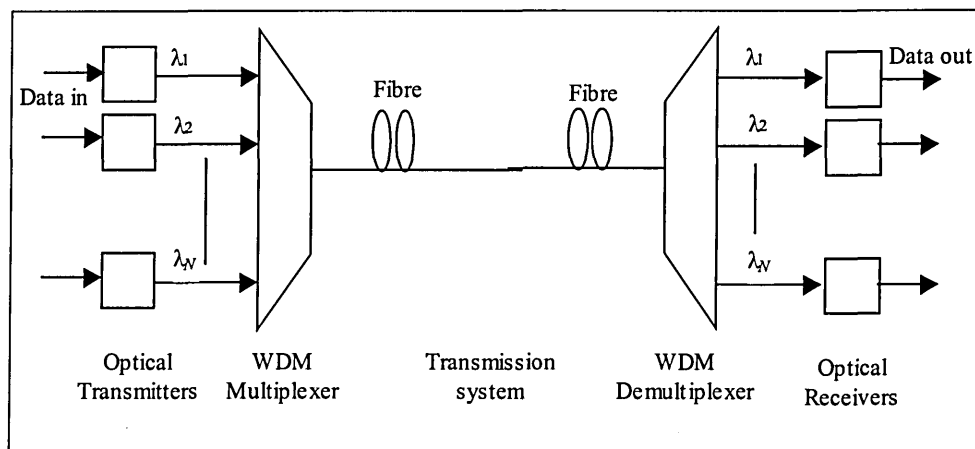
Figure 2.3 Optical WDM system block diagram

Wavelength-division multiplexing (WDM) is an approach that can be used to exploit the huge opto-electronic bandwidth. Here end-user's equipments generate data at electronic rates, which are then used to modulate multiple WDM channels. A number of end users may be multiplexed onto the same fibre as shown in Figure 2.3. Using WDM, the usable optical spectrum [32] (see Figure 2.4) is apportioned into a number of non-overlapping wavelength (or frequency) bands, with each wavelength supporting a signal communication channel operating at whatever rate one desires, e.g., peak electronic speed. The corresponding challenges for this technology at the moment are the design and development of appropriate network architectures, protocols and algorithms to support the various networking functions. At the moment WDM devices are easier to implement since, generally, all components in a WDM device need to operate only at electronic speed; as a

17

result, several WDM devices are available in the marketplace today, and more are emerging.
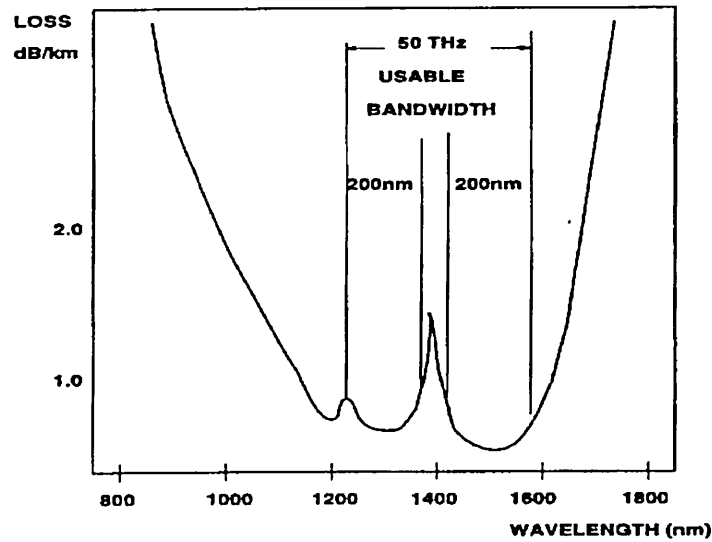
Figure 2.4 The low attenuation regions of an optical fibre

Research and development on optical WDM networks have matured considerably over the past few years, and they seem to have suddenly taken on an explosive form, as evidenced by recent publications [28] as well as overwhelming attendance and enthusiasm at the WDM workshops during recent conferences: E.g. the optical fibre communication (OFC'2002) conference and the IEEE International Conference on Communications (ICC'2002). A number of experimental prototypes have been developed and are currently being deployed and tested mainly by telecommunication providers in the U.S., Europe, and Japan. With the rapid emergence of WDM, it is anticipated that the next generation of Internet will employ WDM based optical backbones.

Current activities indicate that some sort of WDM network will be deployed mainly as a backbone network for large regions, e.g., for nation-wide or global coverage. Figure 2.5

18

shows a passive-star-based optical WDM network [32]. An end-user sends its transmission to the passive star on one wavelength. The information streams from multiple sources are optically combined by the star and the signal power of each stream is equally split and forwarded to all of end-users on their receiving fibres. An end-user's receiver is turned to only one of the wavelengths, hence it can receive the information stream. End-users, for whom the architecture and operation of the backbone will be transparent except for significantly improved response times, will attach to the network through a wavelength-sensitive switching/routing node. An end-user in this context need not necessarily be a terminal equipment, but the aggregate activity from a collection of terminals include those that may possibly be feeding in from other regional and/or local subnetworks. So that the end-user's aggregate activity on any of its transmitters is close to the peak electronic transmission rate.
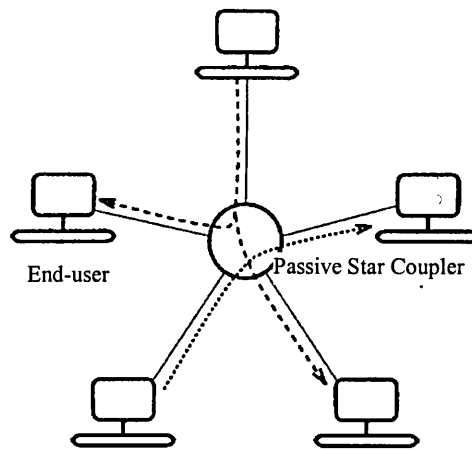
Figure 2.5 A passive-star-based local optical WDM network

2.2.2.2 limitation with WDM used in networks

End-users in a WDM based backbone network may communicate with one other via all optical WDM channels, which are referred to as lightpaths. A lightpath may span multiple

19

fibre links, e.g., to provide a "circuit- switched" interconnection between two nodes, which may have a heavy traffic flow between them and which may be located "far" from each other in the physical fibre network topology. Each intermediate node in the lightpath essentially provides an all-optical bypass facility to support the lightpath.

In an N-node network, if each node is equipped with N-1 transceivers [transmitters (lasers) and receivers (filters)] and if there are enough wavelengths on all fibre links, then every node pair could be connected by an all optical lightpath, and there is no networking problem to solve. However, it is important that the network size N should be scalable. Transceivers technological constraints dictate that the number of WDM channels that can be supported in a fibre are limited to W (whose value is a few tens today, but is expected to improved with time and technological breakthroughs). Thus, only a limited number of lightpaths may be set up the network.

Under such a network setting, for a given set of lightpaths and a constraint on the number of wavelengths, the challenging problems are how to determine the routes over which these lightpaths could be set up and the wavelengths that should be assigned to these lightpaths, so that the maximum number of lightpaths may be established. Although the shortest-path route may be the most preferable option, this choice may not be adopted on occasions where there is a need for a large number of lightpaths. Thus, one may allow establishment of several alternate routes for lightpaths within the network. In such networks the lightpath probability of blocking is a problem, which requires network optimisation.

In this regard, note that, normally, a lightpath operates on the same wavelength across all fibre links that it traverses, in which case the lightpath is said to satisfy the wavelength-

continuity constraint. Thus, two lightpaths that share a common fibre link should not be assigned the same wavelength. However, if a switching /routing node is also equipped with a wavelength converter, then the wavelength-continuity constraints disappear, and a lightpath may be switched between different wavelengths on its route from its origin to its destination.

This particular problem is referred to as the routing and wavelength assignment (RWA) problem. Returning to the networking problem, the designers of the next generation lightwave networks need to be aware of the properties and limitations of optical fibre and devices available in order for their corresponding protocols and algorithms to take advantage of the full potential of the WDM. Often a network designer may approach the WDM architectures and protocols from an overly simplified, ideal, or traditional-networking point of view. Unfortunately, this may lead an individual to make unrealistic assumptions about the properties of fibre and optical components, and hence may result in an unrealisable or impractical design.

2.2.3 OTDM networks
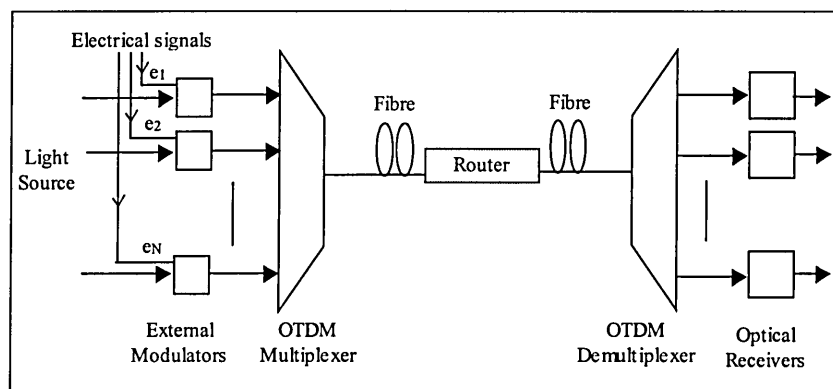
Figure 2.6 OTDM network system block diagram

21

Optical time division multiplexing system networks are considered as alternative to the WDM for future all optical networks. That utilises a single wavelength for high (>100Gbit/s) data rates. A block diagram of a typical OTDM transmission system is shown in Figure 2.6. Instead of WDM, the nodes in Figure 2.6 use a synchronous TDM system for multiaccess communication to implement a local optical TDMA network. The access method at the nodes can be implemented in one of two ways: (1) multiplexing the data from the sources using bit-interleaving or (2) multiplexing based on time slots, each of which can obtain several bits. However, regardless of the above choice, the physical-layer bit rate of the TDMA network would need to be enhanced to N times the data rate of an individual node, where N represents the number of nodes in the networks. In other words, if the user data rate is r bps, the network transmission medium must support a data transmission rate of Nr bps over the entire network span. Thus, in an OTDM based network, if individual nodes have outbound electrical data stream at 10 Gbps with 10 such nodes connected to the network, then each node should be able to transmit at a rate of 100 Gbps on the optical fibre together with the global synchronisation with the other nodes in the network. This is indeed a nontrivial task as opto-electronic interfaces would find it difficult to support the ultra-high transmission rates together with the requirement to preserve the optical pulse shapes against fibre dispersion and timing jitter.

Implementation of the functional units that would constitute an OTDM network requires special considerations to be capable of handling the ultrafast optical signal. These components must be capable of generating narrow optical pulses at high repetition rates and be able to multiplex and demultiplex with complete timing synchronisation [29,30]. In addition consideration must be given to the transmission of the OTDM signal over long

22

fibre spans [31], and possible processing of the optical signals at network nodes using optical buffers and other processing elements [33, 35-37].

In the following subsections, the salient features and operating principles of the basic subsystems in OTDM networks are described.

❖ optical sources (OTDM signal)

❖ modulation and multiplexing

❖ demultiplexing and clock recovery

❖ optical TDM network architectures and proposals

2.2.3.1 OTDM signal

Two types of OTDM signal are illustrated in Figure 2.7. Optical signals representing data streams from multiple sources are interleaved in time to produce a single data stream. The interleaving can be implemented at the bit level as shown in Figure 2.7(a). Alternatively if the data is sent in the form of packets, it can be accomplished at the packet level as shown in Figure 2.7 (b). If the packets are of fixed length, the recognition of packet boundaries is much simpler. In the following description, it is assumed that fixed-length packets are used.

For both bit and packet interleaving, a framing pulse must be used. In the packet interleaving framing pulses mark the boundary between packets. In bit interleaving, if n input data streams are to be multiplexed, then a framing pulse is used every n bits. As will be seen later, these framing pulses are useful for demultiplexing of individual packets from the incoming multiplexed stream of packets.

23

Data in

1 0 0
0 1 1
1 0 1
1 1 1

Bit interleaving time divison multiplexer

Framing pulses

Bit multiplexed stream

(a)

Data in

1 0 0
0 1 1
1 0 1
1 1 1

Packet interleaving time division multiplexer

Framing pulses

Packet multiplexer stream
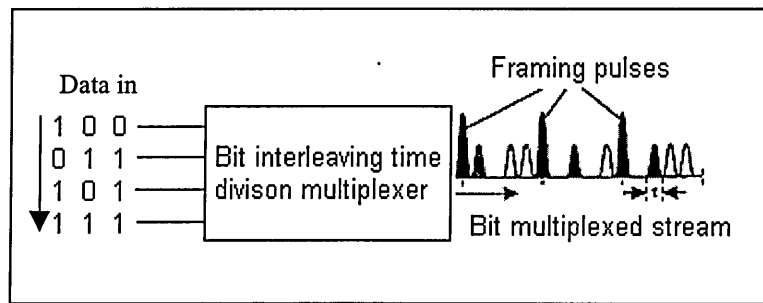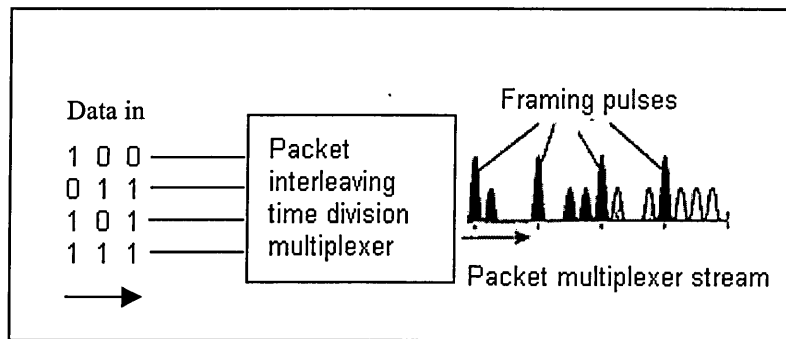
(b)

Figure 2.7 OTDM signal generation (a) Bit interleaving, and (b) Packet interleaving

As shown in Figure 2.7, pulses-much shorter than the bit period must be used in OTDM systems. Ultra short pulses with widths of the order of a few ps can be generated using mode-locked lasers. As the pulse widths are narrow, their spectral width will be large, pulse broadening due to the chromatic dispersion is a problem that needs considering when transmitting over a long span.

2.2.3.2 multiplexing and demultiplexing

At the inputs to the network, lower speed data streams are multiplexed optically into a higher speed stream, and at the output of the network, the lower-speed streams must be

24

extracted from the higher-speed stream optically by means of a demultiplexing function. Functionally, optical TDM is identical to electronic TDM. The only difference is that the multiplexing and demultiplexing operations are performed in the optical domain at high speeds.
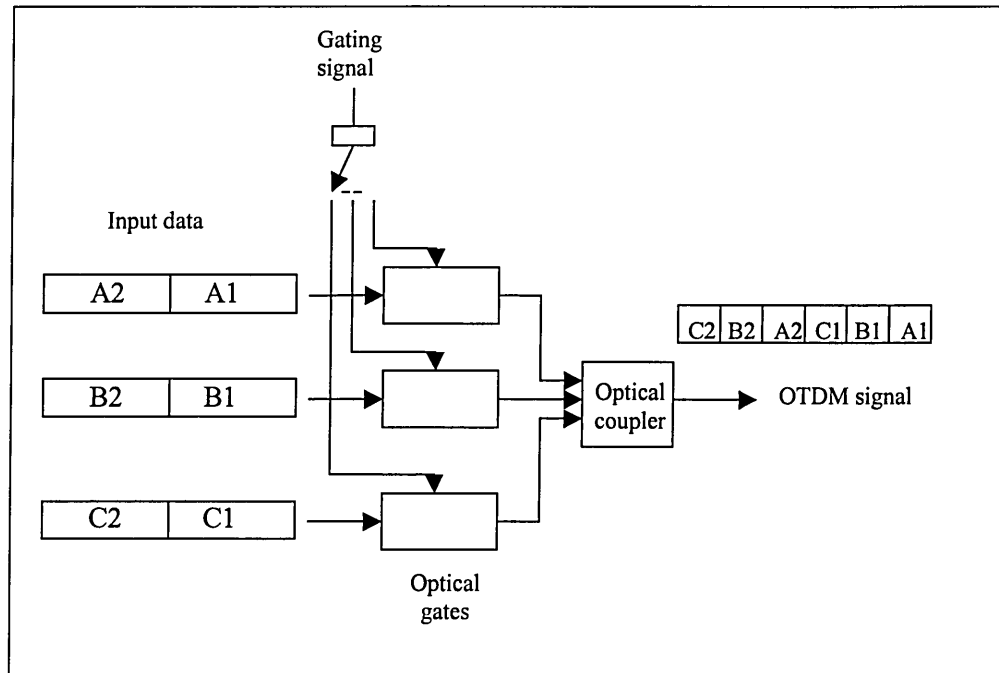
Figure 2.8 Basic elements of an optical time division multiplexer (OTDM).

In OTDM system, data bits for a particular channel, or data packets are allocated a particular time slot, as shown in Figure 2.8. Input channels are optically multiplexed by optically gating each input channel once every bit period.

At the receiver the signals can be demultiplexed using a gating procedure as shown in Figure 2.9, The optical gate could be an electro-absorption modulator or a terahertz optical asymmetric demultiplexer (TOAD) structure, which will be discussed in Section 5.2.
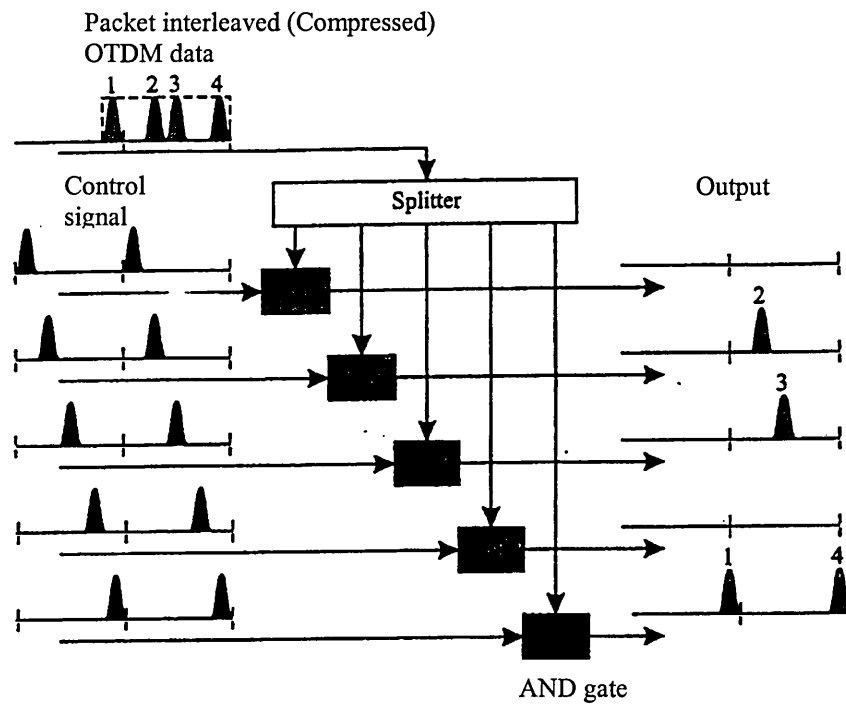
Figure 2.9 An optical demultiplexer to extract one channel from a packet-interleaved OTDM data stream

The demultiplexing operation can be achieved, in principle, by passing the OTDM bit stream or packet compressed OTDM signal through a set of AND gates, to convert the single (serial) high-speed data stream into multiple (parallel) lower-speed data streams that can then be processed electronically [32]. Demultiplexing of a packet interleaved OTDM is illustrated in Figure 2.9. Here, a bank of five AND gates is used to break up an incoming high-speed OTDM packet stream into five parallel streams each with five times the pulse spacing of the multiplexed streams. The procedure is identical to what would be used to receive five bit-interleaved stream. One input to each AND gate is the incoming data stream, and the other input is a control pulse stream where the pulses are spaced five times apart. The control pulse streams to each AND gate are appropriately offset from each other so that they select different data pulses. This approach can also be used to demultiplex a

26

portion of the packet, for example, the packet header. This is useful in switch-based networks for optical routing of packets at intermediate nodes in the networks, and will be explored further in Section 5.4.2.

The logical AND operation shown in Figures 2.8 and 2.9 is performed optically at very high speed. A number of mechanisms have been devised for this purpose. Note that the logical AND operation between two inputs is that one input is the data signal and the other is the control signal.

2.3 Optical TDM Network Architectures and Proposals

In common with WDM networks, OTDM networks can also be implemented using a broadcast topology or more dynamically using optical switching. In the case of a broadcast OTDM network, the topology used is usually a star or a bus. Photonic packet switching networks that incorporate photonic switching and routing will be referred to as switch-based networks.

In broadcast networks there is no routing or switching within the network. Switching occurs only at the periphery of the network by means of tuneable transmitters and receivers. Note that tuneability in the case of TDM networks refers to the ability to select one of several time-multiplexed streams. E.g. for a bit-interleaved multiplexed signal, a tuneable receiver, in a particular tuning state, will be able to receive a fixed time slot in a frame. The switch-based networks perform routing and switching functions optically within the network in order to provide packet-switched service at very high bit rates. The goal of

photonic packet-switching networks is to provide packet-switched service at rates that are outside the capabilities of electronic packet-switched networks. The tradeoff between broadcast and switch-based photonic packet-switching OTDM networks are similar to those of WDM networks. The broadcast networks suffer from large splitting losses, and are not practically scalable. They are generally only suitable for LAN applications. The switch-based networks, on the other hands, are scalable and suited for LAN/MAN applications.

Chapter 3

All Optical Switches

3.1 Introduction

The speed and bandwidth of the world's fast-growing fibre optic communications networks and of the Internet are limited by the speed constraints of the electronic switches required to properly identify and route signals and information packets. Switching light in the light domain eliminates these "bottlenecks". In the emerging field of optical switching, there are a number of competing technologies [38-44]. These include:

❖ Mach-Zender Interferometers

❖ Ultrafast Nonlinear Interferometer (UNI)

❖ Four Wave Mixing

❖ Nonlinear Waveguide (NLWG) Switch

❖ Micro-Electro-Mechanical Systems (MEMS)

❖ Nonlinear Optical Loop Mirror (NOLM)

These techniques should be able to satisfy the bandwidth demand of future routers. The type of device used in router will determine the system reliability, cost and scalability. Many techniques have been demonstrated to perform all optical switching and demultiplexing. This chapter will look at the operation of each device and compare it with a

common set of evaluation criteria, which are switching window temporal size, switch repetition rate, control pulse energy requirements, noise figure, ease of integration and practicality.

3.2 Mach-Zender Switch

Figure 3.1 shows a typical Mach-Zender switch, which is formed by placing two waveguides in close proximity to each other. Light intensity is input to port 1 and splits equally between the two waveguides via coupler 1. The second coupler combines the signals and dependent on their relative phase of signals, output is via port 3 or 4. When a phase shift of π is imposed by the phase shifter on the signal, transmission (after interfering at coupler 2) is via port 4. Port 3 output occurs when the phase shift is zero (i.e. both arms undergo equal phase shift). The switching speed is determined by how fast the phase shift can be turned on and off. One of major disadvantages of Mach-Zender switch is the difficulty in manufacturing waveguides of equal length and dimensions. Using fused fibre technology, the problem can be overcame somewhat by manufacturing the device on similar lengths of fibre and forming the couplers at two points on the fibre by fusion.
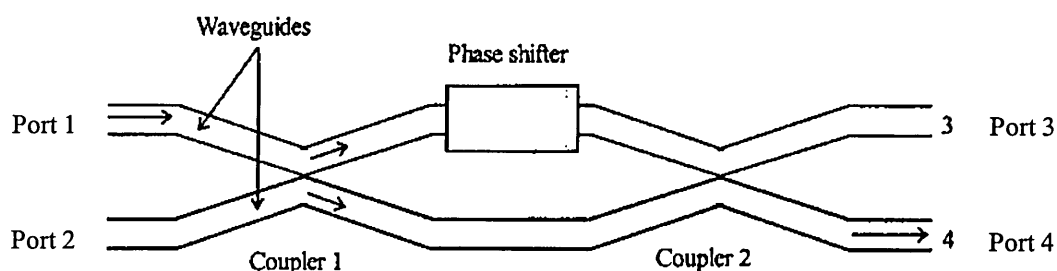
Figure 3.1 Mach Zender switch

Initial investigations on this configuration have been carried out by Shipley [45]. To produce the phase shift, thermo-optic method has been used. By heating the fibre in one arm of the switch, a phase shift ϕ is produced which obeys the following differential equation:

$$\frac{\partial \phi}{l_f \partial T} = k\left(\frac{n_f}{l_f}\frac{\partial L}{\partial T} + \frac{\partial n_f}{\partial T}\right) \qquad (3.1)$$

where l_f is the heated length of fibre, n_f is the fibre index, and k is the propagation constant. With electro resistive heating producing the thermal effect, the power output of the switch follows a periodic response given by:

$$P_o = P_i \cos^2(\pi P / 2P_\pi) \qquad (3.2)$$

where P_π is the electric power required for a π phase shift. Switching speeds were slow due to the long time constant of the heating effect. Modulation frequencies of ≈ 25 Hz were achieved with a heating power of 25 mW.

A novel type of all optical Mach-Zender devices, which is incorporating travelling wave semiconductor laser amplifier (TWSLA), has been demonstrated by Kang [46]. Here, in each arm of the interferometer a TWSLA is placed asymmetrically as shown in Figure 3.2. An additional control signal is fed into port 3 of Figure 3.2. The resolution of the switch is related to the length L_{SLA} and refractive index N_{SLA} of the TWSLA respectively and is given by $2L_{SLA} N_{SLA}/c$. With this configuration a switching speed of 11 ps has been achieved. The time required before switching can be performed is determined by the relaxation time of the TWSLA and is reported to be 1 ns with a contrast ratio between the on and off state of 5:1.

31

This configuration permits integrated assembly and has been demonstrated in a 4 x 1.5 mm device by [47] with a switching speed of 20 Gbit/s with an extinction ratio of 10 dB. A similar device (size 9 x 1.3 mm) [48] produced an extinction of 20 dB. Note that this asymmetric TWSLA device also had an overall gain of ≈5 dB (which is a feature of this configuration) compared with the previous Mach-Zender devices which exhibited an overall insertion loss for the data signal. Both types of the MZS are polarisation sensitive.
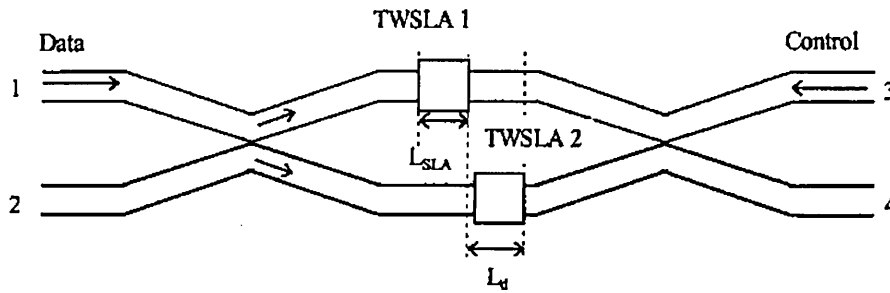
Figure 3.2 Asymmetric TWSLA switch

3.3 Ultrafast Nonlinear Interferometer (UNI)
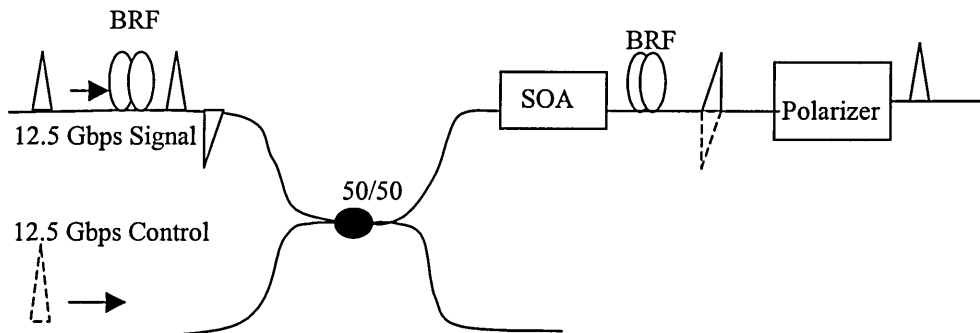
Figure 3.3 Ultrafast nonlinear interferometer

The UNI as shown in Figure 3.3, developed at MIT Lincoln Labs, is an ultrafast all-optical OTDM switching, which uses a SOA as the nonlinear element in a single-arm interferometer [50, 51]. Using a long length of birefringent fibre to separate orthogonally polarised components of data pulses in time, a control pulse can be introduced precisely between the components of a data pulse. When these components pass through the SOA, only the data pulse whose components are separated by the control pulse will experience a differential phase change. As a result, when the pulses are realigned by another long length of birefringent fibre, the components will interfere with each other. Only the pulse which experiences the differential phase change induced by the control pulse will be passed to the output port through the polarizer. The integratability and practicality of the UNI are limited by the long length of birefringent fibre needed to induce the polarization walk-off.

The switching window of UNI switch is determined primarily by the birefringence of the fibre used to separate orthogonally polarised components of the data pulses in the time. Enough walk-off time is required to insert a control pulse between these two pulses. As a minimum, the walk-off should be longer than the control pulse width. Like any other SOA based switch, the UNI is limited by intraband carrier dynamics and carrier heating. Switching repetition rate is limited by the carrier recombination time in the SOA. 100 GHz repetition rates for bitwise logic functions has been reported [52]. Switching windows of about 1 ps can be expected.

The biggest and most important drawback of the UNI is system integratability. This is because UNI requires at least 15 m of birefringent fibre to produce picosecond switching window [38]. Other approaches to achieve the switching window such as briefringent

crystals are not monolithically integratable into semiconductor substrates. Therefore, with the current state of optical-electronic integrated circuits (OEIC) integration technology, Fully integrated UNI may not become practical.

While the lack of integratability adversely impacts UNI, other practical systems considerations limit its applicability. Since UNI is dependent on birefringence to achieve switching, the system must use extensive polarisation control throughout the network to maintain reliability. Polarisation maintaining components and polarisation control devices increase the cost of a practical system. Furthermore, the UNI concept doesn't universally apply to a variety of interferometer configurations. The UNI is for the most part limited to a single-arm interferometer. Without flexibility in the device design, integration and systems applications will be limited.

3.4 Four Wave Mixing
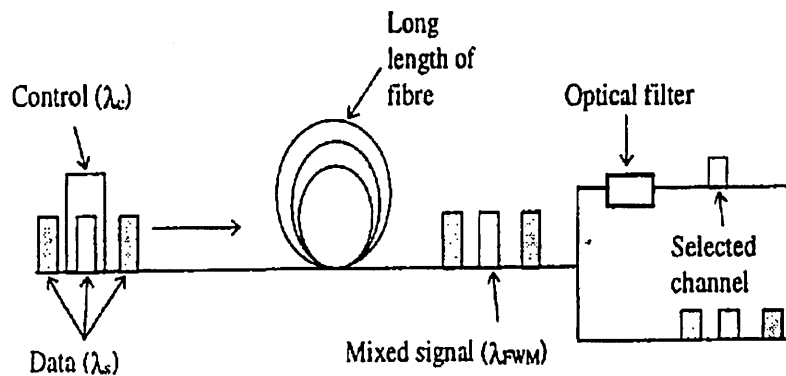
Figure 3.4 Four wave mixing switch

34

Four wave mixing (FWM) switching as shown in Figure 3.4 is achieved by the mixing of two signals of different wavelengths in a non-linear medium [55]. The non-linearity in this case arises from the third order non-linear susceptibility χ^3 of an optical fibre such that polarisation P induced on an electric field propagating through the fibre obeys the relationship given by [55]:

$$P = \varepsilon_0 \chi^3 E^3 \tag{3.3}$$

where ε_0 is the vacuum permitivity of the medium, and E is the electric field. The electric field is the sum of the control signal and data signal ($E = E_c + E_s$), which are given by:

$$E_c = \exp j(\omega_c t - k_c z) \tag{3.4}$$

$$E_s = \exp j(\omega_s t - k_s z) \tag{3.5}$$

The mixing of the two signals takes place in a long length of fibre in which the control signal propagates alongside the selected channel, thus introducing a non-linearity in the fibre, see Figure 3.4. In such case FWM causes a new component to be generated with a frequency f given by:

$$f = c_f / \lambda_{FWM} = 2c_f / \lambda_s + c_f / \lambda_c \tag{3.6}$$

where c_f is the speed of light in the fibre.

Demultiplexing is carried out by filtering the FWM component. In this scheme, although the rise time of the non-linear effect is fast (a few femtoseconds), long interaction lengths are required to generate the non-linearity, thus it is not likely to be in an integrated form. Andrekson [53] have experimentally shown that 14 km of dispersion shifted fibre were needed to generate the required non-linearity. The data and control signal wavelengths were

1.531 μm and 1.48 μm, respectively, with corresponding powers of 4.3 dBm (17mW) and

5.2 dBm (3 mW). Alternatively non-linearity can be achieved by increasing the control

power to 380 mW using 3 km fibre, as demonstrated by [50]. This approach also results in

reduced pulse broadening, which occurs in a long haul OTDM transmission system. In

situations where longer length of fibre is required, an equalising circuit is used to

compensate for the fibre dispersion [54]. This method offers a trade off between fibre

length and control power / circuit complexity. Although this method has been successfully

demonstrated to demultiplex high bit rate data (100 Gbit/s to 6.3 Gbit/s [55]), it remains to

be an inefficient scheme as power is wasted in the unused frequency components.

3.5 Nonlinear Waveguide (NLWG) Switch

Record breaking optical demultiplexing has recently been reported by a group at NEC

research laboratories based on a device known as a nonlinear waveguide (NLWG) switch

[40]. The group has achieved 1.5 Tbit/s demultiplexing with a 200 fs switching window at a

repetition rate of 10 GHz. The device uses a Mach-Zender interferometer configuration and

passive semiconductor waveguides spatially offset within the arms to produce switching,

see Figure 3.5.
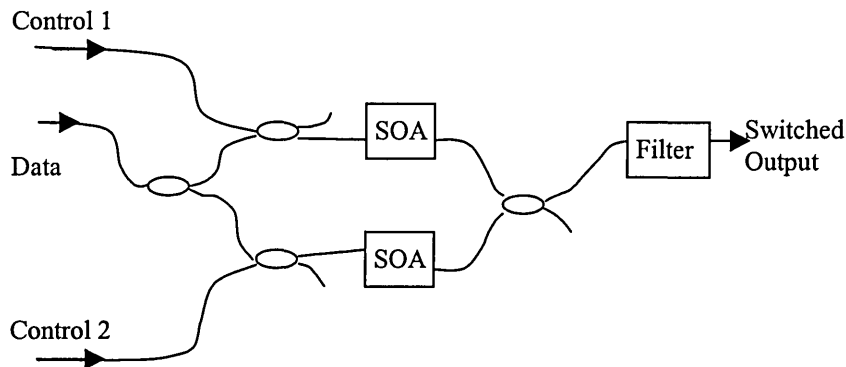
Figure 3.5 Nonlinear waveguide switch

36

The NLWG switch uses data and control pulses sufficiently separated in wavelength to produce a bandfilling effect in the semiconductor waveguide. First, an interferometer is built by using NLWGs in the arms (this may include a Sagnac, Mach-Zender, or even single-arm interferometer like the UNI). When a control pulse is introduced into the device at an appropriate wavelength, its energy is absorbed by the NLWG. The absorption creates an instantaneous refractive index change in the material through the bandfilling effect. Subsequently, data pulses, which traverse the NLWG immediately after the control pulse, can experience a differential phase change needed to produce switching and demultiplexing. The data and control pulses, which have different wavelengths, are separated at the output of the device using a bandpass filter.

While the performance of NLWG switches is outstanding in terms of switching window temporal duration and repetition rate, the device suffers from some important practical considerations. In order to induce a significant amount of bandfilling (the nonlinear mechanism used to induce switching by the control pulse), the control pulse must lie near the absorption edge of the material. For InGaAsP, the communication wavelengths in the 1.55 μm region are strongly absorbed, thus it is used for the control signal. However, for data signals to pass through the device transparently, they must be located tens of nanometers away from the absorption edge. Experimental results presented so far show that the data signal has been set at 1.7 μm wavelength-separated from the control by nearly 150 nm [50]. This data wavelength is impractical for standard fibre based networks as absorption and dispersion would greatly hinder the performance of the network. Additionally, wavelength of 1.7 μm is also difficult to manufacture. Although the performance of NLWG switches is among the best, it is likely that the device will remain a

research interest until control and data signal wavelengths can be accommodated by standard fibre and commercially available optical amplifiers.

3.6 Micro-Electro-Mechanical Systems (MEMS)

Except for time division switches, other mechanisms for optical switching are pursued vigorously. The most common optical switching fabric that is currently being integrated into commercial packet switching system is based on MEMS [77] as shown in Figure 3.6. Simple embodiments of the MEMS technology include movable mirrors which route optic beams of light according to their destination.
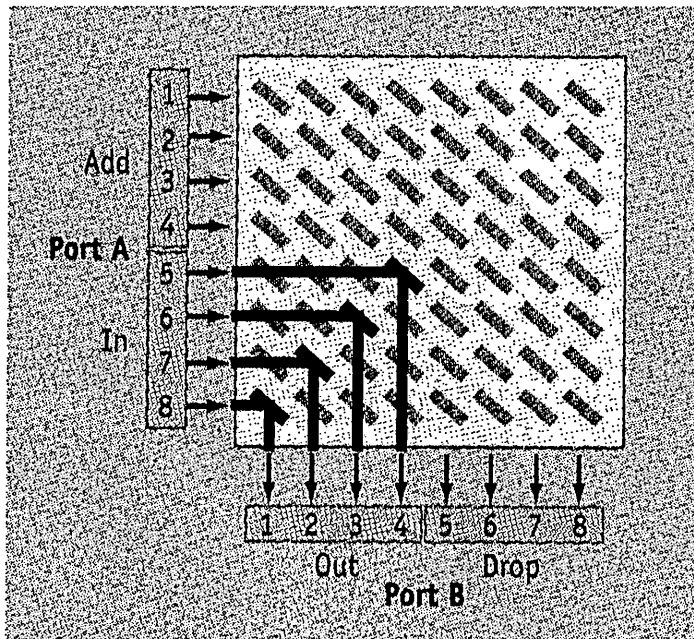
Figure 3.6 MEMS switch

The leader in MEMS technology today is Lucent Technologies. Lucent offered their first all optical routing system in 2000 called WavesStar LambdaRouter [80]. The LambdaRouter

38

uses a 256 x 256 array of movable mirrors to direct light from one fibre to another. Advantages of the MEMS architecture include scalability, low power consumption, low loss, compact size, and protocol transparency. Lucent's current system can support single channel data rates as high as 40 Gbit/s [80]. Other architectures based on the movable mirror technologies are also being developed by the Nortel which uses MENS technology [82].

MENS offers a simple solution to the optical switching problem and avoids the electronic conversion required in standard routers, but the applications area is somewhat limited. Since MEMS are inherently mechanical, they are limited in speed. The Lucent LambdaRouter can move its mirrors only on a time scale of 10 ms. While this is appropriate for optical circuit switching and optical layer restoration protection switching, it is not nearly fast enough to support switching on a packet-by-packet basis required by IP routing. Furthermore electronic hardware must still be used to obtain the routing information to control the switch. Due to the mechanical nature of MEMS, long-term reliability and packaging are still critical issues in these systems. Further advances in MEMS will most likely not be able to upgrade the speed of the switches much beyond a few hundred microseconds. As a result, packet switching with MEMS technology will not replace current electronic IP routers on the Internet backbone. The MEMS based switches will most likely interconnect service providers and large cities where continuous traffic streams are established for long periods of time between fixed locations.

3.7 Nonlinear Optical Loop Mirror (NOLM)

The first successful ultrafast demultiplexing experiments used nonlinear optical loop mirrors (NOLMs) [41]. British Telecom (BT), Michigan, Nippon Telephone and Telegraph (NTT), and many others have performed pioneering work in the development of NOLMs.
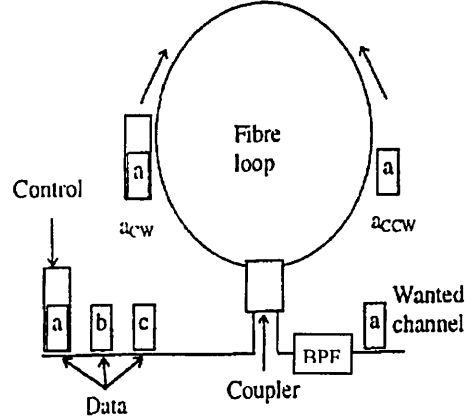
Figure 3.7 Nonlinear optical loop mirror switch

The NOLM switch is composed of a coupler, a band pass filter and a long loop fibre as shown in Figure 3.7 [41]. In the NOLM switch an inherent non-linearity of optical fibres is used known as the Kerr effect. This effect results from variations in the refractive index of the propagation medium as a result of variations in optical intensity. The phase velocity of any light beam passing through the fibre will be affected by its own intensity and the intensity of any other beams present. When the intrinsic third order non-linearity of silica fibres is used, the signal phase shift can be expressed as [56]:

$$\Delta\Phi_{signal} = \frac{2n_2\pi}{\lambda_{sig}}L\left(I_{sig} + 2I_{con}\right)$$

(3.7)

where n_2 is the Kerr coefficient, I_{sig} is the intensity of the data signal to be switched , I_{con} is the intensity of the control signal, λ_{sig} is the data wavelength, and L is the length of the fibre.

The loop itself consists of a long length of fibre, which may be kilometre or more in length, which is necessary to produce the non-linear effect. The data splits at the coupler and propagates around the loop in contra directions (clockwise (CW) and counter clockwise (CCW)) and recombines at the coupler. In the absence of a control pulse the pulse exits via the input port. If a particular pulse in the loop (in this example: clockwise) is straddled by a control pulse then that pulse experiences cross phase modulation and undergoes a relative phase change. The result back at the coupler is a difference in phase between the CW and CCW pulses and the pulse exits via the output port. For more detail, see [57].

Since the switching action in the NOLM is dependent on a passive nonlinearity, subpicosecond operation has been demonstrated. Switching window sizes of about 0.6 ps have been achieved for optical sampling applications [59] as well as demultiplexing. The size (width) of the switching window mainly depends on the duration of the control pulse since the duration of the index change in the fibre is related to the control pulse width. This may impose practical limitation on the size of window and therefore high data rate. There are also other considerations, such as high control pulse intensity (energy) required to achieve non-linearity within the fibre, which limits the device's commercial potential.

The repetition rate of NOLMs can be extremely high due to the passive nature of the fibre nonlinearity. Since the refractive index change induced by the control pulse relaxes very

41

rapidly, the repetition rates are therefore limited only by the practical pulse rates of the laser source. 100 GHz switching rates, although not yet demonstrated, are feasible.

The noise figure of NOLMs is usually not significant, as the fibre nonlinearity is passive. Additionally, the control pulse is easily separated at the output of the loop mirror by a narrow bandpass filter. The best noise figure of about 0 dB is expected for these devices [60].

Although the NOLM has been successfully demonstrated in research laboratories, it has not seen commercial application because of long fibre lengths required to achieve nonlinear interaction. The first NOLM used fibre length > 1 km to achieve enough nonlinearity for full demultiplexing and switching. Using special fibres and other techniques, the length of fibre has been reduced to about 10 m in laboratory. However, in short length fibre, the nonlinearity is still weak, and therefore it is not possible to integrate the long waveguides that could be needed to achieve switching.

Other practical considerations for NOLMs, which make their implementation difficult, include walk-off of control and data pulses as a result of dispersion and birefringence. Since the control and data signals have different wavelengths, each travel at different velocities in the fibre. In order to cause the phase shift in the demultiplexed data signal, both wavelengths must co-propagate together along the entire length of the fibre. Dispersion compensation and cross splicing are two methods that are used to ensure that both data and control signals travel at the same speed [62].

3.8 Summary

This chapter has presented a review of current technologies for the switching of signals in the optical domain. Switches are characterised by switching time, repetition rate, control pulse energy and practicality. Table 3.1 summarises the key device criteria for the all-optical switches. The most likely candidate for an optical router is TOAD, the detail of which will be given in Section 5.2. Its low control energy requirement, reasonable noise figure, integratability, and overall practicality distinguish it among other similar all optical routers. Therefore TOAD will be adopted to investigate the performance of all optical router in this project. The detailed analysis of TOAD will be given in Chapter 5.

A detail explanation of SLA will be represent in following Chapter 4. SLA is an important component used in a number of switches, such as UNI, NLWG, and TOAD. Therefore, it is essential that the operation of SLA be described in details.

Table 3.1 Summary of comparative study among five types of all optical switches

Device	Switching Time	Repetition Rate (GHz)	Control Pulse Energy (pJ)	Noise Figure (dB)	Ease of Integration	Practicality
TOAD	< 1ps	100+GHz	0.25	6	Yes	High
UNI	<1ps	100+GHz	0.25	6	No	Medium
NLWG	0.2ps	40+GHz	50	<2	Yes	Low
NOLM	0.8ps	100+GHz	50+	0	No	Low
MENS	10 ms	< 1 kHz	N/A	N/A	Yes	High

Chapter 4

Optical Amplifier

4.1 Introduction

As Optical amplifier is an important component used in a number of switches, such as UNI, NLWG, and TOAD. Therefore, it is essential that the operation of SLA be described in details. Optical amplifiers are designed to operate on optical signals without recourse to an electro-optic or opto-electronic conversion. Thus electronic repeaters in fibre optical links can be replaced by optical amplifiers, if no reshaping and/or retiming of the signal is necessary. There are two fundamentally different types of optical amplifiers, semiconductor laser amplifiers (SLAs) and fibre amplifiers. Semiconductor laser amplifiers have a distinct advantage over fibre amplifiers in that they can be used for optical switching.

The operating principle of both devices is stimulated emission. In a fibre amplifier the amplification process is affected by feeding an optical pumping signal into a section of fibre that has been doped, usually by a rare earth element such as Erbium. The pump inlet forms part of a directional coupler and the amplifying section of fibre the other.

A semiconductor laser amplifier however is based on a semiconductor laser structure and the interface between the signals is formed from the coupling of an optical fibre to an area of semiconductor. The efficiency obtainable from this coupling is a main contributor to the coupling loss of these devices. The laterally based structure of the device means that polarisation dependence is also an inherent feature.

This chapter presents a literature review of SLAs as used in industrial and laboratory applications. Initially a brief introduction to the use of SLAs in optical communication systems will be given. It is prudent at this stage to divide the SLA into the two broad categories, namely, the Fabry-Perot (FP) SLA and the travelling wave SLA (TWSLA). A description of each is given with the accompanying equations that describe the characteristics of the device under continuous wave input. The main emphasis here is to focus on the TWSLA and will be described in some detail after a brief description of FPSLAs. The concept of noise and how it originates from amplified spontaneous emission will be described and its contribution to receiver generated noise will be shown with the introduction of noise equations. Pulse amplification in TWSLAs will also be reviewed and the special case of ultrashort pulse amplification will also be discussed.

4.2 Semiconductor Laser Amplifiers

The distinction between the FPSLAs and TWSLAs is made from a consideration of the level of reflectivity displayed at the two end facets of the device.

An FP amplifier is a resonant device in which the factor $G\sqrt{r_1 r_2}$ is close to unity, where G is the single pass again through the device, r_1 and r_2 are input and output facet reflectivities. An anti-refection coating is added to the facets in the TW-type SLA in order to allow the input optical power to pass straight through the SLA without encountering any internal feedback. The advantages of travelling wave amplifiers are wide bandwidth, less sensitivity to temperature and signal polarisation and improved gain saturation and noise characteristic.
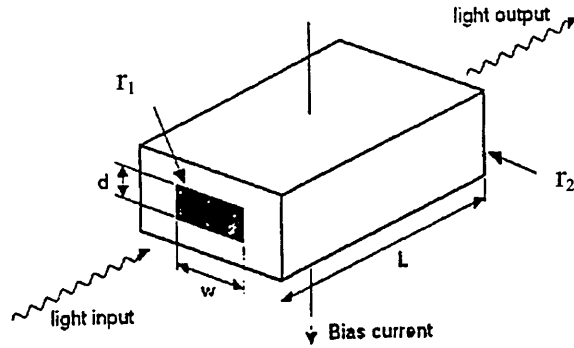
Figure 4.1 Semiconductor laser amplifier schematic

Figure 4.1 shows a basic schematic of a semiconductor laser amplifier with an active area of width w, thickness d and length L. The input and output facet reflectivities are labelled r_1 and r_2, respectively, derived from the difference in the refractive index between the semiconductor and its surrounding. The reflectivity for a GaSb-air interface can be determined using the Fresnel relationship:

$$r = \left(\frac{n_2 - n_1}{n_2 + n_1}\right)^2 = \left(\frac{3.8 - 1}{3.8 + 1}\right)^2 \cong 0.34 , \tag{4.1}$$

where n_1 is the refractive index of the surroundings (air), and n_2 is the refractive index of GaSb.

4.2.1 Theoretical model of a semiconductor laser amplifier

The operation of a semiconductor laser amplifier is based on the interaction of incoming light with the active medium. When an electron undergoes a transition between two energy states it either emits or absorbs a photon (phonon). An electron excited by the absorption of a photon can re-emit a photon in two distinct ways by spontaneous emission, where the electron drops in a random way, or stimulated emission, which is triggered by another photon. In the case of stimulated emission the emitted photon and the triggering photons have equal frequencies and travel in same phases.

Rate equations are often used to describe the interaction between photons and electrons inside an active medium, note the electrons are given the generalised name of "carrier" in this description. There are a number of different forms of rate equations reported in the literature [85-90], differing slightly in the manner in which they attribute different phenomena arising from this process [68] and it is quite usual to omit some of the less effective contributions. The form of rate equations, which includes a number of factors contributing to the changes of carrier density inside the SLA, is given by [68]:

$$\frac{dN}{dt} = \frac{J}{qd} - \frac{N}{\tau_{sp}} - \frac{\Gamma a(N - N_0)P_{in}}{A_{eff}E_p} \qquad (4.2)$$

And the propagation equation used to describe the signal power along the active length is given by [68]:

$$\frac{dP}{dz} = \Gamma a (N - N_0) P - \alpha_{SLA} P \qquad (4.3)$$

where N is the carrier density, J is the bias current density, q is the electron charge, d is the active area depth, τ_{sp} is the carrier lifetime due to spontaneous emission, Γ the mode confinement factor, a is the material gain coefficient, P_{in} is the optical power of the input signal within the transverse waveguide, z is the longitudinal position of light propagation, N_0 is the carrier density required for transparency, A_{eff} is the cross-section area of SLA, E_p is the photon energy, and α_{SLA} is the photon loss coefficient. The first term on the right hand side of equation 4.2 accounts for the influx of electrons provided by the bias current. The second term accounts for the decrease of electron density due to spontaneous emission of photons and the third term for the decrease or increase caused by stimulated emission or absorption of photons. The first term on the right hand side of equation 4.3 accounts for the increase of optical power due to stimulated emission, the decrease, due to (stimulated) absorption of photons, which are described by the third term on the right hand side of equation 4.2. The second term on the right hand side of equation 4.2 takes into account the spontaneous emitted optical power. In most cases this can be neglected as only a small proportion of the randomly directed spontaneous emitted photons are coupled in the guided mode. The second term on the right hand side of equation 4.3 represents a loss of optical power in the laser amplifier cavity, this may also be neglected as the stimulated emission term is dominant in (4.3).

Taking these factors into consideration the rate equations used in this thesis are:

$$\frac{\partial N}{\partial t} = \frac{I}{q \cdot V_{SLA}} - \frac{N}{\tau_{sp}} - \frac{\Gamma \cdot g \cdot P^+}{A_{eff} \cdot E_p}, \qquad (4.4)$$

$$\frac{dP^+}{dz} = \Gamma \cdot g \cdot P^+ . \qquad (4.5)$$

where P^+ is the optical power propagating in the direction of the signal waveguide, I is bias current, V_{SLA} is volume of the active medium of an SLA, A_{eff} is cross-section area of SLA, and g is differential gain of an SLA. Equation 4.5 is subject to the following boundary condition.

$$P^+ = P_{in} , \quad \text{at } z{=}0. \qquad (4.6)$$

4.2.2 Gain of SLA

The localised differential gain of the amplifier can be determined by solving the equations 4.2 and 4.3 and as (4.2) is non-linear numerical techniques are used. The gain coefficient in (4.2) is actually wavelength dependent [68] and usually takes the value of the peak gain g_p of the gain spectrum. If the input light has a wide bandwidth, an integration of the stimulated emission-wavelength curve could be used to replace the third term in (4.2) for improved accuracy. Peak gain g_p of the gain spectrum is given as [92]:

$$g_p = a \cdot (N - N_o), \qquad (4.7)$$

where N is the carrier density, N_o is the transparent carrier density, and a is the gain coefficient. There will be neither gain nor loss if the carrier density is at the transparency level N_o. The gain spectrum and its wavelength of peak gain are both dependent on the carrier density.

The spectral curve of differential gain is different for different semiconductor materials and can be obtained by experimental measurement [92]. The spectral curve of differential gain follows the empirical formula defined in [88] and is given as:

$$g(\lambda) = g_p - a \cdot N \cdot \left(\frac{\lambda - \lambda_p}{\Delta \lambda_g} \right)^2,$$
(4.8)

where g_p, a and N have been defined in (4.7), λ_p is the wavelength of peak gain, and $\Delta\lambda_g$ is the spectral width of the differential gain. The spectral curve of the differential gain in (4.8) does not represent the internal gain spectrum of the SLA. But is defined as the ratio between the amplified output power and the input power to the SLA. The internal gain spectrum is given as:

$$G = \exp(\Gamma \cdot g \cdot L_{SLA}),$$
(4.9)

where L_{SLA} is the length of the SLA.

Equation 4.9 is obtained by integrating (4.5) with the SLA length. It is assumed in (4.9) that the input power is not large enough to cause spatial variation of carrier density along the longitudinal dimension of the SLA.

The peak wavelength λ_p shifts to a lower value as the carrier density increases [92], which is modelled as [88]:

$$\lambda_p = \lambda_o + \left(1 - \frac{N}{N_{th}} \right) \cdot b,$$
(4.10)

where λ_o and b are constants, and N_{th} is the carrier density of lasing threshold. The threshold carrier density depends on the reflectivity of the facets. The lasing threshold in TW-type SLA is larger than in FP-type as there is no oscillation of optical signal inside TW-type SLA to boost the optical gain.

4.2.3 Non-linear gain effects
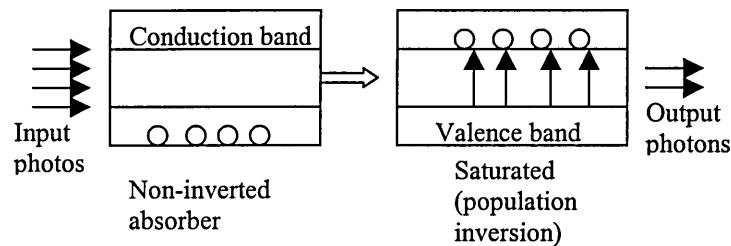
Figure 4.2 Absorption saturation in a semiconductor

It is instructive initially to consider an absorptive medium as shown in Figure 4.2. When a strong signal is sent through such a medium absorption immediately takes place with a corresponding increase in the population inversion. A point is reached where the rate the material absorbs energy is less than the power input and saturated absorption occurs. The point to note is that the shape of the signal is changed by the rate of absorption since the leading edge of a signal (which saturates the absorber) will be absorbed more (attenuated) than the trailing edge. Energy transmission is increased in the saturation region due to inverted carriers during the absorption process and distortion of the signal takes place. In an absorber with an energy gap between conduction bands of E_a and an active area A_{eff}, a common definition of the saturation power is given as [94]:

$$P_{sat} = E_a A_{eff} / (\Gamma \tau_{sp} a) \qquad (4.11)$$

51

Saturable amplification is described fundamentally by the same physics as saturable absorption except for a change of sign between the two processes (the signal is now amplified instead of absorbed). In this case the pump (current) will replenish any stimulated emissions in the amplification process. If the pump injects carriers at a rate greater than that used by the signal then the carrier density does not change. If the stimulated emission rate is greater than the pump rate the carriers are reduced and the gain is reduced leading to a gain that is dependent on the signal power and is given as [98]:

$$G = G_{ss} \exp(-(G-1)P_{in} / P_{sat})$$

(4.12)

where G_{ss} is the small signal gain of the amplifier, P_{sat} is defined in equation 4.11 and describes the value for a steady state gain reduction of ½. Figure 4.3 shows a plot of gain versus input power using equation 4.12, and depicts the saturation of gain due to signal power.
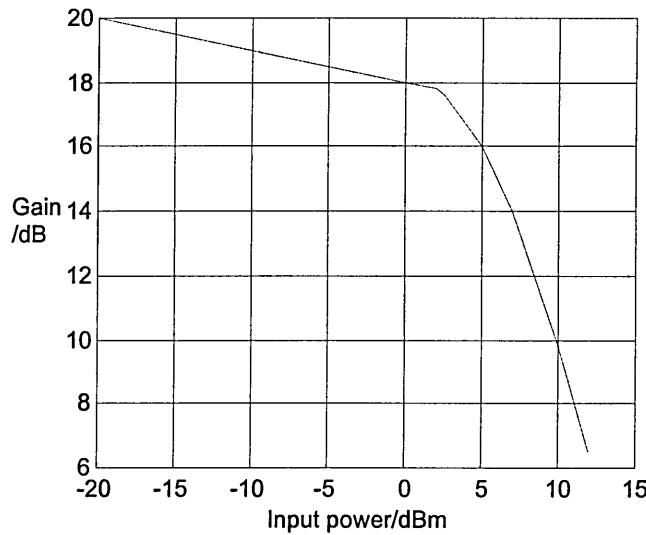
Figure 4.3 Gain saturation in SLA

4.2.4 Carrier density

The carrier density is directly proportional to the bias current when there is no input optical power. This is borne out by (4.4). If P^+ in (4.4) is set to zero and the bias current kept constant, then (4.4) is reduced to:

$$N = \frac{I \cdot \tau_{sp}}{q \cdot V_{SLA}}.$$

(4.13)

The carrier density reaches an equilibrium state when biased by a constant current. The time derivative of N is equal to zero under these conditions. Equation 4.13 shows that the carrier density increases with the bias current. However, when an optical signal enters the SLA for amplification, the stimulated emission (the last term in (4.4)) will deplete the carrier density. This leads to a decrease of differential gain (see (4.7)). Thus increasing the input power will saturate the internal gain. The saturation effect limits the dynamic range of the amplifier. The saturated gain corresponds to a 3dB reduction, from its unsaturated peak value, of the internal gain. The saturated input power is defined as the input power at the onset of saturation. It is desirable to have high-unsaturated gain and high saturated input power in an SLA for a larger amplification and wider dynamic range. However there is always a compromise between high and saturated input power in an SLA. The mathematical model developed by Adams, *et-at* [94] shows the tradeoff that occurs between unsaturated gain and saturated input power. The equation relating the input optical power with the internal gain is given as [94]:

$$P_{in} = \frac{E_p \cdot V_{SLA}}{(G-1)} \cdot \left[\frac{I_b}{q \cdot V_{SLA}} - \frac{N_o}{\tau_{sp}} - \frac{\ln(G)}{a \cdot \Gamma \cdot L_{SLA} \cdot \tau_{sp}} \right],$$

(4.14)

where P_{in} is the input optical power. The other variables have been defined in previous equations. Figure 4.4 shows the internal gain against P_{in} for different values of bias current. As can be seen the plots display a threshold effect above which the internal gain drops rapidly. They also show that the saturated input power decreases as the unsaturated gain increases. The parameters used to generate Figure 4.4 are $E_p = 1.36 \times 10^{-19}$ j, $V_{SLA} = 9 \times 10^{-17}$ m^3, $N_o = 1 \times 10^{24}$ m^{-3}, $\tau_{sp} = 4$ ns, $a = 5 \times 10^{-20}$ m^2, $\Gamma = 0.5$, $L_{SLA} = 300$ μm.
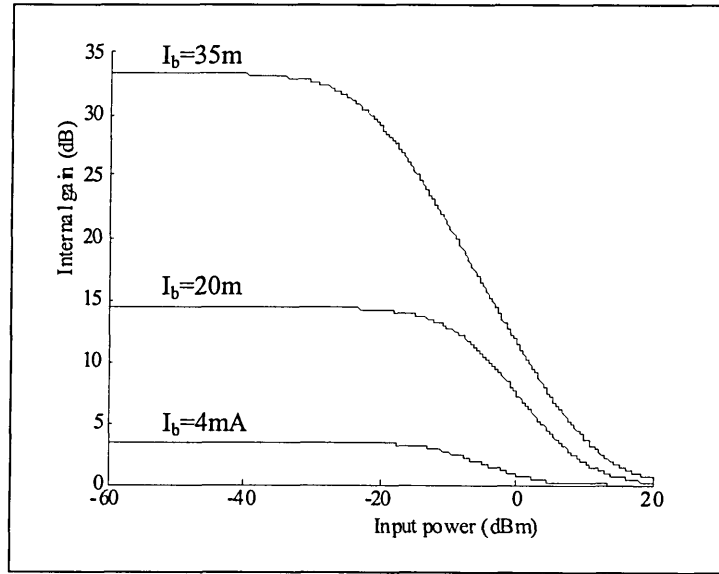
Figure 4.4 The internal gain verses the input power for various bias current I_b

4.2.5 Phase modulation of SLA

In addition to a dynamic gain response these amplifiers also exhibit a phase response that is refractive index dependent, which in turn depends on the carrier density. The refractive index carrier density dependence is given by [98]:

$$n = n_0 - \frac{dn}{dN}(N - N_i)$$ (4.15)

54

where n_0 is the refractive index in the absence of an input signal, N is the carrier density, N_i is the carrier density without signal applied, and dn/dN is the refractive index differential coefficient.

Phase change can also be expressed by (4.16) using the linewidth enhancement factor α_{LEF}, which is a commonly used alternative parameter for quantifying the phase modulation effects in an SLA [92].

$$\frac{\partial \phi}{\partial z} = -\tfrac{1}{2}\alpha_{LEF} \cdot g \tag{4.16}$$

where g is the differential gain, z in (4.16) is related to the reference frame of the pulse profile τ by $\tau = t - z/V_g$ where V_g is the light velocity inside the active region of the SLA. The relationship between α_{LEF} and the carrier density derivative of the refractive index is given by:

$$\alpha_{LEF} = -\frac{dn}{dN} \cdot \frac{4\pi}{\lambda_0 a} \tag{4.17}$$

where λ_0 is the centre wavelength of the input signal and a is the gain coefficient, given in (4.7).

4.3 Equation for SLA Dynamic Analysis

The major differences in the analysis of the dynamic gain and phase non-linearities and any effects due to group velocity dispersion are that the pulse width is assumed long and the device lengths short allowing the latter effects to be ignored. These effects tend to dominate

more in subpicosecond amplification [96]. The task now is to develop a differential equation for an optical signal with intensity $I_o(z,t)$ travelling through an amplifier with an inverted population electron density given as $n(z, t)$. Figure 4.5 describes the propagation of an optical signal through a segment of SLA.
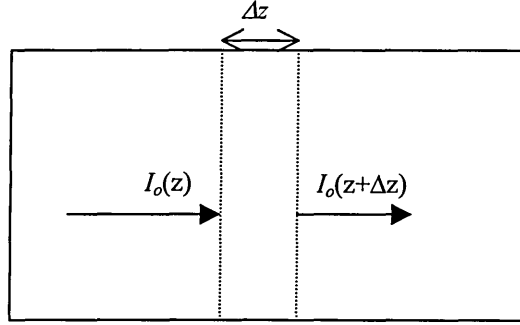
Figure 4.5 Diagram for the calculation of dynamic signal input to an SLA

Considering a short length segment Δz within the amplifier, a simple energy conversion equation in each segment is given by [92]:

$$\frac{\partial E_{tot}(z,t)}{\partial t} = \partial I_o(z,t)A_{eff} - \partial I_o(z + \Delta z,t)A_{eff} - aN(z,t)I_o(z,t)\Delta zA_{eff} \qquad (4.18)$$

where E_{tot} is the total energy within the segment, A_{eff} is the area of segment, and a is the stimulated gain coefficient. The first term of right hand side of equation represents the power into one end of the segment, and the second term is the power out from the other end, the third term indicates the net rate of stimulated emission within the segment.

If ρ is the energy density of the device then the following can be written:

$$\frac{\partial \rho A_{eff}\Delta z}{\partial t} = [\partial I_o(z,t) - \partial I_o(z + \Delta z,t) - aN(z,t)I_o(z,t)\Delta z]A_{eff} \qquad (4.19)$$

Now if the photons move with a velocity of c_d then:

$$I_o(z,t) = c_d \rho \qquad (4.20)$$

giving:

$$\frac{\Delta z \partial I_o(z,t)}{\partial t} \frac{1}{c_d} = I_o(z,t) - I_o(z + \Delta z, t) - aN(z,t)I_o(z,t)\Delta z \qquad (4.21)$$

taking the partial derivative of (4.21) with respect to z gives:

$$\frac{\partial I_o(z,t)}{\partial t} \frac{1}{c_d} + \frac{\partial I_o(z,t)}{\partial t} = aN(z,t)I_o(z,t) \qquad (4.22)$$

which is the propagation equation for the movement of photons within an amplifying medium having an inverted population.

A simplified carrier density equation can be written as:

$$\frac{\partial N(z,t)}{\partial t} = \frac{\Gamma a}{E_p}(N(z,t) - N_0)I_o(z,t) \qquad (4.23)$$

Equations 4.22 and 4.23 are a set of coupled differential equations, which describe the evolution of a time and space varying input to a semiconductor device.

4.4 Noise in Semiconductor Laser Amplifiers

Noise in general is a consequence of the randomness of quantified physical events. Since the mechanisms of light relevant for telecommunications, photodetection and amplification,

57

are theoretically based on the quantum model of light, then it follows that these mechanisms are of a quantum nature. From a quantum mechanical point of view the Heisenberg's uncertainty principle describes the noise phenomena [98]. However this project will aim for a simpler noise model, adequately described in the literature, in order to avoid a quantum mechanical treatment.

The minimum output noise power of an optical amplifier within a bandwidth B_o can be developed from Heisenberg's uncertainty principle and is given by [98]:

$$P_N = (G-1)hfB_o \qquad (4.24)$$

where h is the Planck's constant, f is the frequency, and G is the amplifier gain.

Noise in an SLA can be explained using the concept of spontaneous emission of photons by carrier electrons relaxing randomly from the excited state. The direction these photons are emitted is random and the whole 4π of solid angle is assumed equally likely.

The first approach for noise in a laser amplifier is via blackbody radiation theory. The amount of noise power emitted spontaneously by an element of the amplifying medium at frequencies between f and $f+df$ into the solid angle $d\Omega$ is given by [92]:

$$dP_N = hf \frac{N_2 g(f)}{\tau_{sp}} \frac{d\Omega}{4\pi} dfdV \qquad (4.25)$$

where N_2 is the carrier density or population in the excited state and $g(f)$ is the normalised atomic lineshape function. With consideration of the gain function $e^{\gamma(f)z}$ given by [92]:

$$\gamma(f) = \left(N_2 - \frac{g_2}{g_1}N_1\right)\frac{c^2 g(f)}{8\pi f^2 \tau_{sp}} \qquad (4.26)$$

where g_1 and g_2 are the degeneracies of the two energy levels, N_1 is the population in the lower energy level, and c is the velocity of light in the laser medium. The quantity

$$P_N = hf * df \frac{N_2}{N_2 - \frac{g_2}{g_1}N_1}[G(f) - 1] \qquad (4.27)$$

is usually called the " amount of noise per mode", and it can be shown that it is the amount of noise radiated into a solid angle that can be associated with a single blackbody mode [92].

An alternative theory of noise in optical amplifiers, lasers and masers is the quantum mechanical photon number probability density evolution equation, often called the photon statistics master equation [108], which produces a similar result for the spontaneous emitted power similar to equation 4.24, as derived by Desurvire [96] given by

$$P_{sp} = hfn_{sp}[G - 1]B_0 \qquad (4.28)$$

where B_0 is the optical bandwidth, and the population inversion parameter n_{sp} is given by:

$$n_{sp} = \frac{N}{N - N_0} \qquad (4.29)$$

Using (4.28) as a starting point Olsson has performed semiclassical derivations of the spontaneous-spontaneous beat noise and the signal-spontaneous beat noise [98], by representing the spontaneous emission as a sum of cosine terms, given as:

$$E_{sp} = \sum_{-\frac{B_0}{2df}}^{\frac{B_0}{2df}} \sqrt{hfn_{sp}[G-1]df} \, \cos[(\omega_0 + 2\pi kdf)t + \Phi_k]$$ (4.30)

where Φ_k is a random phase term for each component of spontaneous emission. The total electric field at the output of the amplifier is given by:

$$E_{sp}(t) = \sqrt{2GP_{in}} \, \cos(\omega_0 t) + \sum_{-\frac{B_0}{2df}}^{\frac{B_0}{2df}} \sqrt{ahfn_{sp}[G-1]df} \, \cos[(\omega_0 + 2\pi kdf) + \Phi_k]$$ (4.31)

If the photocurrent is generated by a photodetector with responsitivity R then the photocurrent can be written as:

$$i(t) = R\overline{E^2(t)}$$ (4.32)

The signal-spontaneous beat noise spectral density can also be derived as:

$$N_{s-sp} = 4R^2 GP_{in}n_{sp}(G-1)hf$$ (4.33)

The spontaneous-spontaneous beat noise spectral density near zero can now be written as:

$$N_{sp-sp} = 2R^2 n_{sp}^2 (G-1)^2 (hf)^2 B_0$$ (4.34)

From these two equations for the photocurrent, equivalent noise can be written as:

$$i_N^2 = 2qRL_{opt}\eta_{in}\eta_{out}GP_{in}B_e + 2qRL_{opt}\eta_{out}n_{sp}(G-1)hfB_0B_e +$$
$$4R^4 L_{opt}\eta_{in}\eta_{out}GP_{in}n_{sp}(G-1)hfB_e +$$ (4.35)
$$R^2 L_{opt}\eta_{out}n_{sp}^2 (G-1)^2 (hf)^2 B_e(2B_0 - B_e)$$

where η_{in} and η_{out} are the input and output coupling efficiencies of the amplifier, respectively, L_{opt} is the loss between the amplifier and photodetector, and B_e is the electrical noise equivalent bandwidth of the receiver.

The noise figure of an optical amplifier is given by:

$$F = 2n_{sp}\chi \tag{4.36}$$

where χ is the excess noise coefficient that should approach unity for a travelling wave semiconductor laser amplifier with low mirror reflectivity. In the case of $G \gg 1$, the excess noise factor is given by:

$$\chi \cong \frac{(1 + r_1 G_s)(G_s - 1)}{(1 - r_1)G_s} \tag{4.37}$$

where r_1 is the input mirror reflectivity, and G_s is the single pass gain.

4.5 Summary

The theoretical background of SLA is introduced in this chapter. This chapter presents SLAs with the accompanying equations that describe the characteristics of the device under continuous wave input. The concept of noise of SLA and how it originates from amplified spontaneous emission are described and its contribution to receiver generated noise is shown with the introduction of noise equations. Finally, erbium doped fibre amplifiers (EDFA) are introduced.

Chapter 5

TOAD - Modelling and Simulation

5.1 Introduction

This chapter describes the models developed by the author to simulate the routing action of all optical router based on the terahertz optical asymmetric demultiplexer (TOAD). Although the TOAD model used as demultiplexer has been studied by G. Swift and C. Cheung [104], the TOAD model used for routing action hasn't been investigated yet. The basic TOAD model used for demultiplexer has been modified and developed further by the author. For modelling purposes the TOAD can be described as three components: a fibre coupler, a short fibre loop which could a few meters long, and a non-linear element. Background theories for the non-linear element (i.e. SLA) were described in Chapter 4. The first functional component to be modelled is the input-output coupler. The fibre loop will be assumed initially to consist of a simple time delay until a later section when the polarisation and briefringence effects will also be considered. Fundamental to loop operation is the asymmetry of the SLA within the fibre loop that determine the size of switching window will be discussed along with the need for different SLA models. Equations to describe the special case of small asymmetry are developed in section 5.4.1. Loop performance will be investigated by considering the switching resolution and adjacent pulse crosstalk. The use of a high frequency control pulse is also modelled. A novel application of the system for routing packet signal is also presented.

5.2 Operation Principles of TOAD

The terahertz optical asymmetric demultiplexer (TOAD) [65] was invented at the Princeton University's Lighwave Communications Research Laboratory, which is an enhancement of the fibre loop mirror. Its characteristics suggest that it may be the most versatile and high performance of all optical switches demonstrated to date.
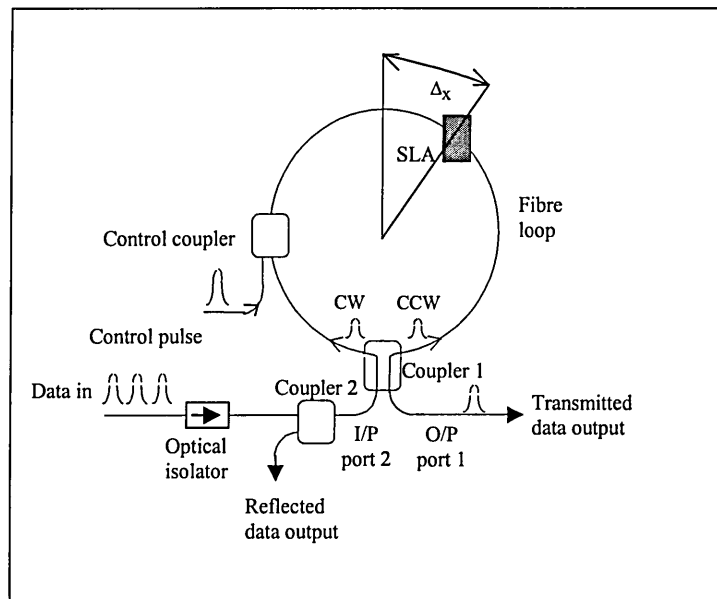
(a)
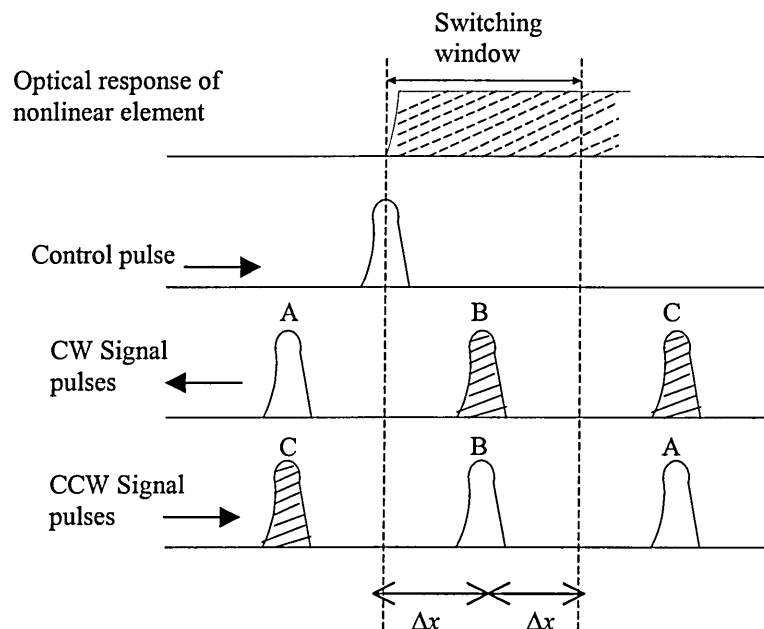
(b)

Figure 5.1 A TOAD switch: (a) schematic block diagram and (b) waveforms

A schematic TOAD is shown in Figure 5.1, which is composed of a short optical loop mirror, a 3 dB 2x2 coupler, a nonlinear element (a semiconductor laser amplifier (SLA)), an intra-loop 2x2 coupler with couplering ratio of 100:0, which injects the control (clock) pulses into the non-linear element, an input coupler with coupling ration of 100:0, and an optical isolator. The states of both the control coupler and the input couplers are selected or set by the switch control unit. These couplers are assumed to have 100:0 ratio whether in 'bar' or 'cross' states. Therefore this is no need to incorporate these in the model, since they act as a short channel with no loss. The optical isolator is used to ensure that the returning pulses do not back propagate towards the source. Note, that with a short length of fibre there is no dispersion penalty, fibre loss is also negligible and polarisation maintenance is not an issue.

When the data pulse train enters the TOAD, each pulse splits into equal clockwise (CW) and counter clockwise (CCW) components. They counter-propagate around the loop and arrive at the SLA at slightly different times as determined by the offset Δx of the SLA from the midpoint of the loop. In the absence of the control pulse, CW and CCW component consequently recombine through constructive interference at coupler 1 and exit the loop via the input port through the coupler 2. Note that the light signal may emerge via the output if CW or CCW component propagating within the loop experience a non-linearity (i.e. a change in the refractive index, relative to CW or CCW or absorption). A control pulse injected via the control coupler arriving at the SLA after both CW and CCW components have passed through the SLA, has no effect on the overall operation of the loop. Thus, the CW and CCW components still emerge via input, see the pulses labelled A in Figure 5.1 (b). However, if CW and CCW components arrive at the SLA after the control pulse has

passed through the SLA will experience the same gain (or phase). Once again the signal will combine at the input coupler and exit via input port, see pulse C in Figure 5.1 (b). In the case where the control pulse reaching the SLA before CW and after the CCW, it saturate the SLA, then causing the SLA to undergo a gain and index changes with short rise time (< ps) and a long recovery time, see pulses B in Figure 5.1 (b). Note the transition in the SLA property does taken place when pulses due to CW and CCW components appear within the switching window. In Figure 5.1 (b), the shaded pulses B indicate that it has experienced post-transition property of the SLA. Thus as a result when the pulses B arrive at the input coupler, the constructive interference between them is incomplete and provided the phase difference between them is π, they will emerge from the output port.

Thus, the rapid changes in the SLA properties (carrier density which leads to gain saturation) followed by a much slower recovery time results in a time window (better known as the switching window) between the TOAD's input and output. Any pulses occurring within the switching window of width $2\Delta x$ will emerge from the output, thus achieving switching. For more detailed information, see [65].

The width of switching window of TOAD is set by location of the SLA within the loop, i.e. Δx, which is the offset from the middle of the loop. The TOAD can perform ultrafast all-optical address recognition by choosing $\Delta x = \tau\ c/2$ (where τ is the bit interval and c is the speed of light in the fibre). When $\Delta x = T\ c/2$ (where T is the length of an optically compressed photonic packet, see Figure 2.7 b), the TOAD can be used as an ultrafast all-optical routing switch.

Note that the control pulse has enough energy to modify the optical property of the SLA (but CW and CCW don't have) to change the optical property of the SLA on a time scale of < ps. The recovery time of the SLA is relatively long much larger than $2\Delta x/v$ but small than the data period or data frame length, see Figure 5.1 (b).

TOAD has achieved a 4 ps timing window in a Sagnac interferometer configuration enabling demultiplexing from an aggregate frame of 250 Gbit/s [30]. Other interferometer configurations have pushed the bandwidth potential to nearly 1 Tbit/s [23]. In terms of the practicality of the TOAD, there are very few devices that can compare with TOAD. The TOAD is primarily suited for applications pertaining to existing all-optical networks operating around the 1.55 μm wavelength. The SLA and other devices used in the TOAD can all be integrated to operate at low loss and low dispersion. TOAD could be used to form pulse or packet switching in an all optical router, by simply changing or setting its switching window width. Cheng [68] and Gao [71] have shown pulse and packet switching at data rate in 250 G bit/s. Simultaneously demultiplexing of 14 wavelength channels from a time multiplexed frame using a TOAD has also been reported, showing TOAD application in hybrid DWDM-OTDM systems [39]. The feature of TOAD enables future optical network routers to exploit the parallelism of optics to push the bandwidth of the technology into the terabit/second regime or beyond.

5.3 Modelling of TOAD

For modelling purposes the TOAD can be described as three components: a fibre coupler, a fibre loop and a non-linear element. The first functional component to be modelled is the input-output coupler. The detail of modelling will be given in this section.

66

5.3.1 Modelling of fibre coupler

Fibre couplers play an important part in TOAD, which is formed by heating a length of two adjacent fibres and elongating to form a tapered fibre with a narrowed length as shown in Figure 5.2.

2x2 roupler
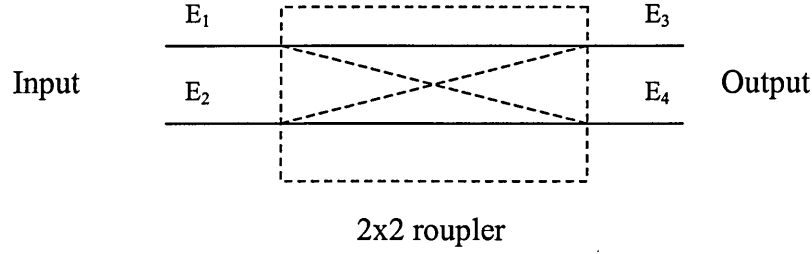
Figure 5.2 Diagram of fused fibre coupler

Coupling action takes place through the interaction of modes along a section of optical fibre. Coupled mode equations are generally used to describe the coupling between the modes of the signal.

The electric field E at the output of a coupler is best described by the coupled theory given by:

$$\begin{pmatrix} E_3 \\ E_4 \end{pmatrix} = (1-\gamma)^{1/2} \begin{pmatrix} (1-K)^{1/2} & K^{1/2}\exp(j\delta) \\ K^{1/2}\exp(j\delta) & (1-K)^{1/2} \end{pmatrix} \begin{pmatrix} E_1 \\ E_2 \end{pmatrix}$$

(5.1)

Where γ represents the excess loss of the coupler, K is the field coupling factor, δ is the phase shift imposed on a cross coupled signal relative to the straight through signal, and E_m (m=1,2,3,4) is the electric field amplitudes at port m.

For the 50:50 couplers, the value of K can be 0.5, which is a function of wavelength demonstrated by Cassidy [102].

5.3.2 SLA model

The SLA model presented is a modified version of that in [68]. The rate equations for the carrier and photon densities inside the active region of an SLA have been given in Chapter 4 and repeated here as:

$$\frac{\partial N}{\partial t} = \frac{I}{q \cdot V_{SLA}} - \frac{N}{\tau_{sp}} - \frac{dP^+}{A_{eff} \cdot E_p dz},$$ (5.2)

where $\dfrac{dP^+}{dz} = \Gamma \cdot g \cdot P^+$, (5.3)

and the differential gain is given as:

$$g = a \cdot (N - N_o)$$ (5.4)

The parameters in (5.2) – (5.4) have been defined before. Assuming that the wavelengths of the control and signal pulses are within the peak and flat region of the gain spectrum, equation 5.4 can be applied to the gains of the signal and control pulses.

ΔL

control
pulse

amplified
control
pulse

m = 1

m = Ln

segment k, time instance t_k

1) $N(k,t_k)$ is calculated from
   $N(k,t_{k-1})$, $P^+(k,t_{k-1})$
2) $P^+(k,t_k)$ is calculated from
   $N(k-1,t_{k-1})$, $P^+(k-1,t_{k-1})$
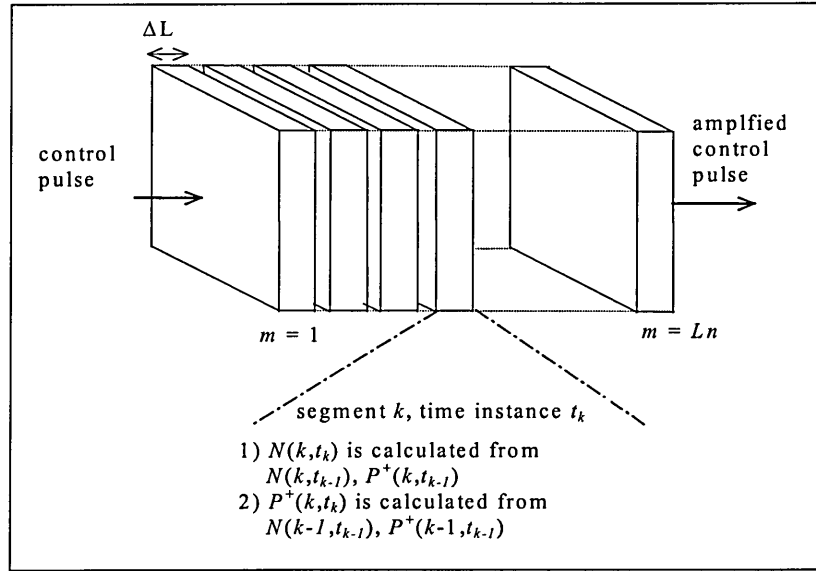
Figure 5.3 SLA model.

N and P^+ may vary across the length of the SLA. The rate equations are solved numerically

by longitudinally breaking down the SLA into L_N number of segments, as shown in Figure

5.3. The segment length is small enough that N and P^+ can be approximated as spatially

independent within individual segments. In each segment, N and P^+ are calculated locally

for a sequence of incremental time instances. N and P^+ for segment k at time instance t_k are

calculated using the following equations:

$$N(k,t_k) = N(k,t_{k-1}) + \Delta N , \tag{5.5}$$

$$P^+(k,t_k) = P^+(k-1,t_{k-1}) \cdot \exp(\Gamma \cdot g(k-1,t_{k-1}) \cdot \Delta L) , \tag{5.6}$$

where

$$\Delta N = \left[\frac{I}{q \cdot V_{SLA}} - \frac{N(k,t_{k-1})}{\tau_{sp}} - \frac{\Gamma \cdot g(k,t_{k-1}) \cdot P^+(k,t_{k-1})}{A_{eff} \cdot E_p} \right] \cdot \Delta t . \tag{5.7}$$

where $\Delta t = \Delta L/V_g$ is the time increment for the numerical calculation, and V_g is the group

velocity of the control pulse. Equation 5.2 is a partial differential equation with time

dependent variables N and P^+, which should generally be solved by complex numerical methods [98]. In order to avoid tedious and time-consuming numerical processes, the change of carrier density ΔN is treated as a time independent value when $\Delta N \ll N$. This condition is satisfied in the SLA model due to the small value of ΔL. The initial values of N can be obtained by setting the last term of (5.2) to zero for the equilibrium state and is given as:

$$N_i = \frac{I \cdot \tau_{sp}}{q \cdot V_{SLA}}.$$

(5.8)

$P^+ = 0$ if no control pulse enters into the SLA. A control pulse entering the SLA will initialise P^+ of the first segment.

Equation 5.2 and 5.3 were solved using the parameters shown in the Table 5.1 and the results are presented in Figure 5.4. It is assumed that the control pulse shape is Gaussian.

Table 5.1 Parameters for calculating the dynamics of carrier density in SLA

Parameters	Value
I	250 mA
V_g	$3 \times 10^8 / 3.5$ m/s
T_{sp}	100 ps
Γ	0.3
E_p	0.8 eV
N_o	1×10^{24} m^3
A_{eff}	2×10^{-20} m^2
SLA length (L_{SLA})	0.35 mm
Total number of SLA segments	100
FWHM control pulse width	2 ps
Peak power of control pulse	1 W
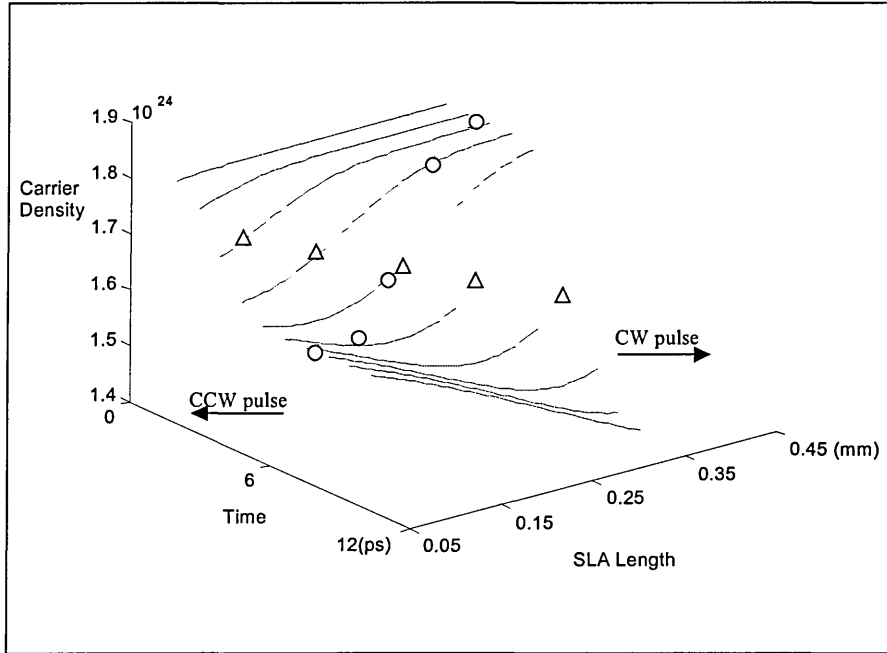
Figure 5.4 Dynamics of carrier density inside the active region of an SLA.

Each solid line in Figure 5.4 represents N versus at a particular time instance. The carrier density is independent of SLA length before the control pulse enters into the SLA, as shown in the first line of the time axis. The carrier density at this state is given by (5.8). When the leading edge of the control pulse propagates into the first few segments of the SLA, the carrier density of those segments depletes somewhat due to the loss of excited electrons by the stimulated emission. The carrier density of other segments to which the control pulse has not reached remains at the initial value. The control pulse propagates further as the time increments increase. The amplitude of control pulse power increases with the propagation distance, as indicated by (5.3). The ever-increasing optical power of control pulse depletes more excited electronics, thus decreasing the carrier density as the propagation length and time increments increase. The carrier density decreases with the

71

SLA length when the control has propagated through the whole SLA, as shown by the last two lines of the time axis in Figure 5.4.

The "Δ" and "o" symbols in Figure 5.4 represent the carrier densities experienced by a temporal points of the CW and CCW pulses, respectively, as they propagate along the SLA. The total gain of the CW and CCW pulses are given as:

$$G_{CW}(t) = \exp\left[\int_0^{L_{SLA}} \Gamma \cdot g\left(z, t + \frac{z}{V_g}\right) dz\right], \tag{5.9}$$

$$G_{CCW}(t) = \exp\left[\int_{L_{SLA}}^0 \Gamma \cdot g\left(z, t + \frac{L_{SLA}}{V_g} - \frac{z}{V_g}\right) dz\right], \tag{5.10}$$

where t is the time at which the temporal point of the CW and CCW pulses entering the first and last segment of the SLA, respectively. The CCW pulse enters the last segment first because its propagation direction is opposite to the CW pulse.

In deriving (5.9) and (5.10) it assumed the SLA is at the mid-point of the fibre loop. With the SLA placed asymmetrically within the fibre loop, the parameter t in (5.9) and (5.10) will take on different values. However, both G_{CW} and G_{CCW} must have the same reference time. Therefore, (5.9) and (5.10) should adopt the time reference either from CW or CCW pulses. Here the time reference adopted is of the CW pulse. With the SLA asymmetry placed within the fibre loop, the modified expression for the G_{CCW} is given as:

$$G_{CCW}(t) = \exp\left[\int_{L_{SLA}}^0 \Gamma \cdot g\left(z, t + T_{asy} + \frac{L_{SLA}}{V_g} - \frac{z}{V_g}\right) dz\right], \tag{5.11}$$

where T_{asy} is the asymmetric arrival time.

5.3.3 Matrix analysis of propagation through TOAD

5.3.3.1 matrix equation

For ease of analysis the TOAD can be broken down into a series of propagation components with individual field transfer functions. The electric fields are representative of a travelling wave signal $E(z,t)$ of amplitude A, radian frequency ω, arbitrary phase shift ϕ and propagation constant k, i.e.,

$$E(z,t) = A\exp(j(\omega t - kz - \phi)).$$ (5.12)
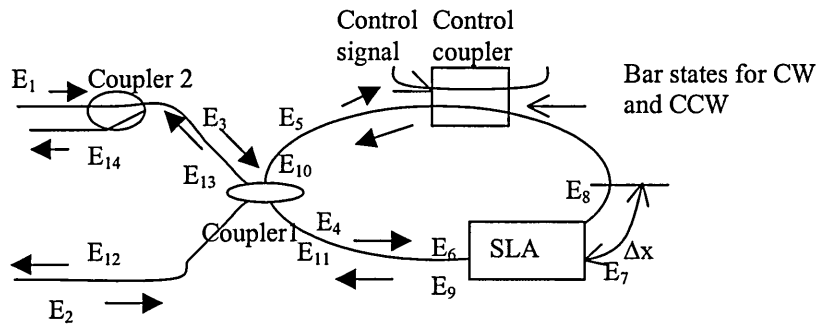
Figure 5.5 A schematic of TOAD showing all the electric fields

Here the main focus is on the TOAD switching characteristics, therefore the power loss of the signal in or out of the loop is not considered. Any loss can be compensated by employing an optical amplifier at the output stage for the returning electric field E_{14}. To

73

simplify the analysis, it is assumed that there is no control pulse, the control coupler is set at the bar state, and the loss of the coupler2 is zero. For non-zero loss coupler optical amplifier may be employed to boost the signal. Following the signal from the input through the couplers 2 and 1, around the loop and returning through the coupler 1 (see Figure 5.5), the following equations can be written:

1. Propagation through coupler 2:

$$E_3 = (1-\gamma)^{1/2}(1-K)^{1/2}E_1 \tag{5.13}$$

2. Propagation through coupler 1:

$$\begin{pmatrix} E_5 \\ E_4 \end{pmatrix} = (1-\gamma)^{1/2}\begin{pmatrix} (1-K)^{1/2} & K^{1/2}\exp(j\delta) \\ K^{1/2}\exp(j\delta) & (1-K)^{1/2} \end{pmatrix}\begin{pmatrix} E_3 \\ E_2 \end{pmatrix} \tag{5.14}$$

3. Propagation through fibre to SLA:

$$\begin{pmatrix} E_7 \\ E_6 \end{pmatrix} = \begin{pmatrix} \exp(\dfrac{j2\pi\alpha n_f(L+\Delta x)}{\lambda_s}) & 0 \\ 0 & \exp(\dfrac{j2\pi\alpha n_f(L-\Delta x)}{\lambda_s}) \end{pmatrix}\begin{pmatrix} E_5 \\ E_4 \end{pmatrix} \tag{5.15}$$

4. Propagation through SLA:

$$\begin{pmatrix} E_9 \\ E_8 \end{pmatrix} = \begin{pmatrix} F_{CW} & 0 \\ 0 & F_{CCW} \end{pmatrix}\begin{pmatrix} E_7 \\ E_6 \end{pmatrix} \tag{5.16}$$

5. Propagation from SLA to coupler1:

$$\begin{pmatrix} E_{10} \\ E_{11} \end{pmatrix} = \begin{pmatrix} \exp(\dfrac{j2\pi\alpha n_f(L-\Delta x)}{\lambda_s}) & 0 \\ 0 & \exp(\dfrac{j2\pi n_f\alpha(L+\Delta x)}{\lambda_s}) \end{pmatrix}\begin{pmatrix} E_8 \\ E_9 \end{pmatrix} \tag{5.17}$$

6. Propagation through coupler 1 (output):

$$\begin{pmatrix} E_{12} \\ E_{13} \end{pmatrix} = (1-\gamma)^{1/2} \begin{pmatrix} (1-K)^{1/2} & K^{1/2} \exp(j\delta) \\ K^{1/2} \exp(j\delta) & (1-K)^{1/2} \end{pmatrix} \begin{pmatrix} E_{11} \\ E_{10} \end{pmatrix}$$

(5.18)

7. Propagation through coupler 2 (output):

$$E_{14} = (1-\gamma)^{1/2} K^{1/2} \exp(j\delta) E_{13}$$

(5.19)

Where L is the half of the length of the fibre loop, λ_s is the signal wavelength, n_f is the refractive index of the fibre, γ is the coupler loss, α is the fibre loss, and F_{CW} and F_{CCW} described in Section 5.3.2 are functions of the gain and phase of the SLA in the CW and CCW directions, respectively. K and δ were defined in (5.1). However, the individual profile of F_{CW} and F_{CCW} are not important, the combination profile is of interest in this work, which determines the switching window and will be discussed in Section 5.3.3.3. The various components can be brought together to give a matrix description of the TOAD thus as:

$$\begin{pmatrix} E_{12} \\ E_{14} \end{pmatrix} = (1-\gamma)^{1/2} e^{-\alpha L} \begin{pmatrix} a_{11} & a_{12} \\ a_{21} & a_{22} \end{pmatrix} \begin{pmatrix} E_1 \\ E_2 \end{pmatrix}$$

(5.20)

where
$$a_{11} = K e^{j(\phi_{cw})} G_{cw} + K e^{j(\phi_{ccw}+\pi)} G_{ccw}$$

$$a_{12} = K e^{j(\phi_{cw}+\pi/2)} G_{cw} + K e^{j(\phi_{ccw}+\pi/2)} G_{ccw}$$

$$a_{21} = K e^{j(\phi_{cw}+\pi/2)} G_{cw} + K e^{j(\phi_{ccw}+\pi/2)} G_{ccw}$$

(5.21)

$$a_{22} = K e^{j(\phi_{cw}+\pi)} G_{cw} + K e^{j(\phi_{ccw})} G_{ccw}$$

where G_{CW} and G_{CCW} are the temporal power gains of the CW and CCW components and defined in (5.9) and (5.11), respectively. ϕ_{cw} and ϕ_{ccw} are the SLA induced phase shifts for CW and CCW components, respectively, and K is the field coupling factor.

It is assumed that in the case where the fibre and loop components are free from birefringence and polarisation effects, the electric field x vector and y vector components undergo equal amplitude and phase change. The matrix description of the TOAD gives a comprehensive analysis of the loop. The effects of various field components in the loop can be described by selecting the appropriate element in the field vector. For example to simulate the component reflected from output port 2 in the direction of electric field x polarisation, the following equation is used (assuming input is port 1 only):

$$E_{14} = a_{21}E_1 + a_{22}E_2 \qquad (5.22)$$

Note that the absence of any birefingence effects indicates no contribution from the y direction of polarisation.

5.3.3.2 power transmission coefficients

To obtain power transmission coefficients, consider a field E incidents into the loop with no input to port 2, which is given as:

$$E = \begin{bmatrix} E_1 \\ 0 \end{bmatrix} \qquad (5.23)$$

After loop transmission, the output power can be written in terms of the transmission vector T multiplied by the input field vector. Note that power of a complex wave is written as $(Ee^{j\phi}) \times (Ee^{-j\phi})$ where $Ee^{j\phi}$ represents the complex amplitude then:

$$\begin{bmatrix} T_1 \\ T_2 \end{bmatrix} \begin{bmatrix} E_1 * E_1 \\ E_1 * E_1 \end{bmatrix} = \begin{bmatrix} a_{11}E_1 \\ a_{21}E_1 \end{bmatrix} \begin{bmatrix} a_{11}E_1 \\ a_{21}E_1 \end{bmatrix} \qquad (5.24)$$

Re-writing (5.24) result is:

$$\begin{bmatrix} T_1 \\ T_2 \end{bmatrix} \begin{bmatrix} |E_1|^2 \\ |E_1|^2 \end{bmatrix} = \begin{bmatrix} a_{11} * a_{11} \\ a_{21} * a_{21} \end{bmatrix} \begin{bmatrix} |E_1|^2 \\ |E_1|^2 \end{bmatrix} \qquad (5.25)$$

Then power transmission coefficients T can be written as:

$$\begin{bmatrix} T_1 \\ T_2 \end{bmatrix} = \begin{bmatrix} a_{11} * a_{11} \\ a_{21} * a_{21} \end{bmatrix} \qquad (5.26)$$

5.3.3.3 *switching window equation for TOAD*

Since all the devices in the TOAD are based on the interferometric principle, we can analyse the switching performance by the following interferometric equation:

$$I_{out}(t) = \frac{I_{in}(t)}{4} \left[G_{cw}(t) + G_{ccw}(t) \pm 2\sqrt{G_{cw}(t)G_{ccw}(t)} (\cos(\phi_{cw}(t) - \phi_{ccw}(t))) \right] \qquad (5.27)$$

where $I_{in}(t)$ and $I_{out}(t)$ are the data input and output intensity, $G_{cw}(t)$ and $G_{ccw}(t)$ are the temporal gain response of the CW and CCW pulses respectively, and ϕ_{cw} and ϕ_{ccw} are the temporal responses of the phase shift for CW and CCW pulses respectively. The responses depend on the propagation geometry and occur at different times and will be described in

77

Section 5.3.2. The ± indicates the signal output at different exits. In order to differentiate two different outputs, we call the signal output with "-" sign as the "transmission output" and "+" sign as the "reflection output".

From the equation (5.27), the output signal with respect to the input signal can be normalised. The normalisation factor, also called as switching window, is given as:

$$W(t)_{ROUTER} = \frac{1}{4} \cdot \left[G_{CW}(t) + G_{CCW}(t) \pm 2 \cdot \sqrt{G_{CW}(t) \cdot G_{CCW}(t)} \cdot \cos \Delta\phi(t) \right], \tag{5.28}$$

where G_{cw} and G_{ccw} were defined in (5.27), and $\Delta\phi$ is the phase difference between CW and CCW pulses. Here it is assumed that the I/O coupler1 in Figure 5.5 has an ideal coupling ratio of 50:50. The phase difference $\Delta\phi$, which is related to the gain ratio of CW and CCW pulses, is given as [65]:

$$\Delta\phi = -0.5\alpha_{LEF} \ln(\frac{G_{CW}}{G_{CCW}}) \tag{5.29}$$

where α_{LEF} is the linewidth enhancement factor.

TOAD switching window could be greater than unity. In other words, TOAD routing can provide additional gain to the target pulse. According to (5.29), when linewidth enhancement factor is known, the TOAD switching window can be calculated by knowing the gain profiles of the CW and CCW pulses. G_{CW} and G_{CCW} are obtained by studying the SLA model as outlined in Section 5.3.2.

Table 5.2 Parameters for evaluating TOAD switching profiles

Parameters	Values
I	300 mA
V_g	3×10^8 / 3.5 m/s
T_{sp}	100 ps
Γ	0.3
E_p	0.8 eV
A_{eff}	2×10^{-20} m^2
N_o	1×10^{24} m^3
SLA length (L_{SLA})	0.3 mm
α_{LEF}	4
Total number of SLA segments	100
FWHM control pulse width	2 ps
Peak power of control pulse	3 W
T_{asy}	0

With the SLA placed asymmetrically with the loop to the right of the loop centre, the CCW pulse reaches the SLA T_{asy} ahead of the CW pulse. T_{asy} would be a negative value when the CCW pulse reaches the SLA first. In equations 5.9 and 5.11 it is assumed that the control pulse is co-propagating with the CW pulse, see Figure 5.1. Equations 5.9 and 5.11 are substituted into (5.29) for evaluating the TOAD switching profiles. Using the data shown in Table 5.2, and assuming a Gaussian shape control pulse, a number of plots were generated as outlined below.
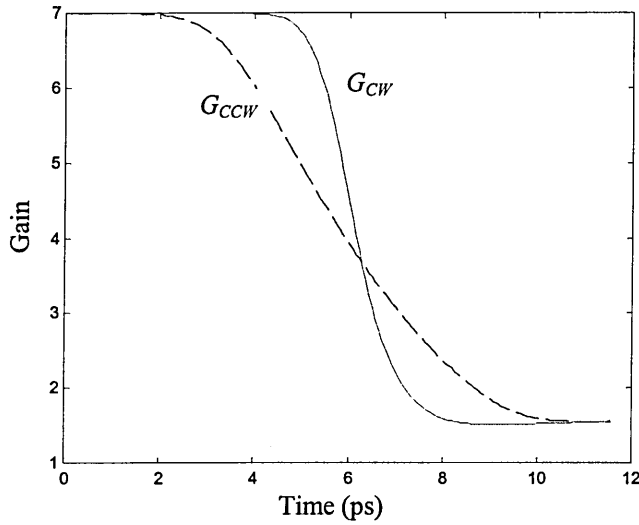
Figure 5.6 Gain response of the TOAD for $T_{asy} = 0$.

Using equations 5.9 and 5.11 to calculate the G_{CW} and G_{CCW}, the result of G_{CW} and G_{CCW} against time for the case when $T_{asy} = 0$ is shown in Figure 5.6. The G_{CW} curve (solid line) in Figure 5.6 has an initial value of 7 before the control pulse enters into the SLA. It drops from 7 to 1.5 due to the decrease of the carrier density by the high intensity control pulse. The fall time of G_{CW} is about 2 ps, which is equivalent to the width of the co-propagating control pulse. The G_{CCW} curve (dashed line) also drops from 7 to 1.5 but at a much slower rate. The fall time of G_{CCW} is about 5.5 ps (equivalent to $\tau_{cp} + L_{SLA}/V_g$) since it is counter-propagating against the control pulse [104].

G_{CW} and G_{CCW} obtained from Figure 5.6 are substituted into (5.29) for determining the TOAD switching window. The result is shown in Figure 5.7, which has two pulse shapes profile. The central dip in Figure 5.7 corresponds to $G_{CW} = G_{CCW}$ at time = 6.2 ps in Figure 5.6.

80
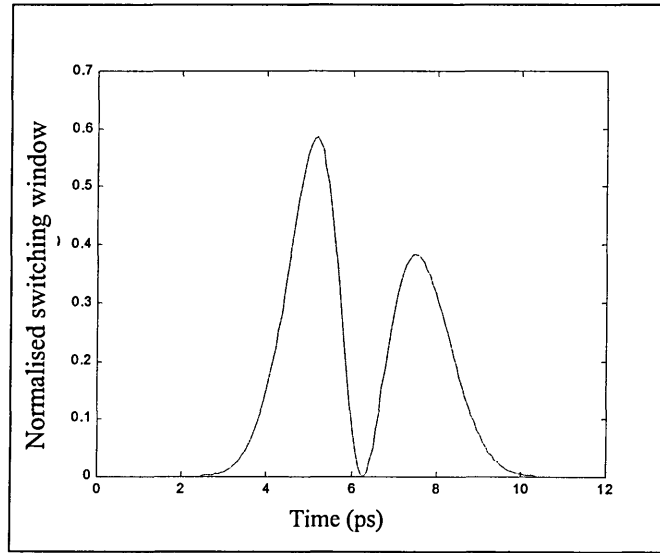
Figure 5.7 TOAD normalised switching window ($T_{asy} = 0$)

The double-peak feature of the switching window displayed in Figure 5.7 can be avoided

by asymmetrically placing the SLA off the mid-point of the fibre loop. Figures 5.8 and 5.9

show the simulation results for the gain profiles in a linear unit and TOAD switching

window using the same set of parameters as in Table 5.2 except for $T_{asy} = 3$ ps.
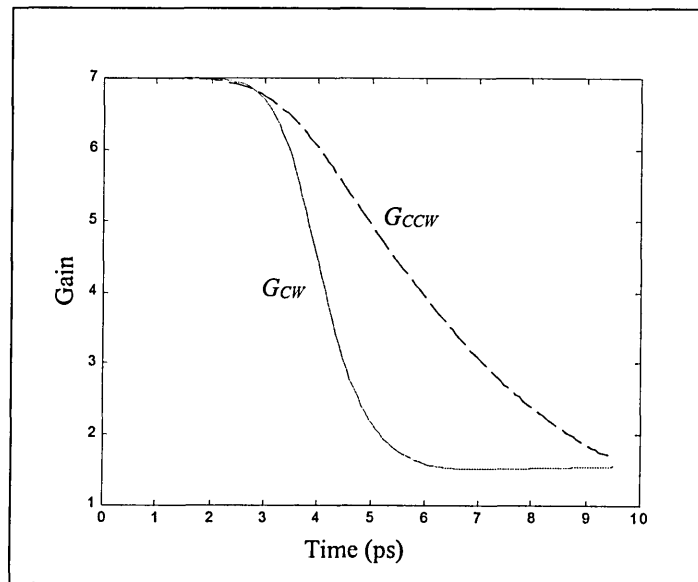
Figure 5.8 Gain response of the TOAD for $T_{asy} = 3$ ps

81
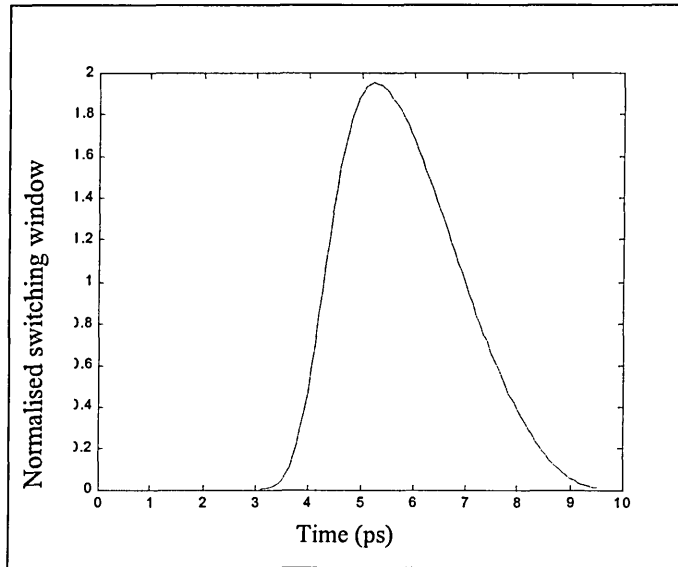
Figure 5.9 TOAD normalised switching window (T_{asy} = 3 ps)

In Figure 5.8 the G_{CW} curve is left shifted by T_{asy} against the G_{CCW} curve, thus eliminating the central dip in the TOAD window for zero asymmetry. A single-peak TOAD window generally has a triangular shape, as shown in Figure 5.9. The rising and declining slopes of the triangle correspond to the fall times of G_{CW} and G_{CCW} as in Figure 5.8, respectively. A triangle-shaped switching window is vulnerable to routing the non-target pulses of neighbour channels from a high capacity OTDM data stream. In order to route only the target pulses, a TOAD router should ideally have a square-shaped switching window profile exactly covering the target time slot of the OTDM signal, with very short rise and fall times. Since the rise time (= τ_{cp}) and fall time (= τ_{cp} + L_{SLA}/V_g) of TOAD switching profile increase with the control pulse width and the SLA length, then it is necessary to keep both of them as small as possible. However, subpico-second control pulse will result in fast and complex gain/phase dynamics of the SLA, as was discussed in Chapter 4. Therefore in this model, the control pulse width is kept at 2 ps, and a range of values used for the SLA length is from 0.1 to 0.5 mm.

82

5.3.4 Optimisation of control energy

The TOAD switching window is a function of G_{CW}, G_{CCW} and $\Delta\phi$, as shown in (5.29). The optimal phase difference $\Delta\phi$ for maximum switching ratio in the TOAD router is less than π and is given as [96]:

$$\Delta\phi_{max} = \pi - \frac{\exp\left(-\dfrac{\pi}{\alpha_{LEF}}\right)+1}{\alpha_{LEF}}.$$ (5.30)

Since $\Delta\phi$ is related to G_{CW} and G_{CCW} according to (5.29), the optimal gain ratio R_G between the CW and CCW components for maximum TOAD switching gain can be given as:

$$R_G = \exp\left[\frac{2}{\alpha_{LEF}^2}\cdot\left(\exp\left(-\frac{\pi}{\alpha_{LEF}}\right)+1-\pi\cdot\alpha_{LEF}\right)\right]\times 100\% .$$ (5.31)

For $\alpha_{LEF} = 4$ using (5.31), R_G is 0.25%. This means that to achieve the maximum switching gain at the peak of TOAD switching window, the control pulse should contain enough energy to saturate the SLA from its initial gain G_o to $G_o R_G$ (in this case $0.25G_o$).

The saturated gain of an SLA driven by an input pulse with an energy of E_{in} is given as [92]:

$$G(E_{in}) = \exp\left\{-\ln\left[1-\left(1-\frac{1}{G_o}\right)\cdot\exp\left(-\frac{E_{in}}{E_{sat}}\right)\right]\right\},$$ (5.32)

where E_{sat} is the saturation energy of the SLA defined by [94]:

$$E_{sat} = \frac{E_p \cdot A_{eff}}{\Gamma \cdot a}.$$ (5.33)

All variables in (5.33) have been defined previously.

In order to attain the maximum TOAD gain, (5.32) can be written as:

$$G_o \cdot R_G = \exp\left\{-\ln\left[1-\left(1-\frac{1}{G_o}\right)\cdot\exp\left(-\frac{E_{CTRL}}{E_{sat}}\right)\right]\right\},$$ (5.34)

where E_{CTRL} is the optimal control pulse energy given as:

$$E_{CTRL} = \frac{E_p A_{eff}}{\Gamma a}\cdot\ln\left(\frac{R_G(G_0-1)}{G_o\cdot R_G -1}\right).$$ (5.35)

If $R_G = 1$, then $E_{CTRL} = 0$, i.e. no gain saturation.

Equations 5.31 and 5.35 are used to optimise the switching energy of the control pulse for maximising the peak of the TOAD switching gain. The following example illustrates the optimisation of the switching energy. Lets assume that the control pulse has a Gaussian shape as given [96]:

$$P_{in}(t) = \frac{0.94E_{in}}{T_{FWHM}}\cdot\exp\left(-(\frac{1.7t}{T_{FWHM}})^2\right),$$ (5.36)

The Gaussian power profile of the control pulse in (5.36) is used as the input pulse to the SLA model for calculating G_{CW} and G_{CCW}. Substituting the parameters shown in Table 5.3 into (5.31) and (5.35), the optimal switching energy E_{CTRL} is calculated to be 2.758 pJ.

Figure 5.10 plots the clockwise and counter-clockwise gains of the TOAD for different values of the switching energy.

Table 5.3 Parameters used for optimisation of the switching energy

Parameters	Values
Unsaturated gain G_o	11
Linewidth enhancement factor α_{LEF}	4
Spontaneous lifetime τ_{sp}	100 ps
Confinement factor Γ	0.3
Gain coefficient a	$3 \times 10^{-20} \ m^{-2}$
Transparent carrier density N_o	$1 \times 10^{24} \ m^{-3}$
Length of the amplifier L_{SLA}	0.3 mm
Cross section area of the amplifier A_{eff}	$2 \times 10^{-13} \ m^2$
Bias current I (calculated from G_o)	335 mA
Photon energy E_p	0.8 eV
FWHM control pulse with T_{FWHM}	1 ps
SLA asymmetry T_{asy}	-4.5 ps
Propagation speed inside the SLA	$(3 \times 10^8 / 3.5)$ m/s
Total number of segments	100

With no control pulse the gain curves in Figure 5.10 have the initial gain value of 11. With the control pulse, the G_{CW} for all values of the control energy remains constant until the time of 5.9 ps, falling to the saturated levels of 4, 2.65 and 1.55 in a linear unit for the control energies of 1 pJ, 3 pJ and 30 pJ, respectively. As expected the G_{CCW} profile drops at a much slower rate than the G_{CW}. The drop in the gain value is dependent on the switching

85

energy and this is due to the saturation of the SLA in the TOAD. Note that for a rusher value of the control energy (30 pJ), the G_{CCW} profile display an exponential profile and reaching the saturation level at time equal to 5 ps much earlier than other two cases. In summary the curves in Figure 5.10 show the cases for under-saturation, optimised saturation and over saturation, for the control energy of 1 pJ, 3 pJ and 30 pJ, respectively.
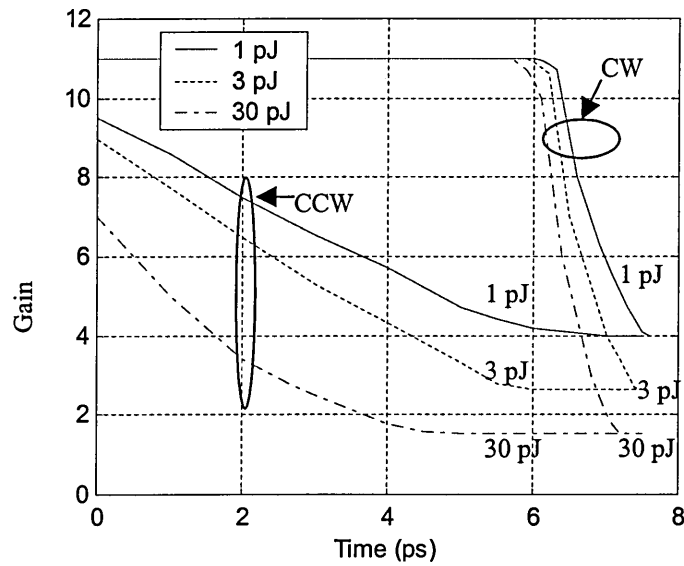
Figure 5.10 G_{CW} and G_{CCW} versus time for different values of the control pulse energies
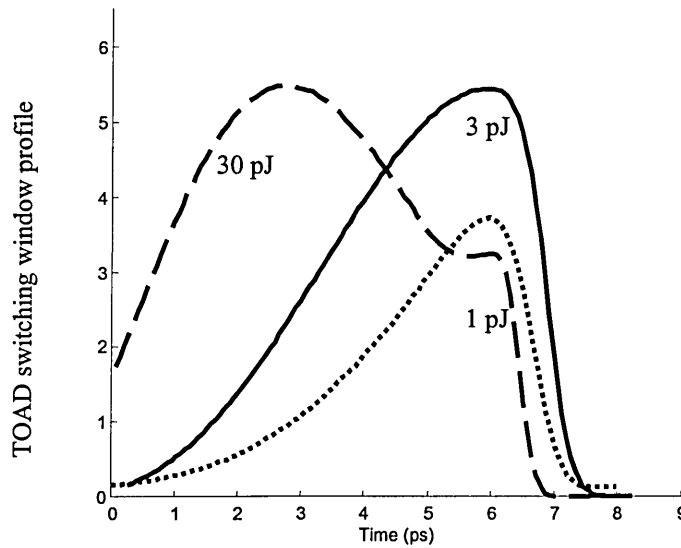
Figure 5.11 TOAD switching window profiles for different values of control pulse energies

The clockwise and counter-clockwise gain obtained from Figure 5.10 are substituted into (5.29) for evaluating the TOAD switching window, and the results in a linear unit are shown in Figure 5.11.

The switching window profiles for the control pulse energies of 1 pJ and 3 pJ are similar except for the peak value and the width of the switching window. Increasing the control energy results in an increase of the peak switching value from 3.5 to 5.5 for 1 pJ and 3 pJ, respectively. For the control energy of 30 pJ, the switching window profile not only peaks at an earlier time of 2.7 ps but also shows a second peak at time equal to 6 ps.

The slow drop in the switching window profile in Figure 5.10 is due to the exponential characteristics of the G_{CCW} as shown in Figure 5.10 for the control energy of 30 pJ.

It was observed that the peak of the switching window ceased to increase further by the increasing the control energy beyond the optimised value.

5.3.5 Limitation on the signal energy

In the TOAD model, the CW and CCW data signal pulses are assumed not to influence the gain and phase dynamics of the SLA because of their low energies. Here we investigate the effect of data signal energy on the SLA gain performance.

Equation 5.32 governs the decrease of the SLA gain by an input signal pulse, where E_{in} in the equation represents the signal energy. The CW and CCW signal pulses are assumed to

have negligible effect on the SLA if the change in the SLA gain is very small compared to the unsaturated gain. Assuming that the change in the SLA gain is less than or equal to 5% when a single input data pulse is applied, the maximum signal energy for the TOAD routing is defined as:

$$0.95 \cdot G_o = \exp\left\{-2 \cdot \ln\left|1 - \left(1 - G_0^{-1}\right) \cdot \exp\left(-0.5 E_{max} E_{sat}^{-1}\right)\right|\right\}, \tag{5.37}$$

where E_{max} is the maximum signal energy for TOAD switching. E_{max} is divided by 2 because the incoming signal pulses are split into CW and CCW pulses with equal energy. Substituting for E_{max} from (5.33) and rearranging (5.37), the maximum signal energy can be written as:

$$E_{max} = 2 \cdot E_{sat} \cdot \ln\left(\frac{G_o - 1}{G_o - 1.05}\right). \tag{5.38}$$

Figure 5.12 plots the maximum signal energy entering the TOAD over an initial gain values of the SLA G_o for $A_{eff} = 2 \times 10^{-13} \text{ m}^2$, $\Gamma = 0.3$, $a = 3 \times 10^{-20} \text{ m}^{-2}$, $E_p = 0.8\text{eV}$. It is shown that E_{max} decreases as G_o increases. A larger initial gain will increase the TOAD output gain, but at the expense of the decrease input dynamic range of the OTDM.
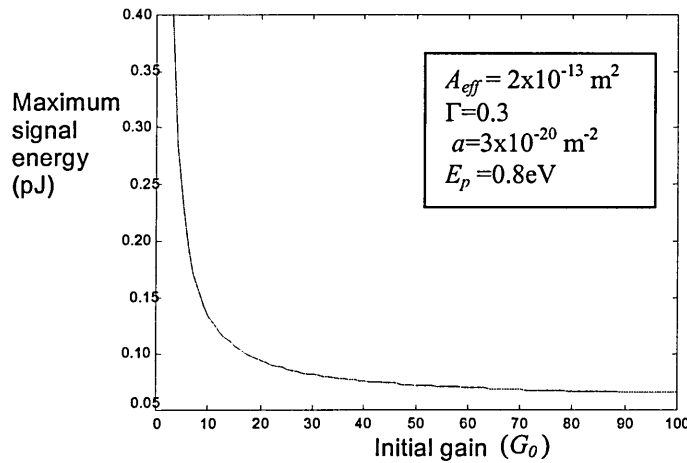
Figure 5.12 Maximum signal energy against the SLA initial gain G_o

88

5.4 Switching Window Size

The gain and phase responses of the CW and CCW data signal passing through the TOAD are simulated using (5.9) and (5.11). The CW data is delayed by a time equal to the asymmetry T_{asy}. These values are then substituted for ϕ_{cw}, ϕ_{ccw}, G_{cw} and G_{ccw} in (5.28) using the values for a_{ij} given in (5.19), which gives the transmission vector of a data signal entering input port 1. Effectively the transmission is simulating the output at port 1 when a continuous wave signal is fed into the input port 1. Here both small and large asymmetries will be investigated, with the former being used for bit switching whereas the latter could be used for packet switching. These will be discussed in the following section.

5.4.1 Small asymmetry

As was previously mentioned, the width of the TOAD switching window is determined by the asymmetry of SLA within the loop. A narrow switching window will be opened with a small asymmetry of SLA in the fibre loop. Reducing the SLA offset from the loop centre will reduced the delay between the G_{CW} and G_{CCW} profiles as illustrated in Figure 5.13 for $T_{ASY} = 3$ ps. The measured delay is about 3 ps that correspond to the FWHM of the switching window as illustrated in Figure 5.14.
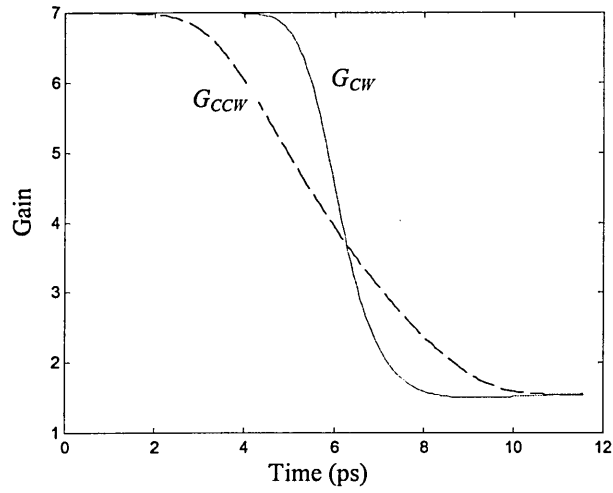
Figure 5.13 Gain profiles of the TOAD for T_{asy} =3 ps
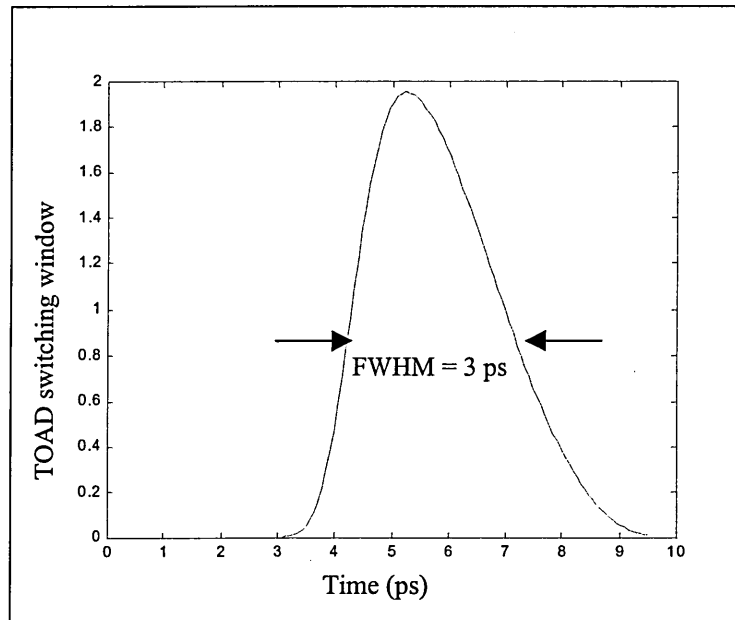
Figure 5.14 TOAD switching window profile for T_{asy} =3 ps

5.4.2 Large asymmetry

Large asymmetry loops are defined as having an asymmetry which is much greater than the

length of SLA, and SLA is assumed to follow the point element model.

90

Consider the case when the SLA is off centre by 0.5 ns, $L_{SLA} = 0.5$ mm, and $\tau_{sp} = 600$ ps. Both CW and CCW gain and phase temporal responses are shown in Figures 5.15 and 5.16, respectively. The responses are separated in the time by $T_{asy} = 1$ ns.
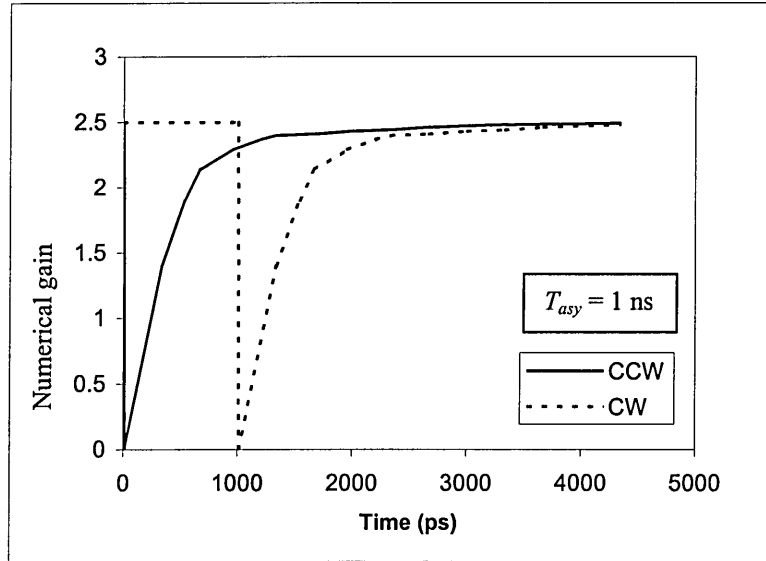
Figure 5.15 Gain response of a large asymmetry loop
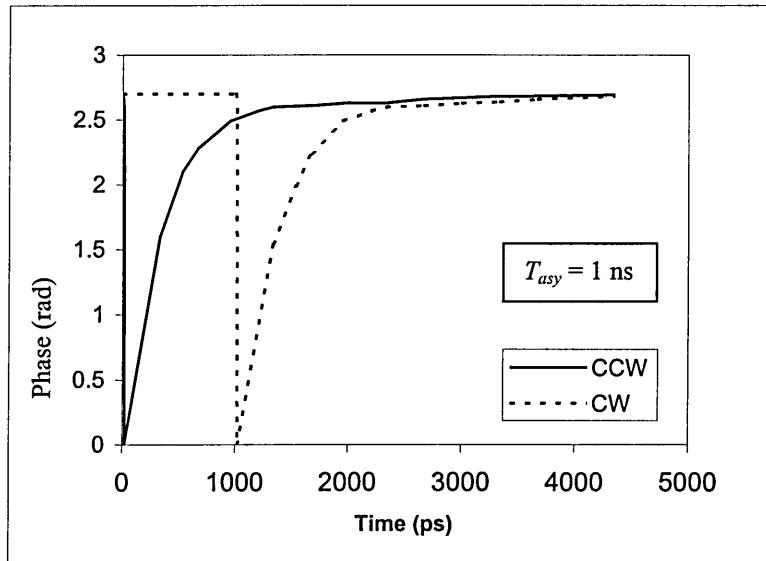
Figure 5.16 Phase response of a large asymmetry loop

The TOAD transmission window profile using the data extracted from Figures 5.15 and 5.16 and (5.28) is shown in Figure 5.17. As expected the switching window shows double windows of width 250 ps that corresponds to the gain /phase response shown in Figures 5.15 and 5.16.
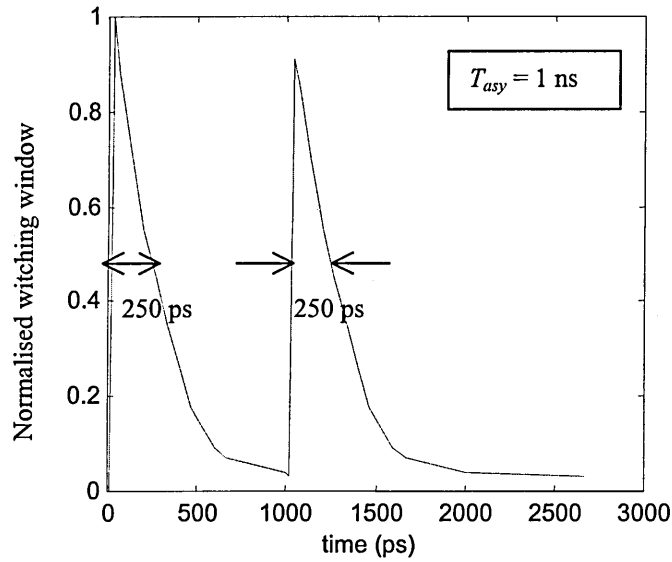
Figure 5.17 TOAD switching windows with a large asymmetry
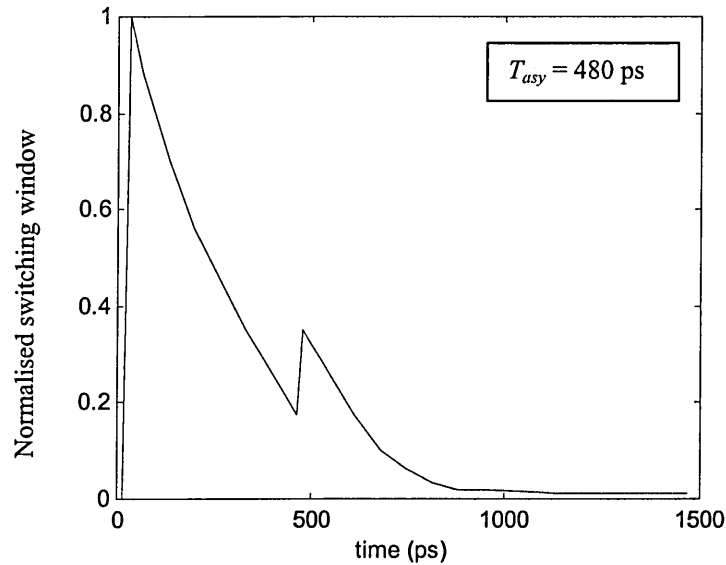
Figure 5.18 TOAD switching window with a reduced asymmetry

What is evident from the Figure 5.17 is that two windows have been opened and separated by T_{asy}. With this switching profile a single OTDM pulse within a period T_{asy} could be detected followed by a second output immediately after the asymmetry time (the frame period is assumed $> T_{asy}$).

Now consider the case where the SLA asymmetry is reduced to 225 ps. The resulting switching window is shown in Figure 5.18, where the width of the first window is increased and it overlaps with the second window, thus resulting in a reduced height of the second window.

Intuitively it is apparent that reducing the asymmetry will result in a gradual disappearance of a second window eventually leaving just one wide window which can be used to select data (or Packet) of length equal to T_{asy}. Experimental results by Sokoloff [106] on an asymmetric semiconductor laser amplifier loop mirror with T_{asy} = 690 ps and τ_{sp}= 600 ps also shows a second switching window appearing at t = 690 ps which confirms the predicted results for the large asymmetry as in Figure 5.17. The configuration required to generate a single switching window will be discussed next.
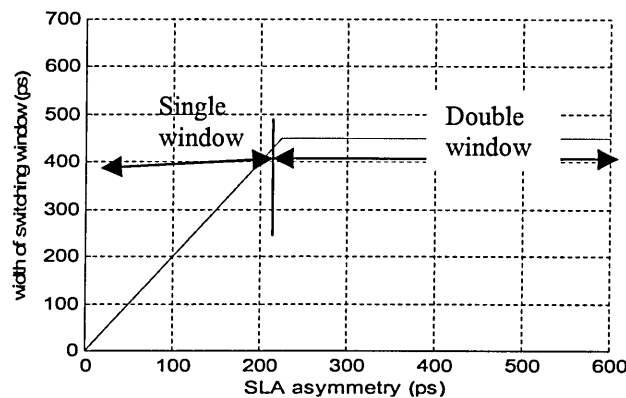
Figure 5.19 Width of switching window versus the SLA asymmetry

93

It is clear to see that the width of the switching window increases linearly as the SLA asymmetry increase up to the point where the SLA asymmetry is equal to 200 ps, which is the relaxation time of the SLA. Beyond this point the switching window width remains unchanged at 500 ps as shown in Figure 5.19. When the SLA asymmetry is comparable to (or near to) the recovery (relaxation) time, a wider width control pulse is needed to keep the SLA saturated or alternatively a train of short duration control pulses may be used to keep the saturation "topped up". Figure 5.20 shows a typical wide switching window of 10 ns obtained using a train of control pulses with width and period of 2 ps and 100 ps.
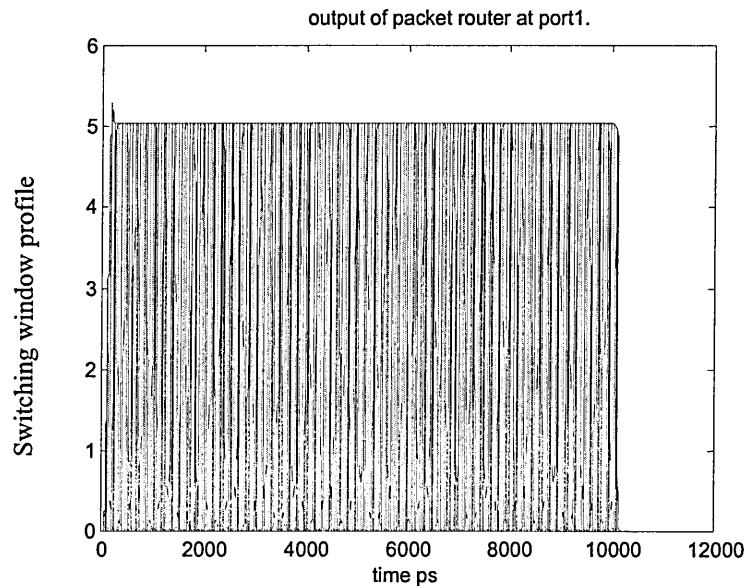
Figure 5.20 TOAD switching window with a width of 10 ns

5.4.3 High frequency control pulse

When a control pulse is fed into the fibre loop via a coupler with a period which is shorter than the recombination time, the carrier density will settle to a value which is determined

by the average power of the control pulse as in Section 4.2.1. With the control pulse separation times $> \tau$ full recovery of the device is allowed and the carrier density settles back to its initial value. For the control pulse with a small separation time, the carrier density can be approximated from the steady state rate equation 5.8 corresponding to N_i. Equation 5.8 results in a smaller ΔN and when substituted in (5.2) the TOAD gives a lower transmitted intensity. To overcome this the SLA is operated with higher bias current, which increases ΔN due to the increase in N_i in (5.8). Figure 5.21 shows the peak of the switching window of the TOAD against the SLA bias current for a 100 GHz control pulse. Other parameters used here is the same as those listed in Table 5.3.
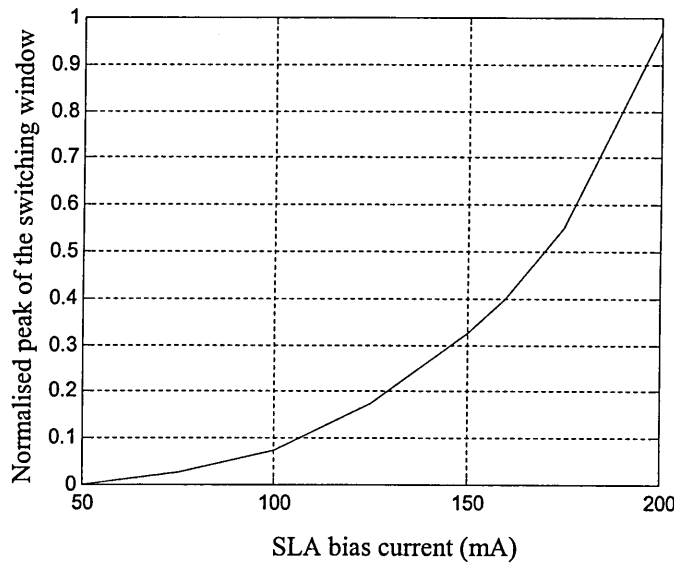
Figure 5.21 Normalised peak of the TOAD switching window against the
SLA bias current for 100 GHz control pulse.

The concept of high SLA bias currents for high input data rate is also observed experimentally in [109] where a current of 200 mA for a 5 GHz control signal is compared to a considerably lower current (35 mA) used [106] using a control pulse of 100 MHz.

5.4.4 Comparison of results

Here a comparison of the simulation results with previously reported data will be made to check the validity of the proposed model. The first comparison will be made with an asymmetric semiconductor laser amplifier loop mirror with an SLA positioned 4 ps from the centre proposed by Kane et al [108]. The second comparison will be made with a medium asymmetry SLA. In this case, the SLA is placed 65 ps from the loop center. Switching window of 140 ps width has been experimentally reported [106].

The experimental and simulated results for various parameters are given in Table 5.4. Table 5.4 indicates a close agreement between the simulated and experimental results.

Table 5.4 A comparison of practical and simulated results for the TOAD

Parameters	Experimental	Simulated	Experimental	Simulated
Width of switching window /ps	9	8	140	130
Control pulse FWHM /ps	2	2	2	2
Rising edge of switching window /ps	11	11.5	11	11.5
Trailing edge of switching window /ps	4	3.5	4	4

5.5 All Optical Router Based on TOAD

TOAD may be used as a switching element in an OTDM based router to extract the header information (i.e. the address bits) and data information (bits or packets). Figure 5.22 shows a schematic of a typical single node TOAD based OTDM router, which consist of two

96

TOADs, an optical fibre loop buffer (OFLB), a 3-dB 1x2 splitter and a polarisation beam splitter (PS).
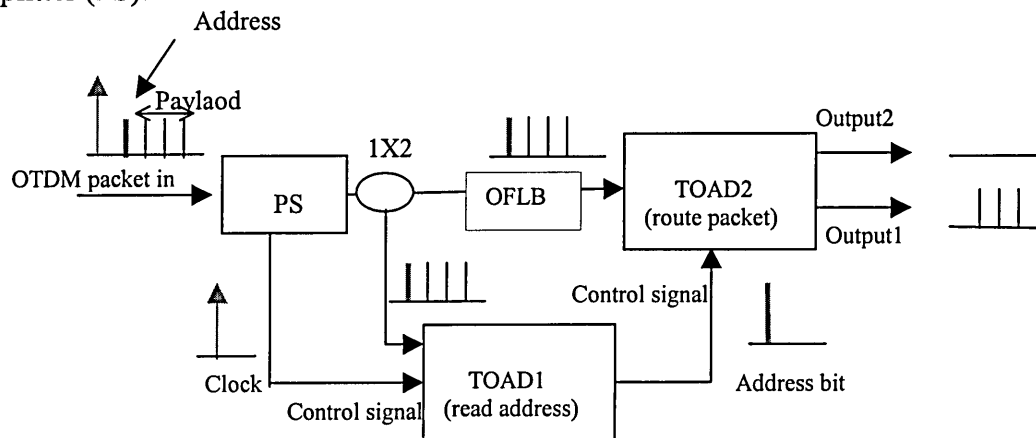
Figure 5.22 Basic elements of an all optical router based on TOAD

A single wavelength incoming OTDM packet is composed of a clock pulse with different polarisation and higher intensity, address bits and payload. A higher intensity clock signal is required since it will be used as a control signal for the TOAD1. The clock pulse is separated from the incoming OTDM packet using a polarisation beam splitter before being used as the control signal for the TOAD1. The remaining part of the OTDM packet (address bit and payload) is split into two using a 1:2 3-dB coupler, feeding TOAD1 and TOAD2 via an optical fibre loop buffer. The TOAD1 with a narrow switching window extracts the packet destination address bit from the incoming address bit and payload. The amplified address bit now acting as a control signal sets the TOAD2 into a switched or unswitched state. The optical fibre loop buffer is employed to match the delay of the address and payload pulses to the control signal before being processed by the TOAD2. The TOAD2 has a much wider switching window compared with the TOAD1. Depending on the address bit, the payload is sent to either output port 1 or 2 of the TOAD2. In a single bit routing scheme, the packets with address bit of value "1" are routed to the output port 1, while packets with an address bit of value "0" are routed to the output port 2.

97

Table 5.5 OTDM packet parameters used in 1x2 router

Parameters	Values
Input data rate	9 Gbit
Input data pulse FWHM	2 ps
Control pulse width	2 ps
Clock pulse width	2 ps
Clock pulse energy	1e-14 J
SLA asymmetry	TOAD1: 2 ps TOAD2: 6 ps

OTDM format could be in one of the following formats:

i)   Single wavelength, constant amplitude and with clock signal of different polarisation to that of the address and payload

ii)   Single wavelength, no polarisation and with the clock signal of high amplitude compared to the address and payload.

iii)   Single wavelength, constant amplitude and no polarisation.

iv)   No polarisation, constant amplitude and with clock signal at a different wavelength to that of the address and payload.

In this work, the generated OTDM packet is based on the first format, and it is assumed that polarisation of the OTDM packet is maintained during the transmission.

The second format is easy to generate but rather complex to implement the clock recovering at the router or receiver. The third format is currently being investigated by

another researcher within the Optical Communication Research Group at Sheffield Hallam University [153].

To investigate the operation of the OTDM router, an input OTDM packet with the following experimental parameters listed in Table 5.5, as in [109], were generated. The simulated waveforms at various points in Figure 5.22 are displayed in the following figures. Figure 5.23 shows the incoming OTDM packet, the extracted clock signal at one of the outputs of the PS (assuming no loss), and the address bit plus payload at the second output of the PS.
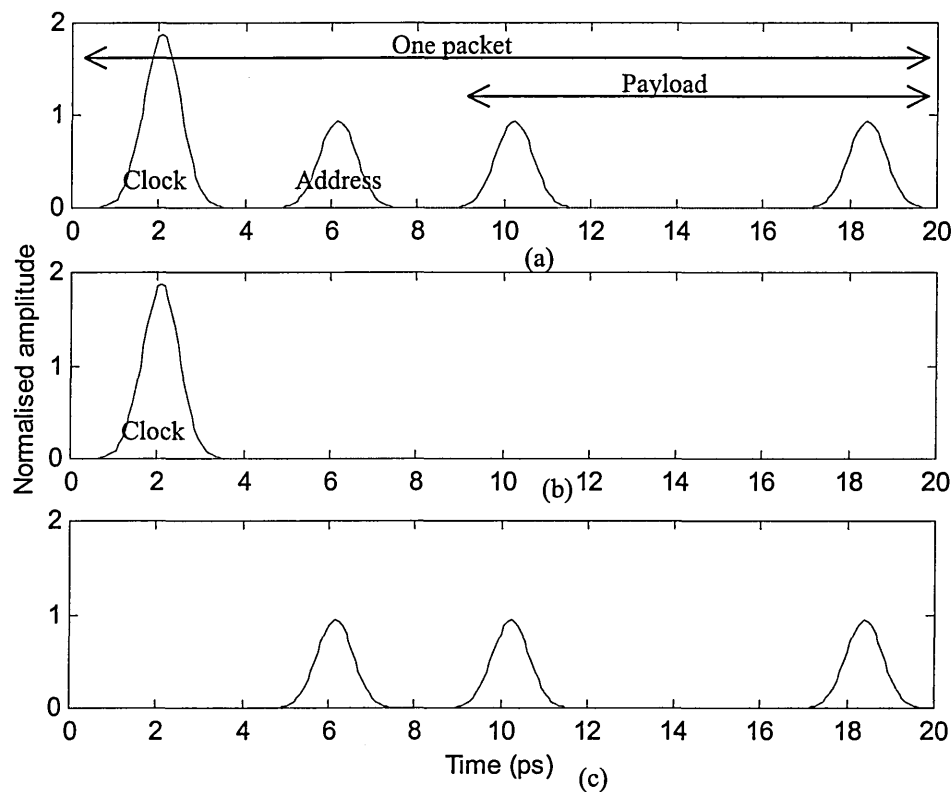
Figure 5.23 (a) OTDM packet, (b) extracted clock and (c) address bit and the payload

Further simulation result demonstrating address recognition from the OTDM signal of 250 Gbit/s is shown in Figures 5.24. Figure 5.24 shows the switching window of TOAD1 and the extracted address bit, which has been amplified and is used as the control signal to saturate the SLA in TOAD2. In this figure, the OTDM data pulse width and the loop asymmetry are reduced to 2 ps and 5 ps, respectively. For the case when the OTDM packet has multi-bit address, the extracted address and the switching window are shown in Figure 5.25. As can be seen the target address bit appears at the center of the switching window as required. But neighbour bit also appears (with reduced intensity) within the windows, which contributes to the crosstalk. Since the extracted address bit has a much higher intensity than the crosstalk bit, it will play the dominant rob in saturating the SLA in the TOAD2. Thus setting the states of the TOAD2 output ports. The crosstalk will have very little or no effect on the operation of the TOAD2. This result has been demonstrated experimentally by Glesk [108].
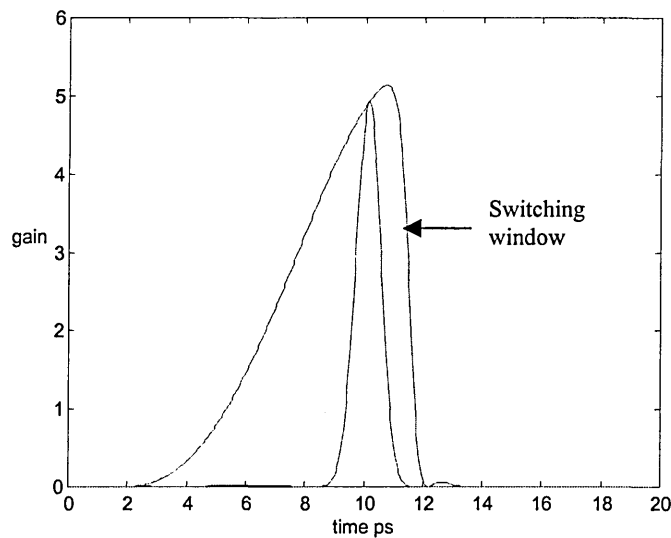
Figure 5.24 Output of TOAD 1 at port 1 (address recognise), also
shown is the profile of the switching window
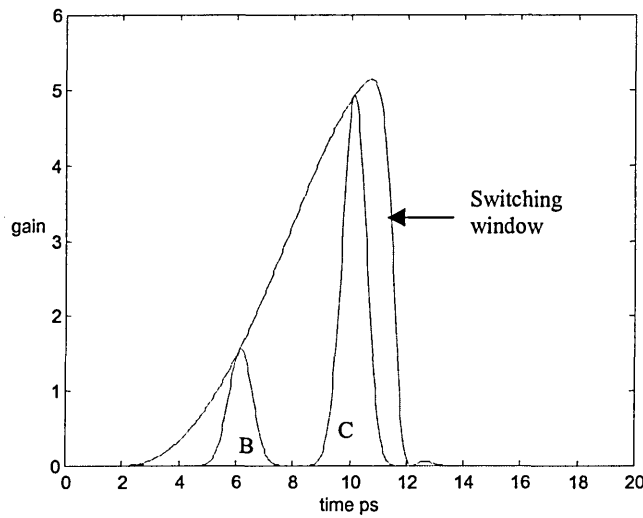
Figure 5.25 Output of TOAD 1 at port 1 (address recognise) for
OTDM packet with multi-bit address

Figure 5.26 shows payload at the output port 1 of the TOAD2. Also shown for information

is the switching window profile of TOAD2, which is wide 15 ps. Also shown in Figure5.26

(b) is the output port2 of the TOAD2. Ideally there should be no signal at all, however,

there is a small amount of crosstalk present. As one can see, there is also crosstalk from the

address bits. This is due to the non-ideal switching window profile (i.e. not a symmetrical

square shape). The crosstalk can be reduced by employing a switch with a truly square

switching window profile or by introducing a guard band between the address bit(s) and the

payload. The problem with the latter is the increase in the packet length.

101
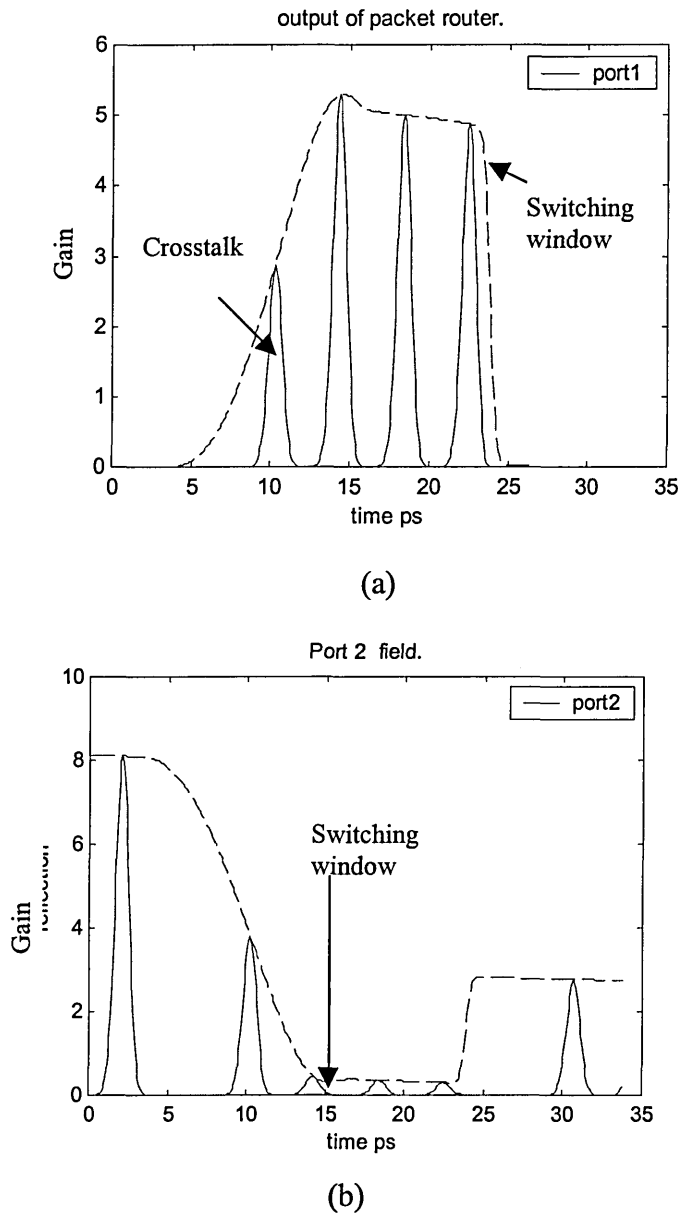
Figure 5.26 Outputs of the TOAD 2 at 250 Gbit/s data stream (a)output port 1 (b) output port 2

5.6 Summary

This chapter described the models developed to simulate the routing action of all optical router based on TOADs. For modeling purposes the TOAD was divided into three components: fibre coupler, fibre loop and non-linear element (SLA). The first functional component to be modeled is the input-output coupler. The fibre loop is assumed initially to

consist of a simple time delay until a later section when the polarization and birefringence effects are considered. Fundamental to loop operation is the asymmetry of the SLA and the effect of this has been considered. An equation to describe the special case of small asymmetry is developed in Section 5.4 and loop performance has been investigated by examining the switching resolution of the system and adjacent pulse crosstalk has been taken into account. The use of a high frequency control pulse has been modeled. The mathematical model of router has been developed for evaluating the switching window. The mathematical models are also used for optimization of the device parameters for maximizing peak transmittance of switching window. A new analytical expression was developed to calculate the width of all optical switching window. The all optical router model architecture using TOADs is based on a system, which has at its input an OTDM packet containing a header and a payload information. The router model simulated extraction of the header information from the data stream using a TOAD, which is subsequently used to make a routing decision. The payload information is routed through a second TOAD according to the information contained in the header.

Chapter 6

Noise and Crosstalk Analysis of All Optical Router Based on TOAD Using A Computer Model

6.1 Introduction

This chapter presents an analysis and subsequent simulations of the noise and crosstalk characteristics of an all optical router based on TOADs. The noise and crosstalk model used in this analysis was derived partly from the mathematical models reported in Refs. [111-116]. The input parameters of the noise and crosstalk model are obtained from the simulation results of the TOAD model described in Chapter 5. The chapter is organised as follows. The origins of the noise and crosstalk associated with an all-optical router are described in Section 6.2. The simulation results of the noise and crosstalk are presented and analysed in Section 6.3.

6.2 Noise and Crosstalk in All Optical Router Based on TOADs

The crosstalk and noise associated with an all optical router are the neighbour channel crosstalk NXT_{ROUTER}, residual crosstalk RXT_{ROUTER}, and relative intensity noise RIN_{ROUTER}. The theoretical analysis of these components are described in sections 6.2.1, 6.2.2 and 6.2.3, respectively.

6.2.1 Relative intensity noise

A major problem of an all-optical transmission system is the timing jitter introduced by optical transmitters, optical amplifiers, and pulse interaction within the TOADs [104]. An all optical routing system based on TOADs, suffers from such timing jitter, meaning the intended target channel (packet) does not always appear at the centre of the switching window (SW) as shown in Figure 6.1. The arrival time of the jittered signal can be described using a Gaussian distribution profile with a root-mean-square timing jitter RMS_{jitter}.
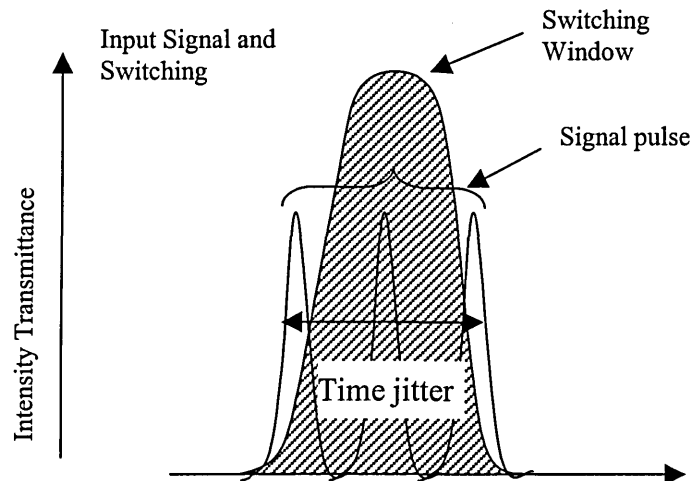
Figure 6.1 The transformation from timing jitter noise to relative intensity noise

The non-square shape of the SW also means the intensity profile of the routed signal will exhibit a variation in its intensity profile according to the temporal location of the target channel [117]. A significant feature of this is that the energy of the routed pulse is maximised when the target pulse is located at the centre of the switching window. As the

temporal position of the target pulses can be described using a Gaussian distribution, the timing jitter noise associated with the target pulses will manifest as a relative intensity noise through different positions within the switching window (see Figure 6.1). The intensity fluctuation of the routed pulses strongly depends on the shape of the switching profile. Chin Cheung [68] has employed soliton pulse as control signal of TOAD to obtain a relatively flat-top switching profile in order to reduce the TOAD intensity noise due to timing jitter.

The output signal power profile of the TOAD router can be described by:

$$w(t) = \int_{-\infty}^{\infty} T_x(t) p(t - \tau) dt , \qquad (6.1)$$

where $p(t)$ is the input data packet power profile, τ is the relative pulse arrival time, and $T_x(t)$ is the switching window profile of the router, which can be obtained by (5.28). The expected value of the output signal energy is then given as:

$$E[w(\tau)] = \int_{-\infty}^{\infty} w(t) p_t (t - \tau) dt . \qquad (6.2)$$

Where p_t is the probability density function of the relative signal pulse arrival time given by:

$$p_t(t) = \frac{1}{\sqrt{2\pi} t_{rms}} e^{-\frac{1}{2} \left(\frac{t}{t_{rms}} \right)^2} . \qquad (6.3)$$

The variance of the output signal energy, as a function of the relative arrival time, is given as:

$$Var[w(\tau)] = \int_{-\infty}^{\infty} w^2(t) p_t(t - \tau) dt - E^2[w(\tau)]. \tag{6.4}$$

Assuming that the mean arrival time of the target channel (packet) coincides with the centre of the TOAD switching window, then the relative intensity noise induced by timing jitter of the signal pulses can be expressed as:

$$RIN_{ROUTER}(\tau) = \frac{Var[w(\tau)]}{E^2[w(\tau)]} \tag{6.5}$$

The numerator on the right hand side of equation 6.5 represents the variance of the routed energy of the target pulses whilst the denominator represents the square of the mean routed energy of the target pulses.

6.2.2 The residual crosstalk
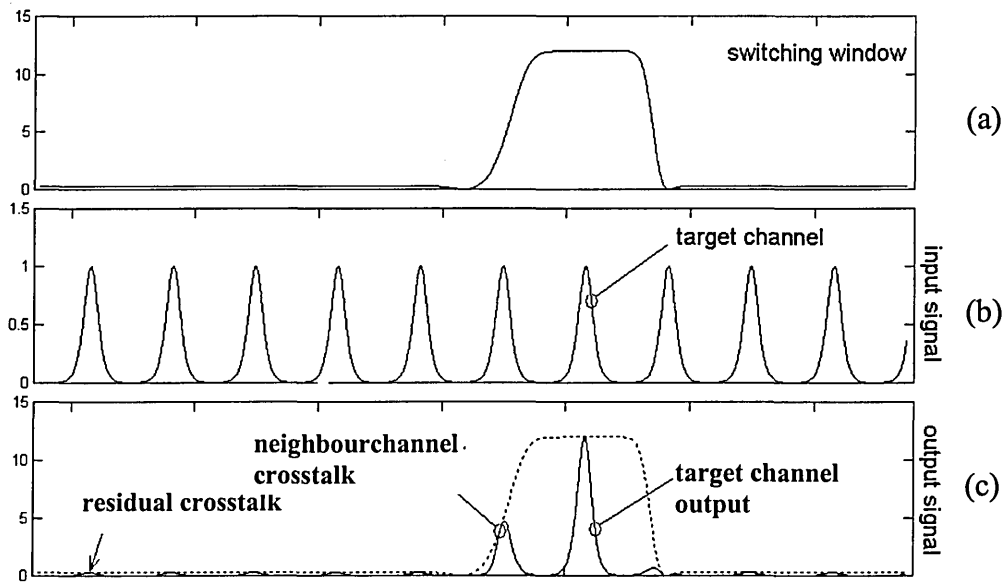
Figure 6.2 (a) the switching window, (b) the input data stream and (c) the recovered channel plus the residual and neighbour channel crosstalk

107

The residual crosstalk of the all-optical router occurs due to transmission of energy from non-target channels during the recovery period of the SLA in the TOAD as shown in Figure 6.2. Also shown in Figure 6.2 are the TOAD switching window, input data (channel) stream and the neighbour channel crosstalk. The latter will be discussed in Section 6.2.3. This phenomenon arise from the relative difference in the recovery times as experienced by the CW and CCW pulses outside the intended switching window of the TOAD. The result is a small difference between G_{cw} and G_{ccw}, and ϕ_{CW} ϕ_{CCW}, which give a small switching window according to (5.25) for non-target channels during the recovery period of the SLA in the TOAD. As this effect resides outside the switching window and can affect adjacent data pulses it is described as crosstalk. The description attributed here is residual crosstalk. The TOAD residual crosstalk is defined, as:

$$RXT_{ROUTER} = \frac{\sum_{r=2}^{M_{TDM}-1} \int_{(r-0.5)T_b}^{(r+0.5)T_b} T_x(t) \cdot S(t - r \cdot T_b) dt}{2 \cdot \int_{-T_b/2}^{T_b/2} T_x(t) \cdot S(t) dt}, \qquad (6.6)$$

where M_{TDM} is the total number of OTDM channels. The crosstalk due to the two channels adjacent to the target channel is excluded from the numerator as they are defined as neighbour channel crosstalk (see Equation 6.7), which will be discussed in Section 6.2.3. The factor 2 in the denominator assumes that the occurrence of a mark and a space is equivalent.

6.2.3 The neighbour channel crosstalk

Neighbour channel crosstalk NXT_{ROUTER} as shown in Figure 6.2 is caused by the routing of the adjacent non-target channels to the output port and is due to the switching window

extending beyond the time slot of the target channel. It can be represented mathematically as:

$$NXT_{ROUTERr} \; = \; \frac{\int_{-T_b/2}^{T_b/2} T_x(t) \cdot S(t+T_b)dt + \int_{-T_b/2}^{T_b/2} T_x(t) \cdot S(t-T_b)dt}{2 \cdot \int_{-T_b/2}^{T_b/2} T_x(t) \cdot S(t)dt}.$$

(6.7)

where T_b is the duration of an OTDM time slot. The expression of equation 6.7 assumes the signal pulse profile $S(t)$ is located at the centre of the FWHM router switching profile. If the TOAD window has double peaks (see Section 5.3.3.3), then $S(t)$ aligns with the peak with the highest gain. As in (6.6), the factor 2 in the denominator assumes that the occurrence of a mark and a space is equivalent.

6.3 Crosstalk and Noise Analysis

Simulation results obtained from the mathematical models presented in Chapter 5 and Section 6.2 are analysed in this section for determining the crosstalk and noise characteristics of an all optical router based on TOADs. The system parameters of the TOAD switching profile used in the crosstalk and noise analysis are optimised using (5.35) to maximise the peak transmittance of the switching window. The switching profile equation 5.28 of the TOAD model is used for evaluating the switching profile. The loss and nonlinearity of fibre loop used for the simulations in this section are ignored due to the short fibre loop of a few meters.

In this analysis, assuming the OTDM data signal power is less than the maximum power limitation discussed in Section 5.3.5 and with a optimised control pulse energy, a normalised signal pulse power profile rather than an actual power profile is used as the

noise and crosstalk values described in Section 6.2 are independent of the signal power. Analysis and simulation results for relative intensity noise, residual crosstalk, neighbour channel crosstalk and total crosstalk of the router are presented in Section 6.3.1, 6.3.2, 6.3.3 and 6.3.4, respectively. The ensuing trade off between the noise and crosstalk will be discussed in Section 6.3.5.

6.3.1 Simulation results of TOAD relative intensity noise

Optimised values of the control pulse energy for maximising the TOAD gain obtained from (5.35) are substituted into (5.28) for calculating TOAD switching profiles. The TOAD switching profiles are then substituted into (6.1) for calculating router relative intensity noise. The results are shown as follows. The parameters used for the simulations are listed in Table 6.1.

Figure 6.3 depicts the TOAD relative intensity noise versus the asymmetry (T_{asy}) for a signal FWHM of 1 ps, RMS_{jitter} = 1 ps and G_0 = 5. The dotted and solid lines represent L_{SLA}=0.3 mm and 0.1 mm, respectively. As can be seen from Figure 6.3, the router relative intensity noise decreases with an increase in the SLA asymmetry and reaches a maximum value of –3dB (-11 dB) when the SLA asymmetry is close to zero due to the double peak switching windows, as shown in Figure 5.7. The TOAD switching window exhibits a marked sensitivity to timing jitter of the signal pulses at small SLA asymmetries. The double peak windows will change to a signal peak window as the SLA asymmetry increases. Consequently in TOADs with a short length SLA, the relative intensity noise of the router is large at small SLA asymmetries and small at large SLA asymmetries. The curves of RIN_{ROUTER} shows a threshold T_{asy} (9 ps), beyond which the router relative

intensity noise attains a steady value (-25.33 dB) for an increase in T_{asy}. The relative intensity noise is insensitive to T_{asy} after the T_{asy} threshold. This is attributable to the widening of the switching window by with increasing T_{asy}.

Table 6.1 Simulation parameters used for evaluating the relative intensity noise

Parameters	Values
Linewidth enhancement factor α	4
Spontaneous lifetime τ_{sp}	100 ps
Confinement factor Γ	0.3
Gain coefficient a	3×10^{-20} m^{-2}
Transparent carrier density N_0	1×10^{24} m^{-3}
Cross section area of the amplifier A_{eff}	2×10^{-13} m^2
Phone energy E_p	0.8 eV
FWHM control pulse width T_{FWHM}	1 ps
Propagation speed inside the SLA	$(3 \times 10^8/3.5)$ m/s
Total number of segments	100

Figure 6.3 The relative intensity noise versus the SLA asymmetry for RMS$_{jitter}$ = 1 ps and different SLA lengths
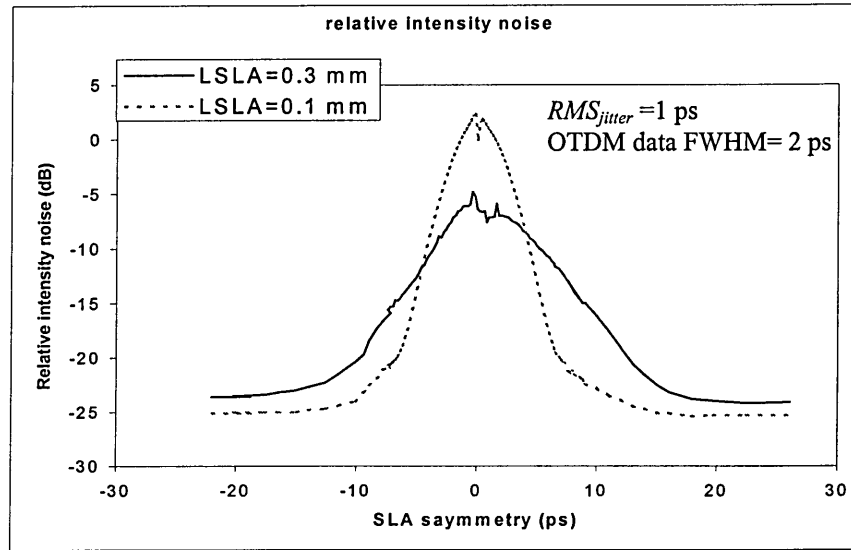
Figure 6.4 The relative intensity noise versus the SLA asymmetry for RMS$_{jitter}$ =
2 ps and different SLA lengths

Figure 6.4 is a plot of router relative intensity noise as a function of the SLA asymmetry

using the same parameters as Figure 6.3, with the exception that the RMS_{jitter} is 2 ps, which

is half bit duration and assumed as the maximum acceptable values of time jitter. As

indicated on intuitive grounds the relative intensity noise increases substantially due to the

severe timing jitter of the signal pulses. The intensity noise values in Figure 6.4 are larger

than those in Figure 6.3 due to the larger root-mean-square jitter of the signal pulses. The

threshold characteristics of T_{asy} can also be observed in Figure 6.4. By increasing RMS_{jitter}

the threshold T_{asy} is increased from 9 ps in Figure 6.3 to 15 ps in Figure 6.4. The value of

relative intensity noise beyond the threshold values is the same (i.e. -25.33 dB) for Figures

6.3 and 6.4. Therefore, when the TOAD is used for wide switching window (the width of

the switching window > 30 ps, i.e. two times threshold value of the T_{asy}), the relative

intensity noise is as low as to –25.33 dB and has very little effect on switching action

compared to the corsstalk of the TOAD.

In high capacity OTDM systems, it is important to investigate how the duty cycle of optical pulses affects the noise performance of all-optical router. Decreasing the duty cycle of the OTDM signal can result in an improved bit-error-rate. This is due to the smaller neighbour channel crosstalk present with narrower signal pulses. To evaluate the effect of the signal pulse width on relative intensity noise, simulations were performed using the same parameters as used to generate the plots of Figure 6.3. The exception was that the FWHM signal pulse width used was 2 ps. Figure 6.5 depicts the result of these simulations with plots of RIN_{ROUTER} versus T_{asy}. The profiles shown in Figure 6.5 are similar to those in Figure 6.3 except for a slight increase in threshold of T_{asy} up to about 16 ps for a FWHM signal pulse width of 2 ps. Therefore, the duty cycle has little effect on the width of switching window with low relative intensity noise. The value of relative intensity noise is smaller for a signal width = 2 ps as compared with a width of 1 ps, see Figures 6.3 and 6.5. The reason for this is signal with large duty cycle has less energy density, and then has less effect on the relative intensity noise of the TOAD. The influence of signal width is more pronounced at small SLA asymmetries. The overall noise characteristics for various SLA lengths in Figure 6.5 are similar to those of Figure 6.3.
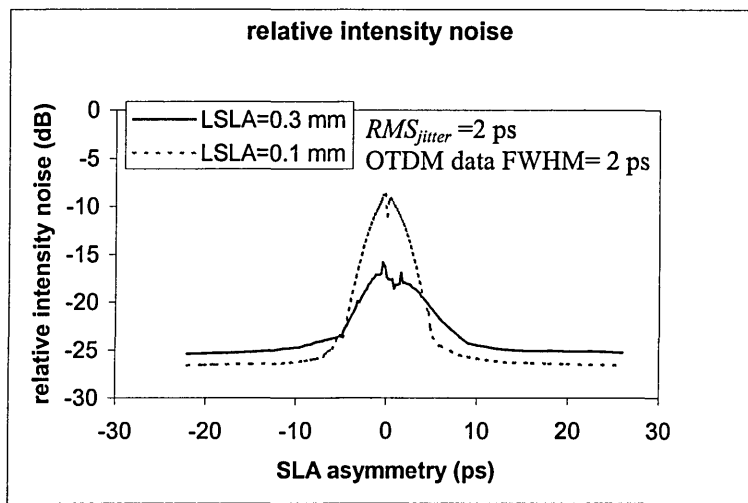
Figure 6.5 The relative intensity noise versus the SLA asymmetry for
signal width of 2 ps and different SLA length

Figure 6.6 shows a plot of the router relative intensity noise against the SLA asymmetry using the same parameters as Figure 6.3 with the exception that G_o =10. There is little difference between the simulation results of Figures 6.3 and 6.6. Similar comparisons made of simulation results using various combinations of parameters (not illustrated here) have shown that the router relative intensity noise is relatively independent of the initial gain of the SLA.

Relative intensity noise in router
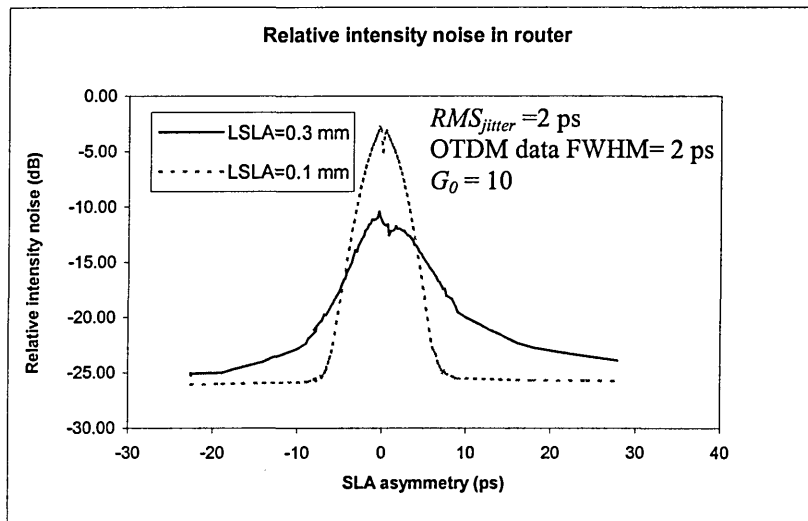
Figure 6.6 The relative intensity noise versus the SLA asymmetry for G_0 =10 and different SLA length

6.3.2 Simulation results for the residual crosstalk

Using equation 6.6 and the data obtained from the TOAD model, the residual crosstalk is simulated. Table 6.2 lists the basic parameters used in the simulation. Additional parameters are specified for individual simulations where appropriate.

114

Table. 6.2 Simulation parameters used for evaluating the residual crosstalk

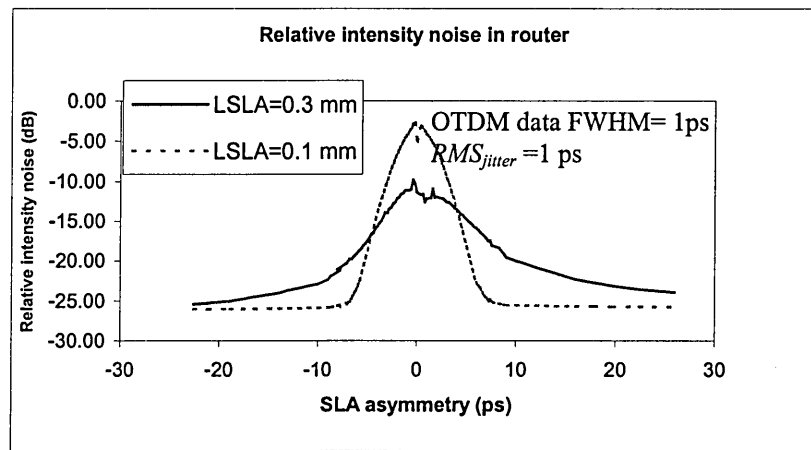| Parameters	Values
Linewidth enhancement factor α_{LEF}	4
Spontaneous lifetime τ_{sp}	100 ps
Confinement factor Γ	0.3
Gain coefficient a	$3 \times 10^{-20} \, m^{-2}$
Transparent carrier density N_0	$1 \times 10^{24} \, m^{-3}$
Cross section area of the amplifier A_{eff}	$2 \times 10^{-13} \, m^2$
Phone energy E_p	0.8 eV
FWHM control pulse width T_{FWHM}	1 ps
Propagation speed inside the SLA	$(3 \times 10^8/3.5) \, m/s$
Total number of segments	100
FWHM signal pulse width	1 ps
RMS_{jitter}	1 ps
G_0	5

Figure 6.7 depicts plots of the router residual crosstalk against the SLA asymmetry using a total bit rate of 100 Gb/s. Other relevant parameters used are $M_{TDM} = 10$, $G_0 = 5$, $L_{SLA} = 0.5$ mm, 0.1mm, and duty cycle = 0.1. The solid and dotted lines represent an SLA length of 0.5mm and 0.1mm, respectively. The curves in the figure illustrate that the residual crosstalks for different SLA length have similar characteristics, having a minimum values when the SLA asymmetry is close to zero and increasing with SLA asymmetry. Choosing different SLA lengths has little influence on the router residual crosstalk.
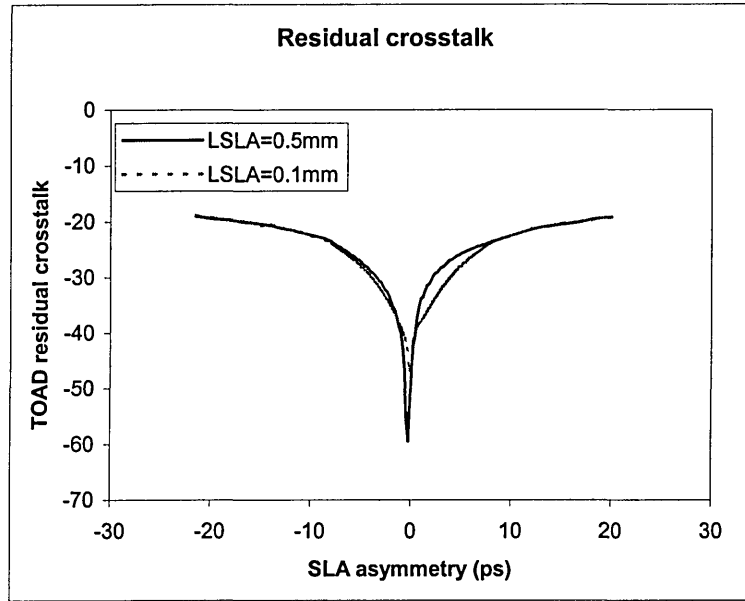
Figure 6.7 The router residual crosstalk versus the SLA asymmetry for total
bit rate of 100 Gb/s for SLA length of 0.1 and 0.5 mm

Figure 6.8 shows simulation plots for the residual crosstalk as a function of the SLA

asymmetry using the same simulation parameters as those in Figure 6.7 except for $M_{TDM} =$

20. The solid and dashed lines represent $L_{SLA} = 0.5$ mm and 0.1 mm respectively. The effect

of SLA length on the residual crosstalk is shown to be insignificant when used in 200 Gb/s

routing. Simulations using other combinations of parameters (not shown here) led to the

same conclusion.
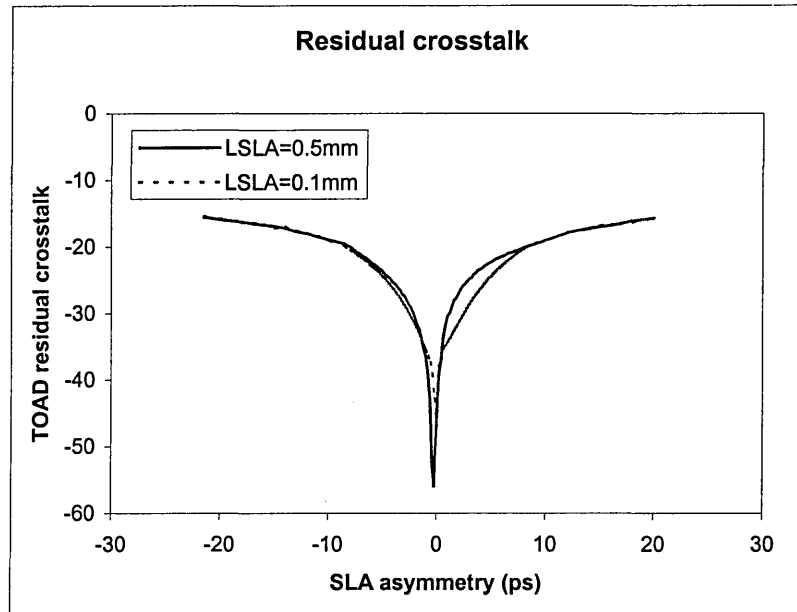
Figure 6.8 The router residual crosstalk versus the SLA asymmetry for
total bit rate of 200 Gb/s for SLA length of 0.1 and 0.5 mm

Summarising, the router residual crosstalk is relatively independent of the SLA length over

all data rates.

In order to assess the effect of changing the amplifier initial gain (G_o) on the residual

crosstalk performance, simulations were performed and the results for the residual crosstalk

for different values of G_o are shown in Figure 6.9. The simulation parameters used were

$L_{SLA} = 0.3$ mm, total bit rate = 200 Gb/s, $M_{TDM} = 10$, and duty cycle = 0.1. The square

dotted, dashed and solid lines represent $G_o = 10$, 7.5 and 5, respectively. The residual

crosstalk in Figure 6.9 shows similar characteristics for various G_o. Thus changing the

amplifier initial gain has little effect on the RXT_{ROUTER}.
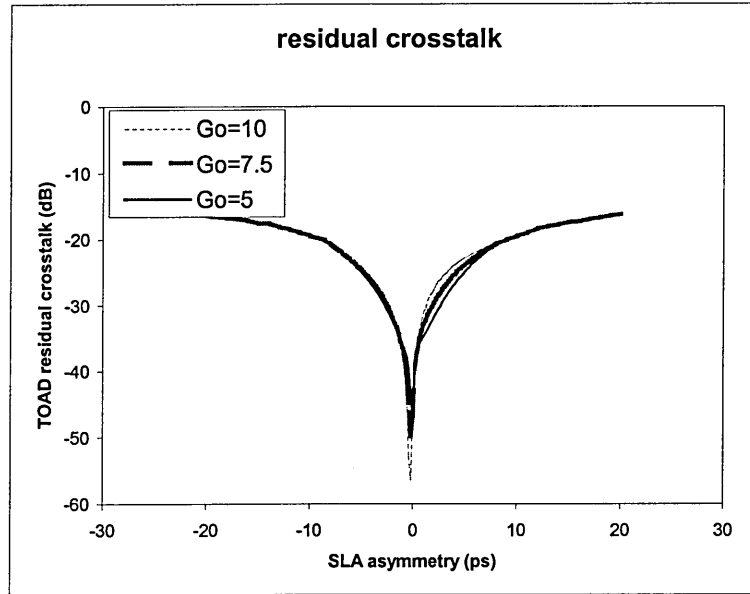
Figure 6.9 The router residual crosstalk versus the SLA asymmetry for
different values of the amplifier initial gain

Figure 6.10 plots results of the residual crosstalk for OTDM channels of 30 and 300 at 300

Gb/s routing in order to evaluate the effect of M_{TDM} on the residual crosstalk performance.

The solid and dashed lines represent M_{TDM} = 300 and 30 respectively. Other simulation

parameters are G_o = 5, L_{SLA} = 0.3 mm, and duty cycle = 0.1.
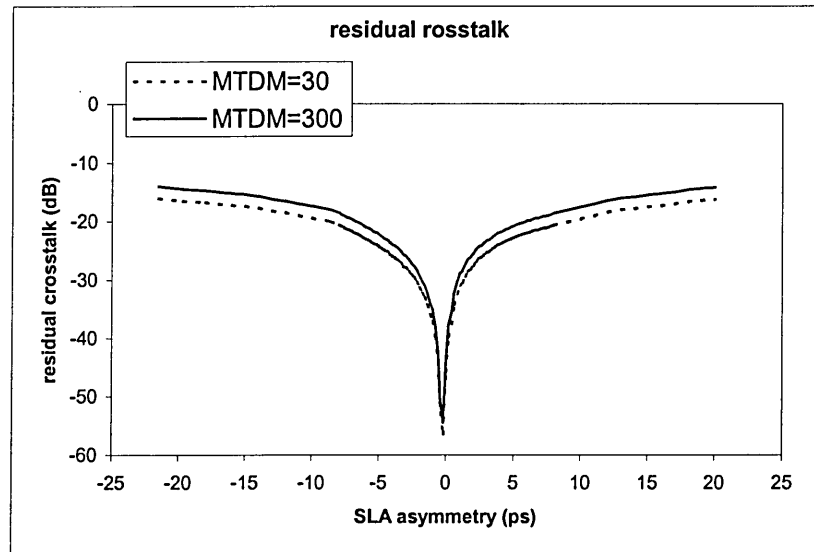
Figure 6.10 The router residual crosstalk versus the SLA asymmetry
for different values of M_{TDM}

As depicted in Figure 6.10, a substantial increase of the number of OTDM channels from 30 to 300 results in only a slight increase of the residual crosstalk. According to the spontaneous life time τ_{sp} in Table 6.2, the saturated G_{CW} and G_{CCW} will recover back to G_o in around 100 ps. After recovering back to G_o, G_{CW} and G_{CCW} will remain at the same value until the next control pulse arrives and saturates the SLA again. At a total bit rate = 300 Gb/s, the OTDM frame periods are 100 ps and 1000 ps respectively for M_{TDM} = 30 and 300. Although the number of non-target channels, described by the parameter M_{TDM} = 300, is 290 more than that of M_{TDM} = 30, the non-target channels outside the first 100 ps of the OTDM time frame contribute little to the residual crosstalk.
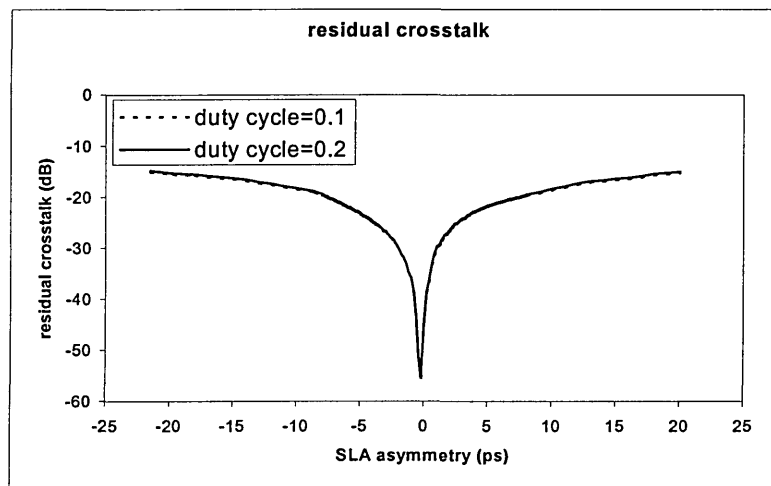
Figure 6.11 The router residual crosstalk versus the SLA asymmetry for
different values of duty cycles

Figure 6.11 shows a plot of residual crosstalk for different values of duty cycle to illustrate the effect of changing the duty cycle on the crosstalk performance. The dotted and solid lines represent a duty cycle of 0.1 and 0.2 respectively. The simulation parameters used here are G_o = 5, total bit rate = 200 Gb/s, M_{TDM} = 20, and L_{SLA} = 0.3 mm. Figure 6.11

indicates that the residual crossstalk is largely independent of the duty cycle. Simulations using other combinations of parameters (not shown here) confirm this.

6.3.3 Simulation results for the neighbour channel crosstalk

Device parameters optimised from equation 5.34 for maximising peak transmittance are substituted into equation 6.7 to calculate the neighbour channel crosstalk. The simulation results are shown and subsequently analysed in this section.
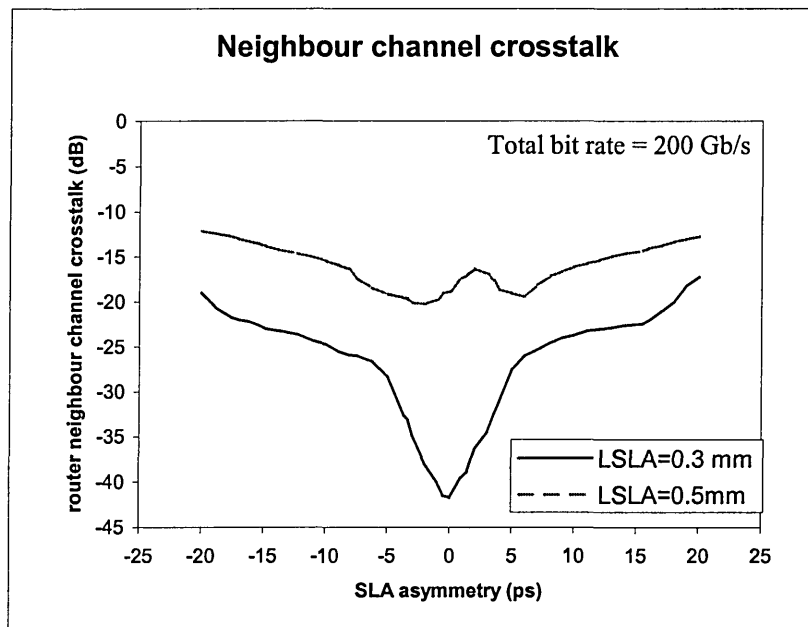
Figure 6.12 The router neighbour channel crosstalk versus the SLA
asymmetry for different length of SLA

Figure 6.12 shows the neighbour channel crosstalk characterises for different SLA lengths using the same simulation parameters as in Figure 6.8. The solid and dotted lines represent SLA lengths of 0.3mm and 0.5mm, respectively. The large vertical separation between the two lines shows that the neighbour channel crosstalk is strongly dependent on the SLA

length. In order to minimise the overall crosstalk in 200 Gb/s routing, a small SLA length should be used for keeping the neighbour channel crosstalk small. However there is a trade-off for the SLA length considering the neighbour channel crosstalk and the relative intensity noise, which will be discussed in Section 6.3.5. The overall crosstalk can be minimised by making the residual crosstalk a dominant one.

The dependence of the neighbour channel crosstalk on the duty cycle of the incoming OTDM data stream (duty cycle in this thesis is defined as the ratio between the FWHM width of the data pulses and the OTDM time slot.) is investigated next. The profiles of two adjacent signal pulses will overlap with each other if duty cycle is greater than 30%. The values of duty cycle used for the computer simulations are 20 and 30%.
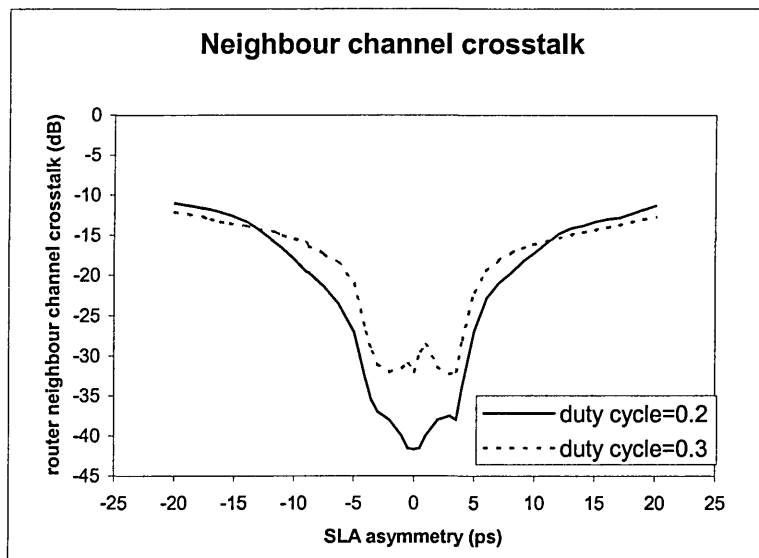
Figure 6.13 The router neighbour channel crosstalk versus the SLA
asymmetry for different values of duty cycles

Figures 6.13 shows the simulation results using the same parameters as in Figure 6.12 with the exception that the duty cycle are 20% and 30%, respectively, and L_{SLA} is 0.2 mm. Note 30% duty cycle corresponds to a FWHM of 3 ps. Comparing plots in Figure 6.13, it can be seen that increasing duty cycle will increase the neighbour channel crosstalk. More energy of adjacent non-target signal pulses will be routed because of the wider pulse width present with larger duty cycles. Comparing the dotted and solid lines in Figure 6.13, for L_{SLA} of 0.2 mm and T_{asy} = 4 ps, the difference in crosstalk for two duty cycles is 5 dB.

Figure 6.14 shows the simulations results for aggregate bit rates of 100 Gb/s, 200 Gb/s and 300 Gb/s, respectively, with duty cycle = 0.3 and other simulation parameters being the same as those used to obtain Figure 6.13. As can be seen from Figure 6.14, neighbour channel crosstalk increases with the bit rate of the incoming signal. Comparing the curves in the figure, the router neighbour channel crosstalk at a bit rate of 300 Gb/s is much higher than that for a bit rate of 100 Gb/s. 300 Gb/s routing shows that the neighbour channel crosstalk for large SLA asymmetry tends to saturate at 0 dB, which represents the same routed energy for both target and non-target pulses.
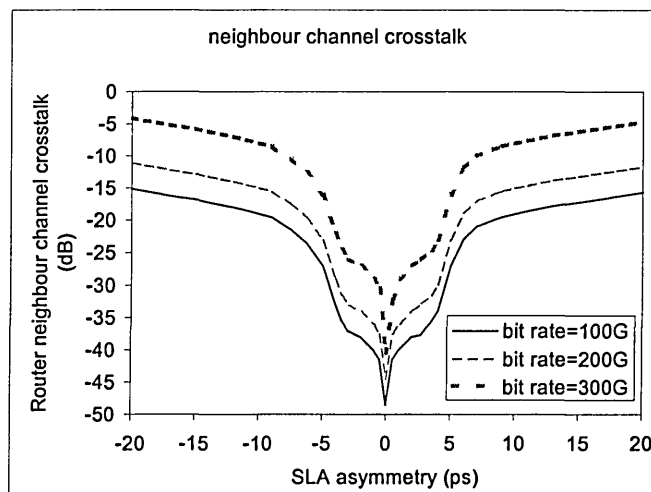
Figure 6.14 The router neighbour channel crosstalk versus the SLA asymmetry for different bit rates

Figure 6.15 shows the effect of amplifier initial gain G_o on the neighbour channel crosstalk performance. The simulation parameters used are L_{SLA} = 0.2 mm, total bit rate = 100 Gb/s, M_{TDM} = 10, and duty cycle = 10%. The solid, dashed and square dotted lines represent G_o = 5, 7.5 and 10, respectively. As shown in Figure 6.15, the neighbour channel crosstalk has similar characteristics for various values of G_o, the amplifier initial gain has very little effect on the router neighbour channel crosstalk.
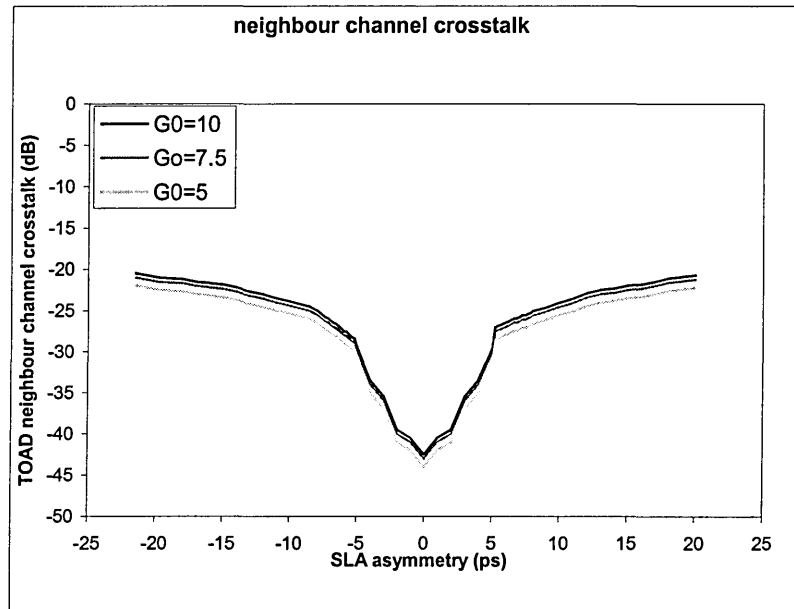
Figure 6.15 The router neighbour channel crosstalk versus the SLA

asymmetry for different values of the amplifier initial gain G_0

6.3.4 Simulation results of router crosstalk

Figure 6.16 depicts plots of the residual and neighbour channel crosstalks against the SLA asymmetry at 100 Gb/s data rate. The simulation parameters are L_{SLA} = 0.1 mm, G_o = 5,

M_{TDM} = 10, and duty cycle = 10%. The solid and dashed lines represent RXT_{ROUTER} and NXT_{ROUTER} respectively. Figure 6.16 shows that both types of crosstalk display a minimum when the SLA asymmetry is close to zero and increase with the SLA asymmetry. As mentioned earlier in this chapter, the width of a switching window is adjusted by the SLA asymmetry. The routing of non-target pulses from neighbour channels will not occur unless the SLA asymmetry induced window width is comparable to or larger than the time slot of an OTDM channel, which is 10 ps in the case of 100 Gb/s routing. Since the range of SLA asymmetry in Figure 6.16 is not wide enough for the switching window to route neighbour channels, the overwhelming contribution to the neighbour channel crosstalk is the residual gain difference between the CW and CCW pulses within the time slots of the neighbour channels. Residual and neighbour channel crosstalks display similar characteristics for 100 Gb/s routing as they are from the same origin. Residual crosstalk is generally larger than neighbour channel crosstalk because residual crosstalk accounts for more non-target channels. Router crosstalk at 100 Gb/s routing can be minimised by setting the SLA asymmetry close to zero, as shown in Figure 6.16.
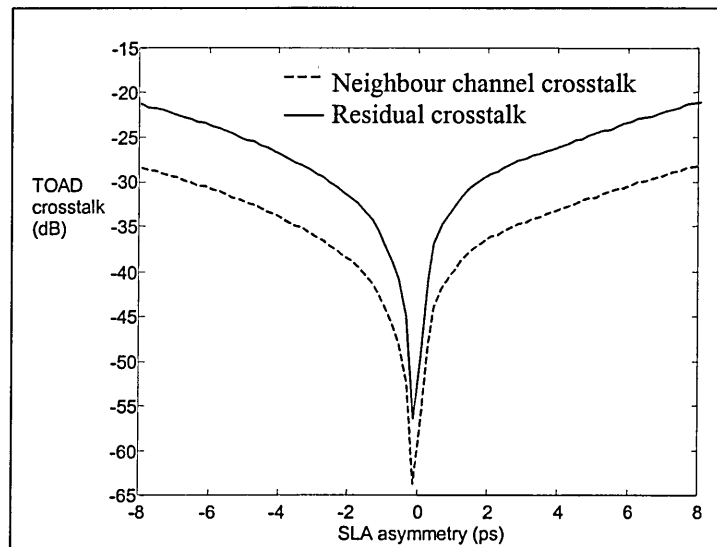
Figure 6.16 The router neighbour channel and residual crosstalks versus
the SLA asymmetry

124

Summarising, it can be concluded that the router crosstalk is fairly independent of the SLA length for medium data rate (100 Gb/s). For high data rate (> 200 Gb/s), shorter SLA length could be used to minimise the overall crosstalk. As one example, to illustrate this point, let's consider the total crosstalk (RXT_{ROUTER} + NXT_{ROUTER}) for a data rate of 100 Gb/s, 200 Gb/s and 300 Gb/s, respectively. Results for these rates are plotted in Figures 6.17, 6.18 and 6.19. The dash and solid lines represent L_{SLA} = 0.5 mm and 0.1 mm respectively. The value of M_{TDM} used in Figures 6.17-6.19 is 10, 20 and 30, respectively. Other simulation parameters are the same as the previous crosstalk simulations.
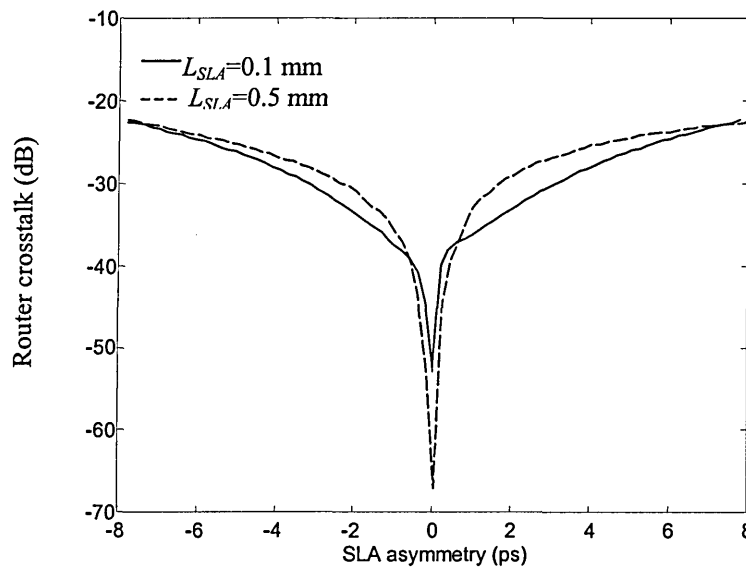
Figure 6.17 The router crosstalk versus the SLA asymmetry for different

SLA length with total bit rate of 100 Gb/s.

Figure 6.17 demonstrates no significant difference for the crosstalk performance for different SLA lengths for 100 Gb/s routing. Figures 6.18 and 6.19 show that a decrease in the SLA length from 0.5 mm to 0.1 mm can greatly reduce the router crosstalk for data

rates > 100 Gb/s. For data rates of 300 Gb/s, the total crosstalk for L_{SLA} of 0.1 mm rises to overtake the total crosstalk for L_{SLA} of 0.5 mm with large SLA asymmetry. This is a result of excess neighbour channel crosstalk induced by the wide switching window and narrow time slot.
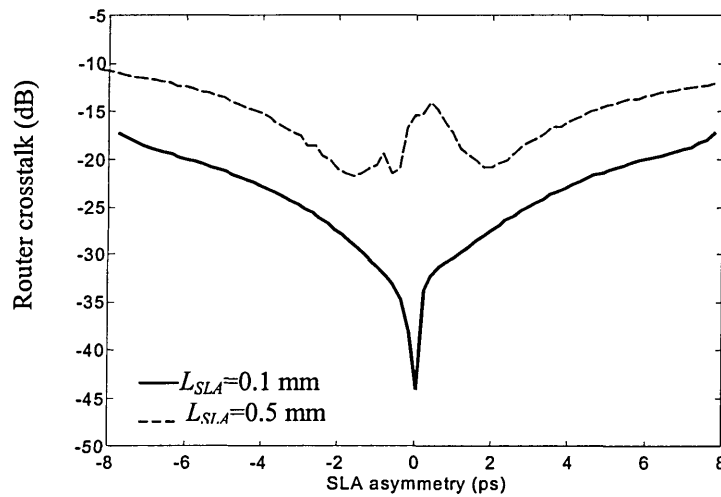
Figure 6.18 The router crosstalk versus the SLA asymmetry for different SLA length with total bit rate of 200 Gb/s
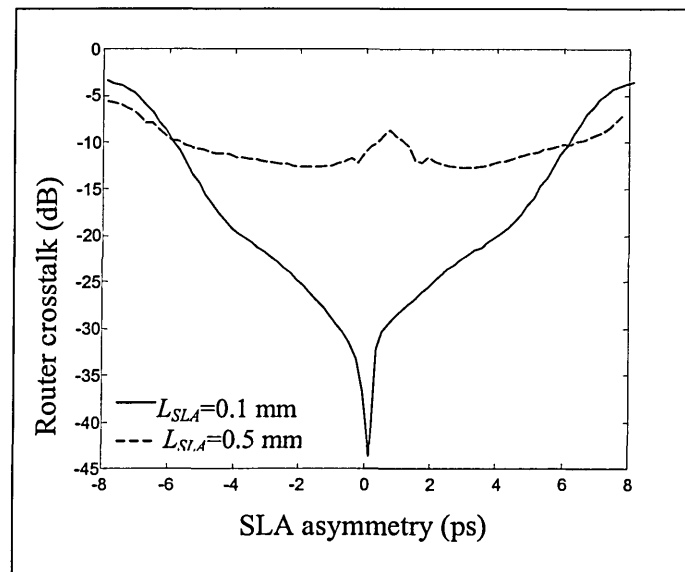
Figure 6.19 The router crosstalk versus the SLA asymmetry for different SLA length with total bit rate of 300 Gb/s.

6.3.5 Trade off between the relative intensity noise and the crosstalk

A trade off between the noise and the crosstalk in TOAD routing is evident for different forms at various bit rate levels. The two TOAD parameters that have a pronounced influence on the noise and crosstalk performance are L_{SLA} and T_{asy}. A compromise of noise and crosstalk can be illustrated from computer simulations with different values of L_{SLA} and T_{asy}.
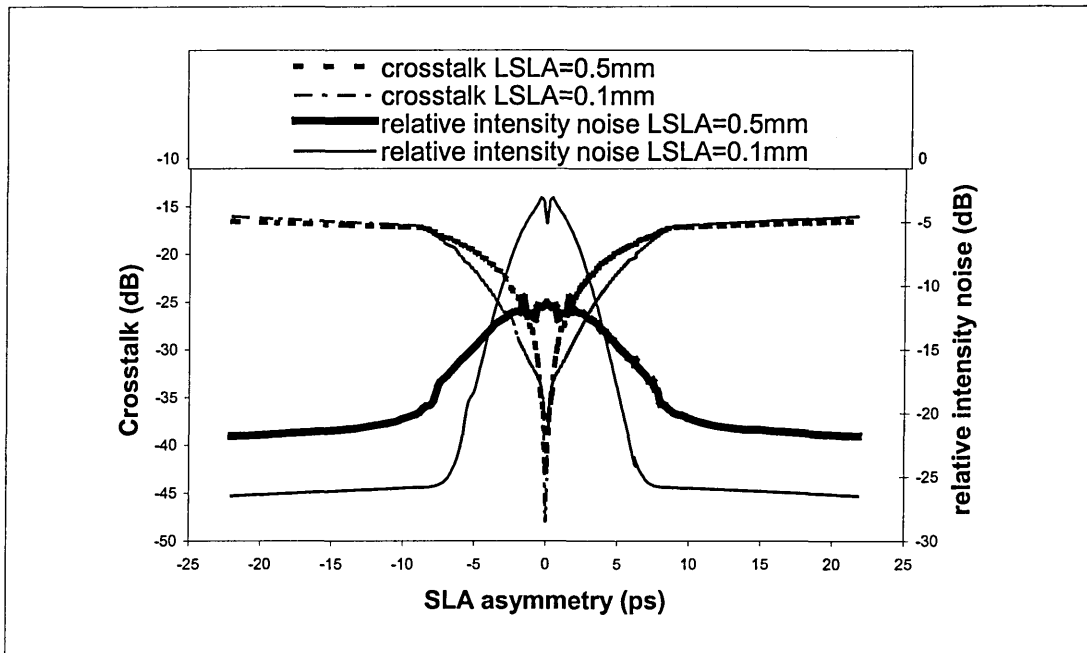
Figure 6.20 Trade off between the noise and the crosstalk of the router for
total bit rate of 100 Gb/s

Figures 6.20 and 6.21 are plots of router relative intensity noise and router crosstalk as a function of the SLA asymmetry for data rate of 100 Gb/s and 200 Gb/s routing, respectively. The bit rate of individual OTDM channels is 10 Gb/s, which makes the value of M_{TDM} equal to 10 for Figure 6.20 and 20 for Figure 6.21. The other parameters are $G_o = 5$, and duty cycle = 0.1. The solid and dashed lines represent RIN_{ROUTER} and router crosstalk

respectively. The bold and thin lines represent L_{SLA} = 0.5 mm and 0.1 mm respectively. The router crosstalk is calculated from $RXT_{ROUTER} + NXT_{ROUTER}$.

The dashed lines in Figure 6.20 show little dependence of the router crosstalk on the length of SLA (L_{SLA}) in 100 Gb/s routing. L_{SLA} has little effect on the crosstalk performance. However relative intensity noise (RIN) is strongly dependent on L_{SLA}, as shown by the solid lines in Figure 6.20. Hence, to minimise the overall effect of crosstalk and noise, the value of L_{SLA} chosen is solely dependent on the relative intensity noise in 100 Gb/s routing. Figure 6.20 shows that the relative intensity noise at L_{SLA} of 0.1 mm is larger for smaller SLA asymmetry and is smaller for larger SLA asymmetry. Large L_{SLA} should be used for small SLA asymmetry and small L_{SLA} should be used for large SLA asymmetry. In order to obtain the optimal SLA asymmetry, other noise contributions from the optical receiver have to be considered for minimising the power penalty of the router. The power penalty calculations of routing will be presented in Chapter 7.
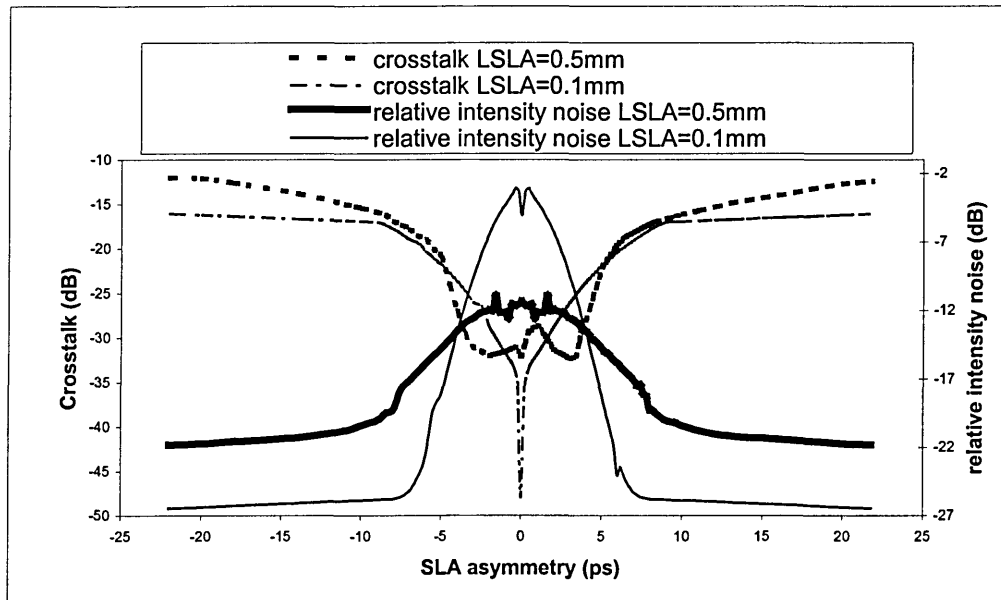
Figure 6.21 Trade off between the noise and the crosstalk of the router for total bit rate of 200 Gb/s

The dependence of noise and crosstalk on L_{SLA} is more complex for 200 Gb/s routing. Router crosstalk in 200 Gb/s routing increases with the SLA length, as shown by the dashed lines in Figure 6.21. The relative intensity noise characteristics displayed in Figure 6.21 are similar to those in Figure 6.20. Relative intensity noise at smaller L_{SLA} is larger for smaller SLA asymmetry and is smaller for larger SLA asymmetry. For small SLA asymmetry, increasing the value of L_{SLA} will decrease relative intensity noise but increase crosstalk. For large SLA asymmetry, increasing the value of L_{SLA} will increase both the crosstalk and relative intensity noise of router, as shown in Figure 6.21. Therefore, in 200 Gb/s routing, small SLA length should be used in large SLA asymmetry. As for the small SLA asymmetry, the SLA length could be optimised in terms of power penalty.

6.4 Summary

In Chapter 6 equations for evaluating crosstalks of all optical router have been developed, which was used to analyse the relative intensity noise, residual crosstalk and neighbour channel crosstalk characteristics of the router. The noise and crosstalk analyses of router were discussed. It was found that both noise and crosstalk are largely independent of the initial gain of the asymmetrically located SLA. Apart from that, the dependences of the noise and crosstalk on the other system parameters display complex characteristics. A trade off between noise and crosstalk in TOAD routing is evident for different forms at various bit rate levels. The two TOAD parameters that have a pronounced influence on the noise and crosstalk performance are L_{SLA} and T_{asy}. A compromise of noise and crosstalk has been illustrated from computer simulations with different values of L_{SLA} and T_{asy}.

Chapter 7

Bit Error Rate Performance of All Optical Router

7.1 Introduction

In OTDM based network employing all optical routers, system BER performance is limited by a number of additional noise sources due to routers. Many researchers [120-126] have investigated theoretically the bit error rate (BER) performance of OTDM systems. In these studies it is shown that the two factors, channel crosstalk, and relative timing jitter associated with the non-linear switching element play a major role in determining the overall system performance. Jepson et al. [117] have shown practically that the interferometic noise is a major problem, which would degrade the BER performance, when pulses before multiplexing have a poor tail extinction ratio. All the analyses reported so far describe a system which is composed of an OTDM demultiplexer, optical pre-amplifier and optical receiver. However, no work has been reported that take into account the presence of an all-optical router within a system. Therefore, to fully evaluate the OTDM system performance, a number of noise sources such as bit pattern noise of router due to crosstalk, the intensity noise of router due to timing jitter between the control and signal pulses, interferometic noise and other noise sources are required to be taken into consideration. The

purpose of this chapter is to investigate the characteristics of these noise sources at speeds exceeding 100Gb/s, and to develop an expression for the overall system BER.

The chapter organised as follows. The system model of the receiver and signal to noise ratio (SNR) analysis is presented in Section 7.2. Two sources that degrade the SNR of routed signals are also considered. (i) the channel crosstalk originating from the leakage of non-target channels and (ii) the relative intensity noise induced by the timing jitter in the router. In Sections 7.3, the impact of crosstalk on BER performance is investigated. Calculations based on the real switching window shapes enable estimation of the timing tolerance width for combining control and signal pulses at the input of the router. Also studied is the power penalty, which is defined as the difference between the minimum average received optical power levels at BER of 10^{-9} of the signal at the output of the transmitter and the router. Section 7.4 predicts BER power penalties from BER simulation results based on the proposed optical receiver model. Finally, in Section 7.5, the concluding remarks are presented.

7.2 Theoretical Analysis

7.2.1 System model (receiver model)

Figure 7.1 shows a typical block diagram of an OTDM system employing OTDM transmitter, an all-optical router, optical demultiplexer, an optical pre-amplifier (EDFA), an optical band-pass filter (BPF) and a conventional optical receiver. The 1x2 all-optical router is based on TOADs as described in Chapter 5. The incoming OTDM packet signal,

composed of header and payload, is input to the all-optical router. The bit rate of OTDM signal is $R_B = M_{TDM}R_b$, where M_{TDM} and R_b are the time division multiplication factor and the base data rate, respectively. The energy of the incoming OTDM packet stream needs to be kept sufficiently low (< 0.4 pJ) in order to avoid nonlinear effects associated with SLAs within the router as discussed in Section 5.3.5. At the router, an optical control pulse, extracted from the incoming OTDM signal, is used for selecting the target packet from the incoming OTDM signal. The packet output of the router is passed through an optical demultiplexer in order to recover a channel within a packet. The output of the demultiplexer is amplified, using EDFA, and then passed through a narrow band optical band-pass filter before being input to the receiver. The narrow band optical filter reduces the spontaneous-spontaneous noise generated by the optical amplifier. Finally, conventional optical receiver, consists of a PIN photodiode, electrical amplifier and a decision circuit, is used to recover the original data. It is assumed that the input to the electrical amplifier is terminated with a standard 50 Ω load resister (a low impedance front-end design). This straightforward approach has the advantage of high bandwidth, but at the expense of high thermal noise.
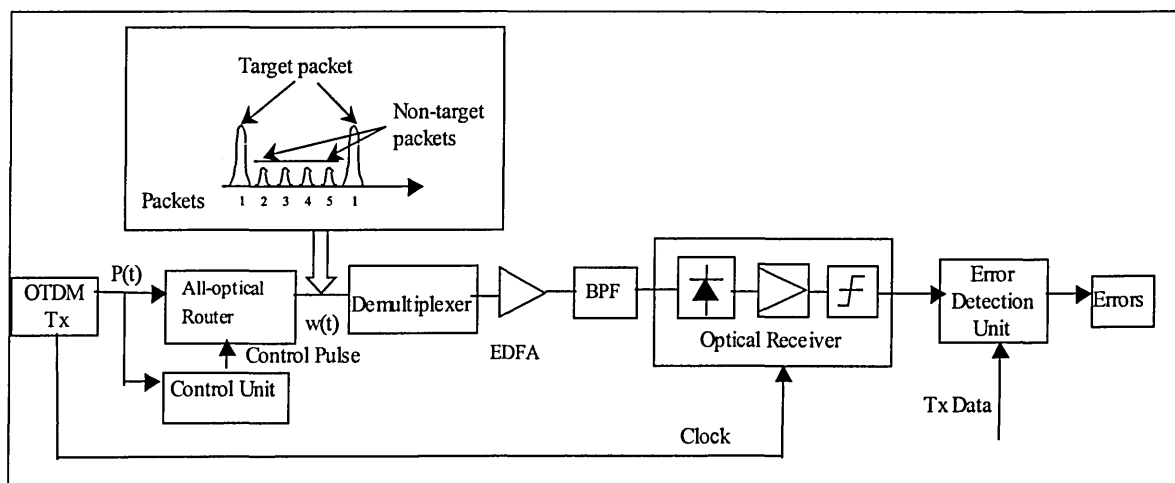
Figure 7.1 Block diagram of an OTDM system

132

7.2.2 Noise analysis

As in any communication systems, the system performance is affected by the noise signals. In the model there are a number of noise sources. They are:

(i) Timing jitter induced relative intensity noise associated with the incoming OTDM signal.

(ii) Timing jitter induced relative intensity noise, spontaneous emitted power and bit pattern noise within the router.

(iii) Timing jitter induced relative intensity noise, spontaneous emitted power and bit pattern noise within the demultiplexer.

(iv) EDFA preamplifier noise.

(v) Thermal noise, shot noise and amplifier noise within the receiver [96,98].

The detailed analyses of all noise sources are presented in the following subsections.

7.2.2.1 router relative intensity noise

One of the major problems in high-speed transmission system is the timing jitter introduced by transmitter, optical amplifier, and pulse interaction within routers. In OTDM system employing TOAD or nonlinear optical loop mirror for routing and demultiplexing, because of timing jitter, the intended target channel (packet) does not always appear at the centre of the switching window. The arrival time of the jittered signal displays Gaussian distribution profile. Because of the non-square shape of the switching window, the intensity profile of the routed signal will vary according to the temporal location of the target channel [71].

133

The details of the router relative intensity noise analysis have been given in Chapter 6. The relative intensity noise induced by the timing jitter of the routed signal can be defined as (6.5).

7.2.2.2 router pattern noise due to crosstalk

The total crosstalk $XT_{T,R}$ observable at the output of the router is composed of two components, channel crosstalk and residue crosstalk. The origin of the channel crosstalk is specified as an induced phase-shift on signals counter-propagating to control pulses within the router (see Chapter 5). The total energy of the signals due to non-target channel (packet) appearing within and outside the switching window at the output of the router can be expressed as:

$$W_{XT_{T,R}}[i,j] = \int_{\pm\left(i+\frac{1}{2}\right)T_D}^{\pm\left(i+\frac{3}{2}\right)T_D} T_x(t)p(t+T_D+iT_D)dt \Leftrightarrow i = 0,1,2,....k, \text{ and } j = 0 \text{ or } 1, \qquad (7.1)$$

where T_D is the packet duration. The first index i is an arbitrary packet number and the second index j corresponds to mark ($j = 1$) and space ($j = 0$). Here timing jitter is neglected, which will be considered in the next subsection. The expected value of the total crosstalk can be expressed as:

$$E[XT_{T,R}] = \sum_{i=0}^{M-2}\left\{\sum_{j=0}^{1}W_{XT_{T,R}}[i,j]f_j(j)\right\}, \qquad (7.2)$$

where M is the number of the packets, and $f_j(j)$ is the discrete probability density function. $f_j(j) = 0.5$ for both $j = 0$ and $j=1$, assuming equally likely bit one and bit zero for NRZ signal. The variance of the crosstalk, referred to as bit pattern noise because of the randomness of the information on the data signal, is expressed as:

$$Var[XT_{T,R}] = \sum_{i=0}^{M-2} \left\{ \sum_{j=0}^{1} W_{XT_{T,R}}^2[i,j] f_j(j) - \left(\sum_{j=0}^{1} W_{XT_{T,R}}[i,j] f_j(j) \right)^2 \right\} \qquad (7.3)$$

7.2.2.3 demultiplexer relative intensity noise

The noises associated with the demultiplexer are relative intensity noise and pattern noise. Both have the same origins as their counterparts in router [68]. More detailed work on the noise analysis of demultiplexer based TOAD can be found in [117]. Following the similar approach as in [117] the relative intensity noise of the demultiplexer RIN_{DEMU} is given as:

$$RIN_{DEMU} = \frac{\int_{-\infty}^{\infty} w^2(t) \cdot P_t(t) dt - \left[\int_{-\infty}^{\infty} w(t) \cdot P_t(t) dt \right]^2}{\left[\int_{-\infty}^{\infty} w(t) \cdot P_t(t) dt \right]^2}, \qquad (7.4)$$

where $w(t)$ is expressed as

$$w(t) = \int_{-\infty}^{\infty} T_x(t')_{TOAD} \cdot S(t'-t) dt', \qquad (7.5)$$

In (7.4) and (7.5), $T_x(t')_{TOAD}$ is the switching window of TOAD, $P_t(t)$ is the probability distribution of the arrival time of signal pulse versus demultiplexing switching profile, which has a Gaussian distribution with a root-mean-square timing jitters RMS_{jitter}. $S(t')$ is the normalised power profile of the target channel. The target channel may be located in

135

one of two positions. For switching window with single peak, $S(t')$ is located at the central point of FWHM TOAD switching profile. In the case of TOAD window having double peaks, $S(t')$ is normally aligned with the peak with higher TOAD gain.

7.2.2.4 demultiplexer pattern noise due to crosstalk

The origin of the pattern noises associated with demultiplexer is the same as their counterparts in router [68], which is due to channel crosstalk and residual crosstalk of demultiplexer.

For channel crosstalk of demultiplexer, the neighbour channel crosstalk NXT_{DEMU} is dominant, which is given as:

$$NXT_{DEMU} = \frac{\int_{-T_b/2}^{T_b/2} T_x(t)_{TOAD} \cdot S(t+T_b)dt + \int_{-T_b/2}^{T_b/2} T_x(t)_{TOAD} \cdot S(t-T_b)dt}{2 \cdot \int_{-T_b/2}^{T_b/2} T_x(t)_{TOAD} \cdot S(t)dt}. \tag{7.6}$$

In (7.6), $T_x(t)_{TOAD}$ and $S(t)$ have the same definition as in (7.5). T_b is the OTDM time slot duration. The factor 2 in the denominator assumes that the probabilities of occurrence of mark and space are the same.

The residual crosstalk of demultiplexer due to a small difference between G_{CW} and G_{CCW} outside the TOAD window, has the same origin as its counterpart in router. The small gain difference between G_{CW} and G_{CCW} manifests itself into demultiplexer residual crosstalk. The demultiplexer residual crosstalk is defined as:

136

$$RXT_{DEMU} = \frac{\sum_{r=2}^{M_{TDM}-1} \int_{(r-0.5)T_b}^{(r+0.5)T_b} T_x(t)_{TOAD} \cdot S(t - r \cdot T_b)dt}{2 \cdot \int_{-T_b/2}^{T_b/2} T_x(t)_{TOAD} \cdot S(t)dt},$$ (7.7)

where M_{TDM} is the total number of OTDM channels. The crosstalk due to the two channels adjacent to the target channel is excluded from the numerator since they are defined as neighbour channel crosstalk (see (7.6)). The factor 2 in the denominator assumes that the probabilities of occurrence of mark and space are the same.

7.2.2.5 the noises associated with receiver and optical amplifier

The noise sources associated with receiver are thermal noise, optical amplifier beat noise between spontaneous emission components and beat noise between signal and spontaneous emission, which are expressed by the equivalent photocurrent given by [126]:

$$\sigma_{th}^2 = \frac{4kTB}{R_L} + \{i_a^2\}B$$ (7.8)

$$\sigma_{sp-sp}^2 = 4(q\eta G)^2 n_{sp}^2 B_o B$$ (7.9)

$$\sigma_{s-sp,p}^2 = 4(q\eta G)^2 n_{sp}^2 B \langle N_p \rangle$$ (7.10)

where k is the Boltzmann's constant, R_L is the load-resistance of the PIN photodiode detector, $\sqrt{\{i_a^2\}}$ is the spectrum density of amplifier input noise current, B is the electrical bandwidth, B_o is the optical amplifier bandwidth, η is the photodiode quantum efficiency, and n_{sp} is the population inversion parameter of the optical preamplifier. In (7.10), $p = m$ or s for mark and space, respectively.

7.3 BER Analysis

Assuming that the probabilities of mark and space are equal, the mean photo current for mark I_m and space I_s at the receiver can be given as:

$$I_m = \eta_{in}\eta_{out}L_{of}GR\{E[w(t)] + E[XT_{T,R}] + E[XT_{T,Dem}]\}R_B,$$ (7.11)

$$I_s = \eta_{in}\eta_{out}L_{of}GR\{r_w E[w(t)] + E[XT_{T,R}] + E[XT_{T,Dem}]\}R_B,$$ (7.12)

where R is the photo-detector responsivity, r_w is the extinction ratio of switching window, τ is the mean pulse arrival time relative to the switching window, η_{in} and η_{out} are the input and output coupling efficiencies of the optical amplifier, respectively, G is the optical amplifier gain, L_{of} is the optical filter loss, $E[XT_{T,Dem}]$ is the expected total crosstalk of the demultiplexer, $E[XT_{T,R}]$ is the expected total crosstalk of the router, and R_B is the channel bit rate.

The standard deviation of the photo currents for mark and space in receiver end are respectively expressed by:

$$\sigma_m = \sqrt{(\eta_{in}\eta_{out}L_{of}GR)^2\{Var[XT_T]\}R_B^2 + \sigma_{RIN,m}^2 + \sigma_{th}^2 + \sigma_{sp-sp}^2 + \sigma_{s-sp}^2 + \sigma_a^2}$$ (7.13)

$$\sigma_s = \sqrt{(\eta_{in}\eta_{out}L_{of}GR)^2\{Var[XT_T]\}R_B^2 + \sigma_{RIN,s}^2 + \sigma_{th}^2 + \sigma_{sp-sp}^2 + \sigma_{s-sp}^2 + \sigma_a^2}$$ (7.14)

Where the total crosstalk $[XT_T] = [XT_{T,R}] + [XT_{T,Dem}]$. The first term of the right-hand side of (7.13) and (7.14) represents the variance due to the total crosstalk within the router and demultiplexer. The second term indicates the relative intensity noise of the signal, and the

remaining terms represent the thermal noise, beat noise between spontaneous emission components, beat noise between signal and spontaneous emission, and the electrical amplifier noise respectively [98]. The relative intensity noise for mark and space are expressed by the equivalent photocurrent given by:

$$\sigma^2_{RIN,m} = (q\eta G)^2 \left[RIN\langle N_m \rangle^2 B + RIN_{ROUTER} \langle N_0 \rangle^2 + RIN_{DEMU} \langle N_0 \rangle^2 \right] \qquad (7.15)$$

$$\sigma^2_{RIN,s} = (q\eta G)^2 \left[RIN\langle N_s \rangle^2 B + RIN_{ROUTER} r_w^2 \langle N_0 \rangle^2 + RIN_{DEMU} r_w^2 \langle N_0 \rangle^2 \right] \qquad (7.16)$$

where q is the electron charge, η is the photodiode quantum efficiency, RIN is the relative intensity noise of the optical signal source, RIN_{ROUTER} and RIN_{DEMU} are relative intensity noises of router and demultiplexer, respectively, and $\langle N_m \rangle$, $\langle N_s \rangle$ and $\langle N_0 \rangle$ are the mean photon number of mark, space and when all the bits are mark at the base rate, respectively.

In order to investigate how the power penalty changes with the crosstalk and the intensity fluctuation RIN_{ROUTER} due to the router, the calculations were carried out. The power penalty is defined as the difference between minimum average received optical power levels at BER = 10^{-9} of with and without the optical router.

The bit error rate in the case of Gaussian approximation of the probability density function of the photocurrent equivalent output signal is given by:

$$BER = \frac{1}{2} erfc\left(\frac{Q}{\sqrt{2}}\right) \qquad (7.17)$$

With the parameter

$$Q = \frac{I_m - I_s}{\sigma_m + \sigma_s}$$

7.4 Results

Using the parameters given in Table 7.1, the performance of the proposed model is investigated.

Table 7.1 Parameters of the receiver mode

Parameters	Values
η_{in}	-2 dB
η_{out}	-2 dB
G (preamplifier gain)	30 dB
L_f	-2 dB
R	1.25 A/W
r_w	-25dB
R_L	50 Ω
T	293 K
n_{sp}	2
$\overline{i_a^2}$	100 pA^2
B	0.7 R_b
B_o	374 GHz
RIN_{DEMU}	$3*10^{-3}$
RIN	10^{-15}Hz^{-1}

Applying the parameters in Table 7.1 to the receiver model, Figure 7.2 shows the plots of BER versus average received optical power for 1 Gb/s and 10 Gb/s with and without an optical router. Also shown for comparison is the results for the base line. The baseline bit rate is 10 Gb/s, which corresponds to M_{TDM} = 10, 20 and 30 for total bit rates 100 Gb/s, 200 Gb/s and 300 Gb/s respectively. And baseline bit rate is 1Gb/s, which corresponds to M_{TDM} = 100, 200 and 300 for total bit rates 100 Gb/s, 200 Gb/s and 300 Gb/s respectively.

Observe that for the baseline case, at the BER of 10^{-9} the power requirement is increased by 5 dB for 10 Gb/s compared to 1 Gb/s.

For 1 Gb/s at BER of 10^{-9} the power penalties for receiver with /without router are 0.4 dB and 0.65 dB, respectively, compared to the baseline. The power penalties increase to 1 dB and 1.45 dB at higher bit rate (10 Gb/s).
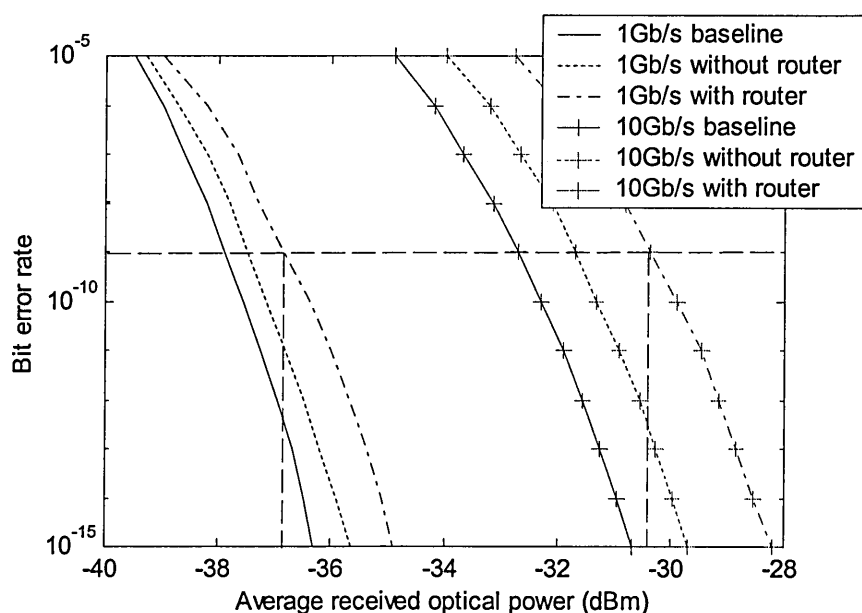
Figure 7.2 BER versus average received optical power for baseline bit rates

141

In the case of system with the router, the optical power requirement increases due to relative intensity noise, crosstalk and router switching ratio. The switching ratio degrades the sensitivity by reducing the energy content of the routed target packet, then resulting in a lower signal to noise ratio.
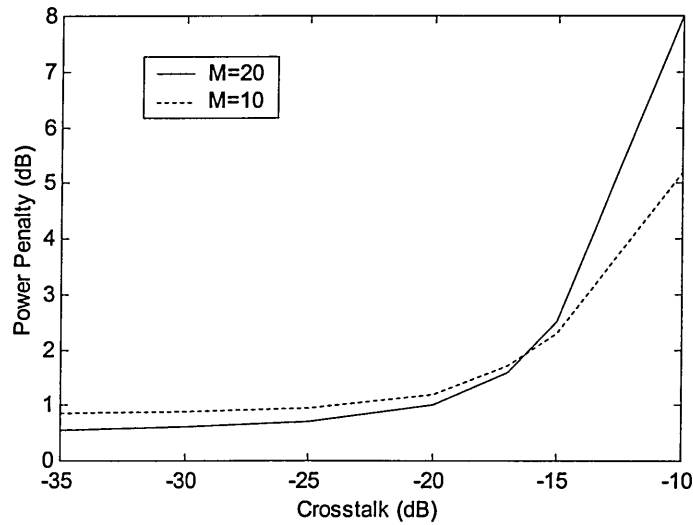
Figure 7.3 Power penalty versus crosstalk of router for 100 Gb/s
OTDM for different values of M_{TDM}

To investigate how crosstalk affect the performance of router in OTDM system, power penalty due to crosstalk of router with different time division multiplication factor have been simulated. Figure 7.3 shows results for the power penalty versus crosstalk for router for 100 Gb/s OTDM system employing a router for two values of time division multiplication factor, i.e. M_{TDM}=10, and 20. As shown in Figure 7.3 the power penalty increases with the increase of crosstalk. The power penalty is small and reaches the value of 0.6 dB and 0.9 dB for M_{TDM}=20 and 10, respectively, when the crosstalk is less than - 20dB. In this range, the power penalty is mainly attributed to the residual crosstalk

142

originated from the phase-shift induced by counter–propagating control pulses, and increases as the M_{TDM} value decreases. For crosstalk larger than –20dB, the power penalty increases exponentially, this is because the channel crosstalk is dominant source. Note for M_{TDM} =20, the power penalty is larger compared with M_{TDM} =10. This is due to the fact that the channel crosstalk value is proportional to the number of nontarget channels, M_{TDM}-1.

The effect of relative intensity noise on the power penalty is illustrated in Figure 7.4. As shown power penalty displays a threshold effect. At below which, there is no change in power penalty. But above threshold level (RIN_{ROUTER} >10^{-3}), there is a big increase in power penalty. Note the router with lower crosstalk value displays the lower power penalty character. Thus, to achieve a low value of power penalty, it is desirable to select a router with crosstalk of less than –20 dB and RIN_{ROUTER} of less 10^{-3}.
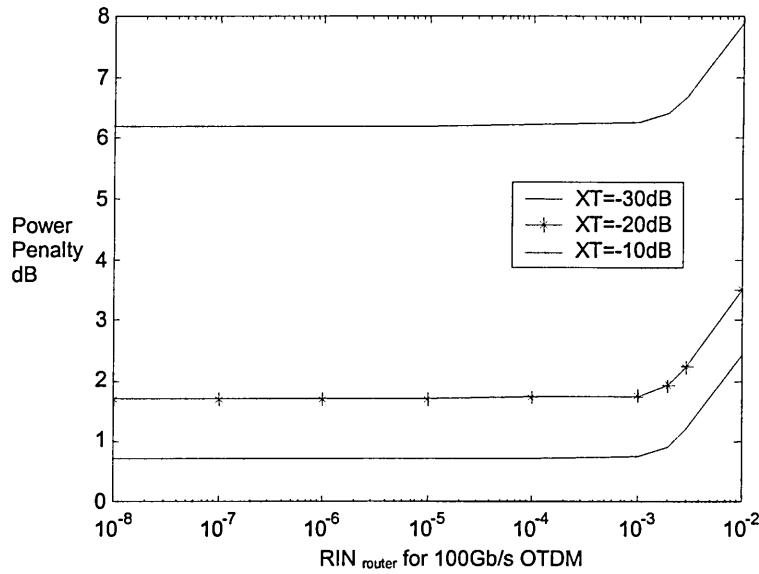
Figure 7.4 Power penalty versus RIN_{ROUTER} for different values of router crosstalks

7.5 Summary

In this chapter, the BER analysis of packet based high-speed OTDM system employing all optical router has been studied by mathematical model considering the time jitter, crosstalk due to router and demultiplexer and the noises due to receiver. An expression for BER presented shows that there is a trade off between the crosstalk and the relative intensity noise in order to minimise BER performance at the receiver. The results obtained show that the RIN_{ROUTER} of 10^{-3} gives a critical value of the intensity fluctuation in order to suppress the power penalty and the router crosstalk of less -20 dB is necessary for the power penalty of less than 1.7 dB in 100 Gb/s OTDM system. Power penalty is router crosstalk dependent and increases as the RIN_{ROUTER} increases.

Chapter 8

All Optical Router with Multi-Input and Output

8.1 Introduction

Growing demands for bandwidth have stimulated the development of high-speed optical shared media networks. All-optical packet based networks offer the potential for high speed and flexible routing. In such systems all optical routers, which overcome the bottleneck of optoelectronic conversion, play an important role. Optical routers with multi-input and output are a fundamental requirement of practical communication systems. A 1x4 router, which uses terahertz optical asymmetric demultiplexers (TOAD) as switching element, is introduced in Section 8.2. The router is described by a mathematical model that is used to simulate a 1x4 router and characterise its performance in terms of crosstalk. 2x2 routers based on TOADs and incorporating input and output buffers are discussed in Section 8.3. Section 8.4 describes multi-port routers used in Banyan network architecture. The mathematical model for the crosstalk of a router with multistage configurations is given in Section 8.5.

8.2 1x4 Router

The performance of a 1x4 optical router based on the terahertz optical asymmetric demultiplexer has been investigated using simulation method. The router operation is based around the TOAD, which is described in Chapter 5. A mathematical model is used to simulate the router and results for crosstalk are presented and compared with the 1x2 router.

8.2.1 Mathematical model
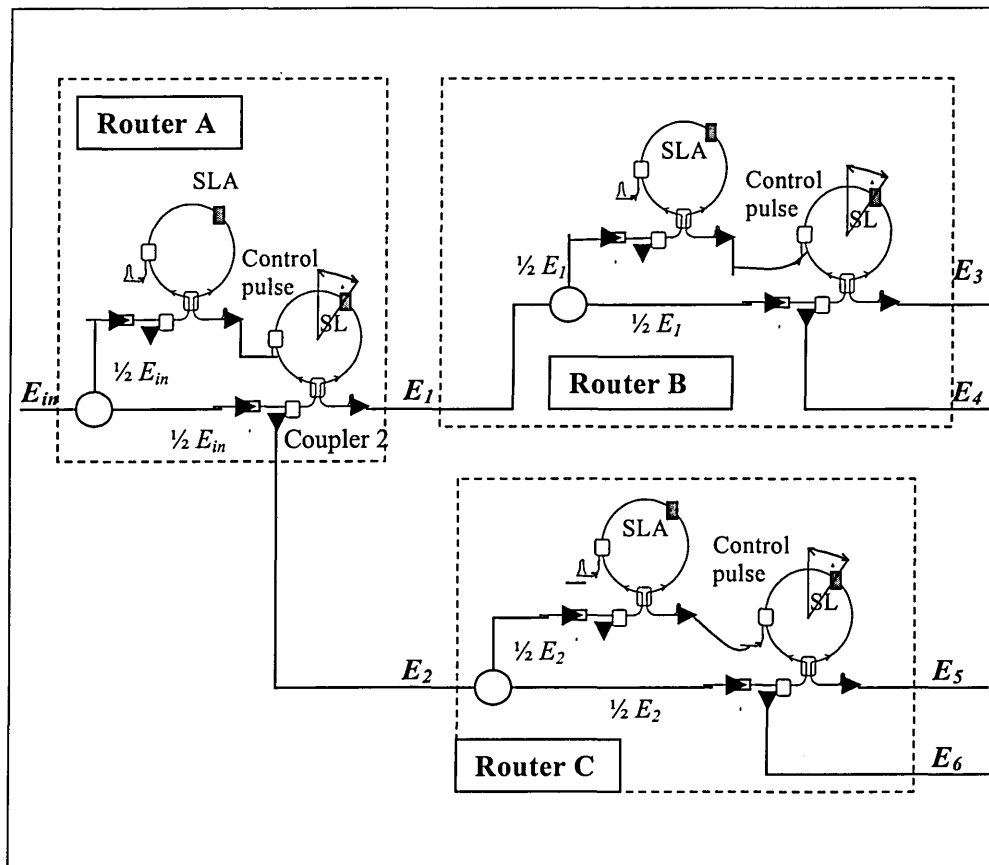
Figure 8.1 Schematic block diagram of a 1x4 router

The schematic diagram of a 1x4 router is shown in Figure 8.1. Each 1x2 router with one input and two output is composed of two TOADs as shown in Figure 5.22. The routers are connected so as to realise single input multi-output switching. As can be seen, the outputs of the router A are connected to the inputs of the routers B and C, respectively. The principle of operation follows 1x2 router as described in Section 5.5. The coupler 2 at the reflection port of router A is a 2x2 cross bar switch which is set at the "bar" state for the returning (reflected) signal E_2. Assuming the loss of the coupler is negligible, then there is no need for further amplification. However, in practical case an optical amplifier will be require at the input port of router B just after the coupler 2 of routerA to compensate for any power loss.

Substituting for $E_2 = 0$ in (5.20), and changing the notation, the matrix for the transmittance of a single 1x2 router, e.g. router A, is given as:

$$\begin{pmatrix} E_1 \\ E_2 \end{pmatrix} = (1-\gamma)^{1/2} e^{-\alpha L} \begin{pmatrix} a_{11} & a_{12} \\ a_{21} & a_{22} \end{pmatrix} \begin{pmatrix} \frac{1}{2} E_{in} \\ 0 \end{pmatrix},$$

(8.1)

where the matrix coefficients are defined as:

$$a_{11} = K e^{j(\phi_{cw})} G_{cw} + K e^{j(\phi_{ccw}+\pi)} G_{ccw}$$

$$a_{12} = K e^{j(\phi_{cw}+\pi/2)} G_{cw} + K e^{j(\phi_{ccw}+\pi/2)} G_{ccw}$$

$$a_{21} = K e^{j(\phi_{cw}+\pi/2)} G_{cw} + K e^{j(\phi_{ccw}+\pi/2)} G_{ccw}$$

$$a_{22} = K e^{j(\phi_{cw}+\pi)} G_{cw} + K e^{j(\phi_{ccw})} G_{ccw}$$

ϕ_{cw} and ϕ_{ccw} are the respective field gains of SLA for the clockwise and the counter-clockwise signals in the router, γ is the coupler excess loss, α is the fibre loss, and L is the half of the length of the fibre loop.

Here it is assumed that the insertion loss of the coupler and the fibre loss are both zero as short fibre length is used.

The outputs of the 1x2 routers B and C are written in a similar way as:

$$\begin{pmatrix} E_3 \\ E_4 \end{pmatrix} = \begin{pmatrix} a_{11} & a_{12} \\ a_{21} & a_{22} \end{pmatrix} \begin{pmatrix} \frac{1}{2} E_1 \\ 0 \end{pmatrix},$$

(8.2)

$$\begin{pmatrix} E_5 \\ E_6 \end{pmatrix} = \begin{pmatrix} a_{11} & a_{12} \\ a_{21} & a_{22} \end{pmatrix} \begin{pmatrix} \frac{1}{2} E_2 \\ 0 \end{pmatrix}.$$

(8.3)

Note the E_1 at the output of the TOAD2 in the router A is split in to two by an optical splitter at the inputs of the router B and C.

Substituting for E_1 and E_2 from (8.1) into (8.2) and (8.3) results in

$$\begin{pmatrix} E_3 \\ E_4 \end{pmatrix} = \begin{pmatrix} a_{11} & a_{12} \\ a_{21} & a_{22} \end{pmatrix} \begin{pmatrix} \frac{1}{4} a_{11} E_{in} \\ 0 \end{pmatrix},$$

(8.4)

$$\begin{pmatrix} E_5 \\ E_6 \end{pmatrix} = \begin{pmatrix} a_{11} & a_{12} \\ a_{21} & a_{22} \end{pmatrix} \begin{pmatrix} \frac{1}{4} a_{21} E_{in} \\ 0 \end{pmatrix},$$

(8.5)

The outputs of the 1x4 router can now be expressed as:

148

$$\begin{pmatrix} E_3 \\ E_4 \\ E_5 \\ E_6 \end{pmatrix} = \frac{1}{4} \begin{pmatrix} a_{11}a_{11} & a_{11}a_{12} \\ a_{11}a_{21} & a_{11}a_{22} \\ a_{21}a_{11} & a_{21}a_{12} \\ a_{21}a_{21} & a_{21}a_{22} \end{pmatrix} \begin{pmatrix} E_{in} \\ 0 \end{pmatrix}, \tag{8.6}$$

$$\begin{pmatrix} E_3 \\ E_4 \\ E_5 \\ E_6 \end{pmatrix} = \begin{pmatrix} B_{11} & B_{12} \\ B_{21} & B_{22} \\ B_{31} & B_{32} \\ B_{41} & B_{42} \end{pmatrix} \begin{pmatrix} E_{in} \\ 0 \end{pmatrix}, \tag{8.7}$$

where

$$B_{11} = \tfrac{1}{4}a_{11} * a_{11} = \tfrac{1}{4}(K^2 e^{j2(\phi_{cw})}G_{cw}^2 + K^2 e^{j2(\phi_{ccw}+\pi)}G_{ccw}^2 + 2K^2 e^{j(\phi_{cw}+\phi_{ccw}+\pi)}G_{ccw}G_{cw})$$

$$B_{12} = \tfrac{1}{4}a_{11} * a_{12} = \tfrac{1}{4}(K^2 e^{j(2\phi_{cw}+\pi/2)}G_{cw}^2 + K^2 e^{j(2\phi_{ccw}+3\pi/2)}G_{ccw}^2 + K^2 e^{j(2\phi_{cw}+2\phi_{ccw}+2\pi)}G_{ccw}G_{cw})$$

$$B_{21} = \tfrac{1}{4}a_{11} * a_{21} = \tfrac{1}{4}(K^2 e^{j(2\phi_{cw}+\pi/2)}G_{cw}^2 + K^2 e^{j(2\phi_{ccw}+3\pi/2)}G_{ccw}^2 + K^2 e^{j(2\phi_{cw}+2\phi_{ccw}+2\pi)}G_{ccw}G_{cw})$$

$$B_{22} = \tfrac{1}{4}a_{11} * a_{22} = \tfrac{1}{4}(K^2 e^{j(2\phi_{cw}+\pi)}G_{cw}^2 + K^2 e^{j(2\phi_{ccw}+\pi)}G_{ccw}^2 + K^2 e^{j(2\phi_{cw}+2\phi_{ccw}+2\pi)}G_{ccw}G_{cw})$$

$$B_{31} = \tfrac{1}{4}a_{21} * a_{11} = \tfrac{1}{4}(K^2 e^{j(2\phi_{cw}+3\pi/2)}G_{cw}^2 + K^2 e^{j(2\phi_{ccw}+3\pi/2)}G_{ccw}^2 + K^2 e^{j(2\phi_{cw}+2\phi_{ccw}+2\pi)}G_{ccw}G_{cw})$$

$$B_{32} = \tfrac{1}{4}a_{21} * a_{12} = \tfrac{1}{4}(K^2 e^{j(2\phi_{cw}+\pi)}G_{cw}^2 + K^2 e^{j(2\phi_{ccw}+\pi)}G_{ccw}^2 + K^2 e^{j(2\phi_{cw}+2\phi_{ccw}+2\pi)}G_{ccw}G_{cw})$$

$$B_{41} = \tfrac{1}{4}a_{21} * a_{21} = \tfrac{1}{4}(K^2 e^{j2(\phi_{cw}+\pi/2)}G_{cw}^2 + K^2 e^{j2(\phi_{ccw}+\pi/2)}G_{ccw}^2 + 2K^2 e^{j(\phi_{cw}+\phi_{ccw}+\pi)}G_{ccw}G_{cw})$$

$$B_{42} = \tfrac{1}{4}a_{21} * a_{22} = \tfrac{1}{4}(K^2 e^{j(2\phi_{cw}+3\pi/2)}G_{cw}^2 + K^2 e^{j(2\phi_{ccw}+\pi/2)}G_{ccw}^2 + K^2 e^{j2(\phi_{cw}+\phi_{ccw}+\pi)}G_{ccw}G_{cw})$$

8.2.2 Simulation results

Figure 8.2 shows the format of two consecutive packets used for the simulation. Framing bits indicate the inter-packet boundaries providing frame synchronisation. The two address bits indicate the destination port to which the payload information is routed. A value of '0' ('1') results in the payload information being reflected (transmitted) during each stage.

Frame Sync.	Address (11)	Payload information (00)	Frame Sync.	Address (10)	Payload information (00)

Figure 8.2 Format of OTDM packets signal
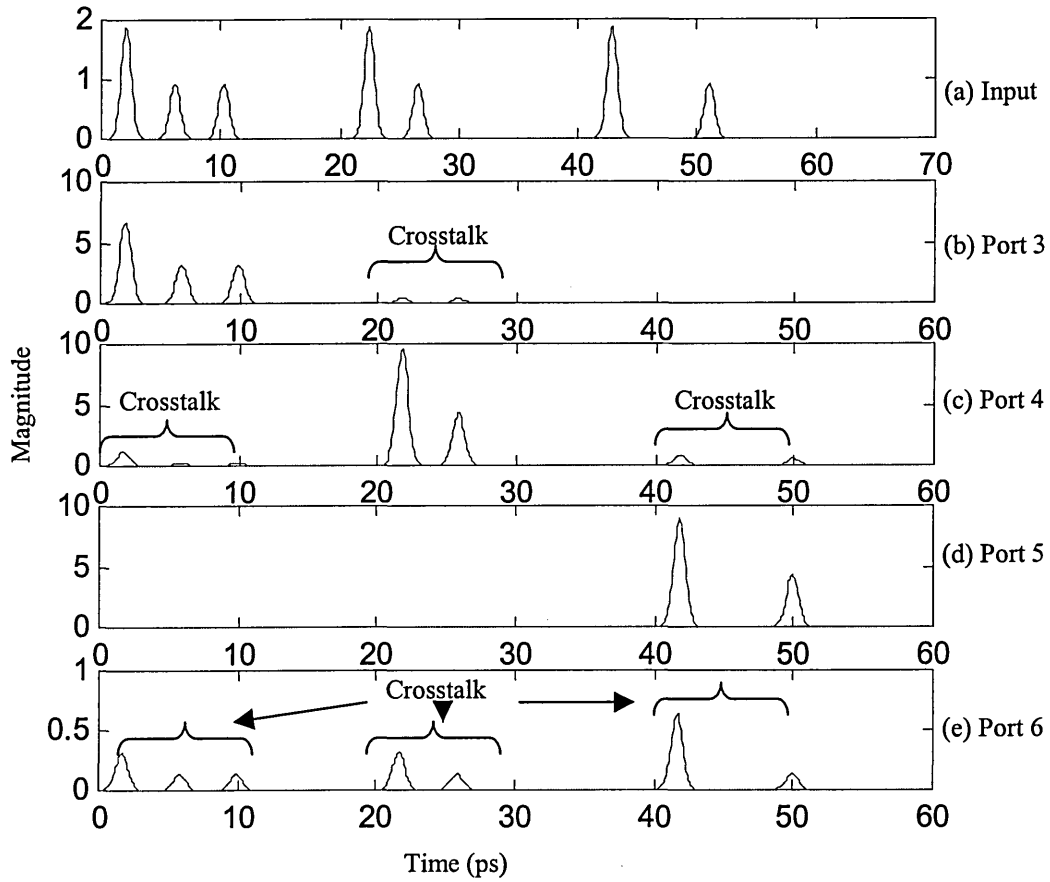
Figure 8.3 Time waveforms of the 1x4 router, (a) input, (b) output port 3, (c) output port 4, (d) output port 5, and (e) corsstalk at the output port 6.

Substituting (5.2) (5.4) (5.9) (5.11) and (5.28) into (8.7) the waveforms at the output of the 1x4 router is investigated. The model used for the TOADs is the same as that given in Section 5.3.3.1, with the parameters used given in Table 8.1.

Table 8.1 Simulation parameters for 1x4 router

Parameters	Values
K	0.5
Control pulse width FWHM	2 ps
Control pulse wavelength	1500 nm
Control pulse power	0.8 pJ
Control pulse period	100 ps
Data signal width FWHM	2 ps
Data signal wavelength	1550 nm
Data frame time	100 ps
SLA length L_{SLA}	300 μm
Total number of SLA segments	300
SLA active area A_{eff}	$0.3e^{-12} m^2$
SLA carrier lifetime τ_{sp}	300 ps
SLA transparent carrier density N_0	$10^{24} m^{-3}$
SLA confinement factor Γ	0.3
Material gain coefficient a	$3 \times 10^{-20} m^{-2}$
SLA asymmetry T_{asy}	TOAD for address: 2ps TOAD for packet: 10 ps
The half of the length of the fibre loop L	1 m
Linewidth emhancement factor α_{LEF}	4
Photon energy E_p	0.8 eV
Propagation speed inside the SLA	$(3 \times 10^8 /3.5)$ m/s

Figure 8.3 shows the simulated waveforms at the input and output ports of the 1x4 router. The three packets used at the input are 21100, 21000, and 20100 with a 2 indicating a frame with twice the magnitude of the data pulses (see Section 5.5). The packet framing signal is shown graphically by its higher amplitude, followed by two bit address bits and the payload information. According to the routing convention established earlier, packets 1, 2 and 3 are routed to ports 3, 4 and 5, respectively. Also present are small amount of crosstalk due to the inter-channel crosstalk and residual crosstalk associated with the router at the output ports 3, 4 and 6.

Simulation results show that the 1x4 router can recognise the address bits and route optical packets containing data with a bit period of only 4 ps, which corresponds to a bit rate of 0.25 Tb/s. The crosstalk performance will be investigated and compared to a 1x2 router in the next subsection.

8.2.2.1 crosstalk versus bit rate

The crosstalk components of a 1x4 router are composed of inter-channel crosstalk and residual crosstalk. The former is caused by the non-target channels appearing within the switching window, whereas the latter is due to the differences in the gain and phase profiles during the recovery period. The inter-channel crosstalk increases with the data rate because of an increase in the number of bits appearing within the switching window whose width is constant. Using the parameters shown in Table 8.1, the output of the 1x4 router was determined by using equation 8.7, and the crosstalk results over a range of OTDM bit rates are shown in Figure 8.4. The crosstalk is seen to increase with increasing the rate reaching

152

−11.97 dB at 200 Gbit/s for the 1x4 router. Comparing this result with that of 1x2 optical router, the crosstalk is approximately 4 dB greater for all bit rates considered. This is due to an increase in the number of TOADs in 1x4 router.
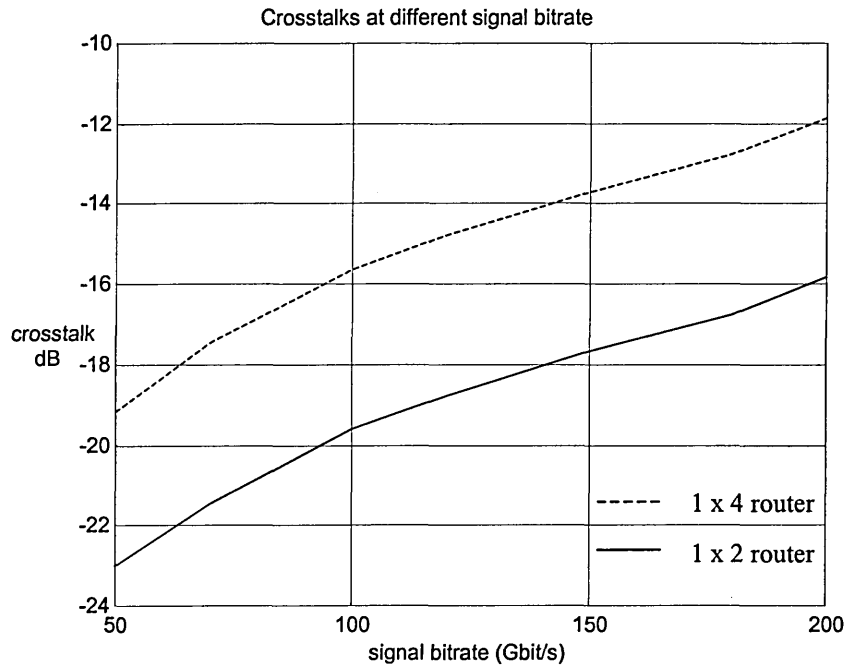
Figure 8.4 Crosstalk versus signal bit rate for 1x4 and 1x2 routers

8.2.2.2 crosstalk versus control pulse energy

The width of switching window is determined by the position of the SLA within the loop. By placing the SLA asymmetrically, one can reduce the time resolution to a value of the order equal to twice the propagation time through the device. Loops with such small asymmetries are capable of ultrafast all optical switching [71]. The control pulse induces the non-linearity property of the SLA, which ultimately determines the output profile of the router.

153
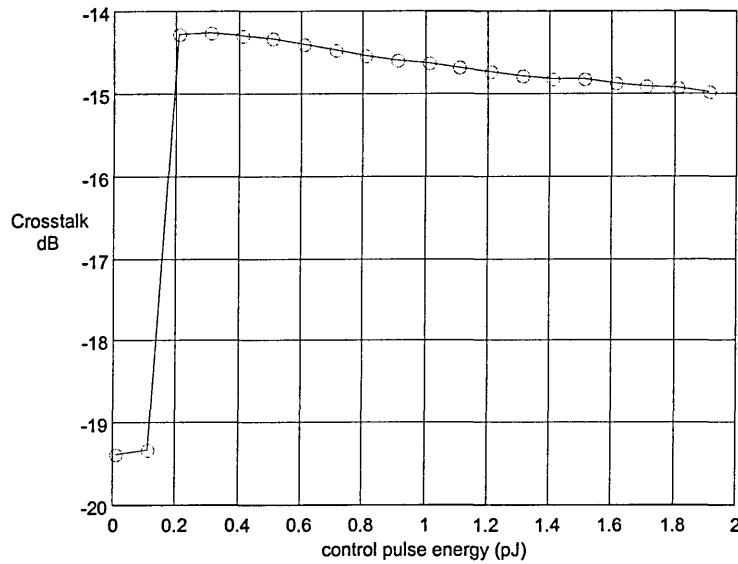
Figure 8.5 Crosstalk versus control pulse energy

To see the effect of the control pulse energy on the crosstalk, different control pulse energies were used in the simulations using (8.7) substituted by (5.2) (5.2) (5.9) (5.11) and (5.28). The results are shown in Figure 8.5, where it can be seen that the crosstalk is relatively low (about -19.5 dB) at control pulse energies < 0.2 pJ. Low values of control pulse energy induce little SLA non-linearity, consequently, data signals, after propagating through the loop, are reflected back to the input port of the TOAD. The crosstalk is at a peak value of -14.4 dB when the control pulse energy is 0.2 pJ, decreasing to -15 dB at a control pulse energy of 1.9 pJ. The reason for sudden increase in the crosstalk is because the control pulse energy affects the carrier density of the SLA, which determines the gain of the switching window. In other words, the more power, the more gain within the region of 0.2 pJ to 1.9 pJ. The simulation results are in good agreement with the experimental results [140]. It has been shown that it is possible to route OTDM packet signals at 200 Gbit/s with

154

switching energy of 0.2 pJ or more, assuming that the data signal energy is 0.1 pJ and there is no influence of the data signal on the carrier density among other things.

It is believed that the proposed configuration is a promising as a component for high-speed all optical TDM networks due to its ultrafast switching capability. Further work will extend the concept to investigate networks with multiple inputs and outputs.

8.3 2x2 Router

8.3.1 2x2 router with input and output buffers

We propose here a novel extension to the 1x2 router model to implement a 2x2 routing element and corporate input and output buffering. The basic design of 2x2 router with input and output buffers and simulation waveforms of the 2x2 router are given in this section.

8.3.1.1 design of 2x2 router with input and output buffers

The basic design of 2x2 router with input and output buffers is shown in Figure 8.6. It consists of two 1x2 routers and four buffers. Optical buffers 1 and 2 are used to allow the input signals to wait for access to the router input, whilst buffers 3 and 4 are used to eliminate contention at the output ports. Data can be stored in the buffers or passed straight through without delay.

155
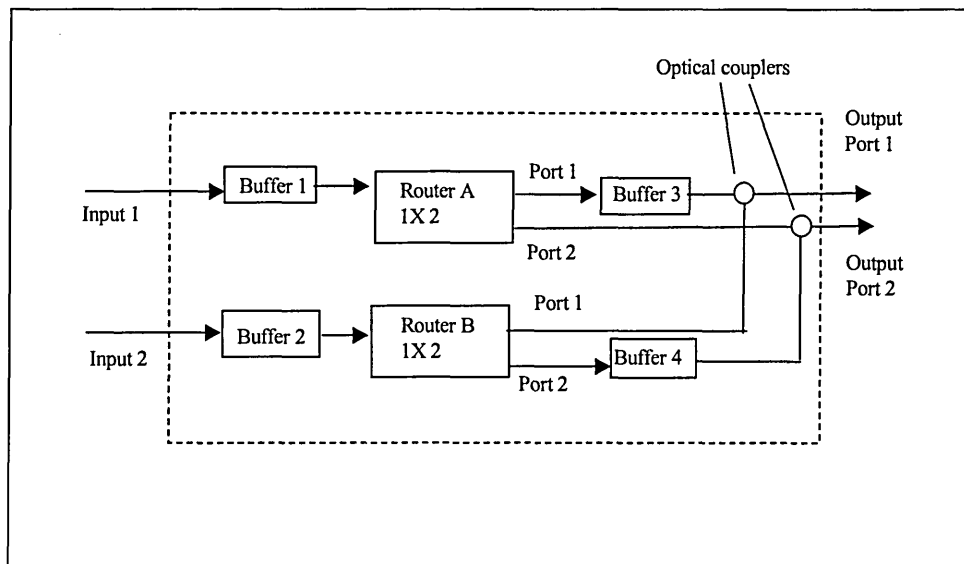
Figure 8.6 2x2 OTDM optical router with input and output buffers

It is the intention that the router should be capable of routing synchronous and asynchronous packets, and for this reason it is important that the router is able to switch packets and resolve output contention regardless of the arrival time and formation of the packets. Figure 8.7 illustrates how employing buffers avoids this problem.

Here three optical packets are incident simultaneously to input ports 1 and 2 of the 2x2 router. Packets identified by letter 'a' are incident at input 1 and whilst those with identifier 'b' are incident at input 2. It is assumed that packets 1a, 2a, 1b and 2b are required to be routed to output port 2 and packets 3a and 3b are required to be routed to output port 1. The sequence of events is implemented successfully depicted in Figure 8.7 and demonstrates how the buffers are used to allow routing to take place.

156

At Stage 1, three packets arrive at each input to the 2x2 router. Both packets 1a and 1b are to be routed to output port 2. One packet can be switched by one of the 1x2 router elements and sent directly to the output port, in this example it is assumed that packet 1a is switched first. The second packet can be switched by the second 1x2 router element but must be stored in the output buffer to avoid contention at the output port as shown at Stage 2.

At Stage 3 packet 1b exits at output port 2 and packets 2a and 2b enter the switch. Both packets 2a and 2b are to be switched to output port 2. It is assumed that packet 2a is given priority and routed directly to output port 2 and packet 2b is stored in the buffer at output port 2.

At Stage 4, packet 2a exits at output port 2 and packet 2b is routed through to the buffer at the output port 2. At the input, packets 3a and 3b enter the switch and both are required to exit at the output port 1.

At Stage 5, Packet 3b is routed to the output port 1, because there is no output buffer for packets entering at input port 2 and exiting at output port 1. Packet 3a is stored in the buffer at the output port 1 to avoid contention at the output port 1.

At Stage 6, packet 3a is able to exit at the output port 1.
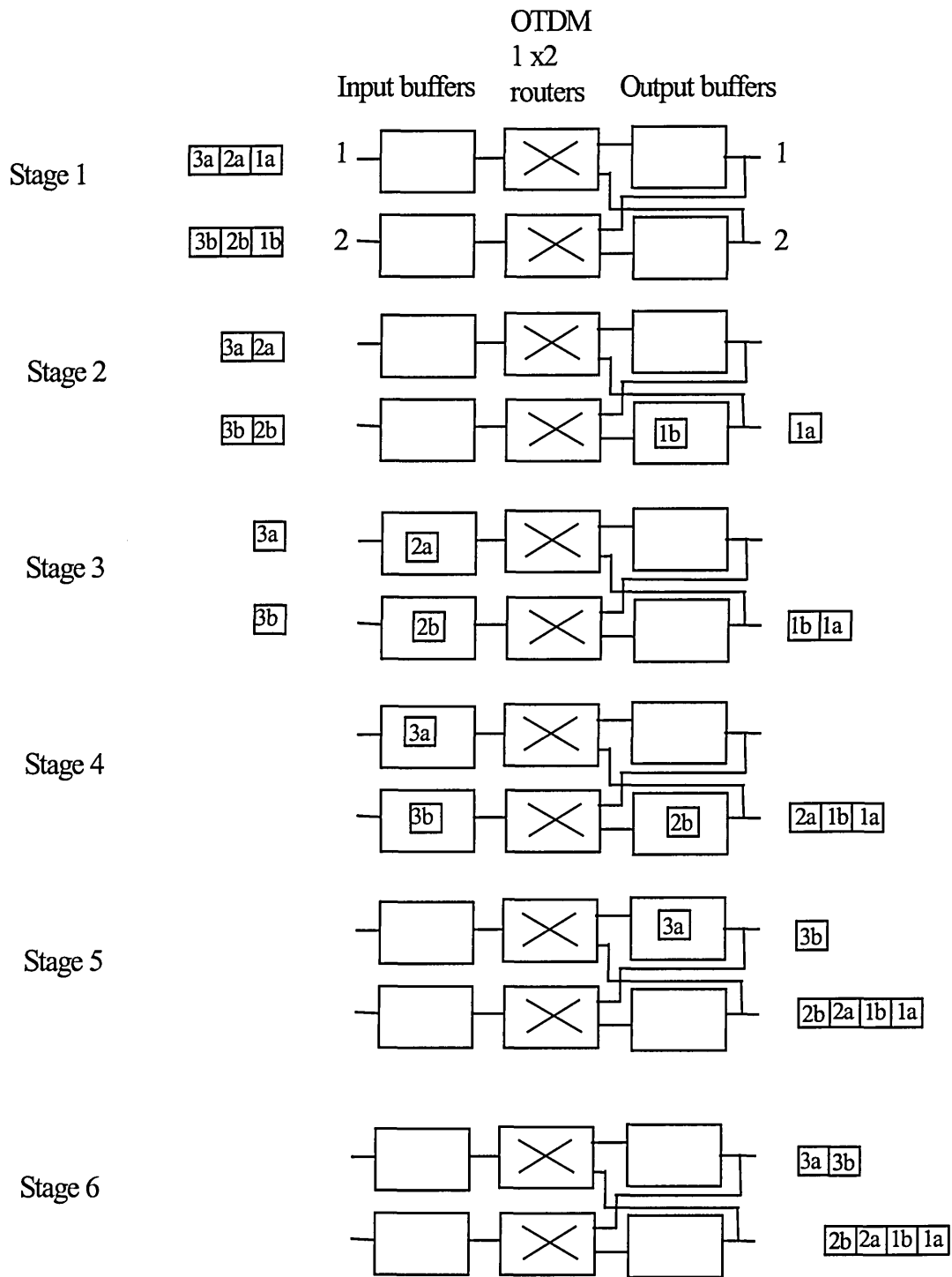
Figure 8.7 Operation of 2x2 OTDM router with input/output buffering

Figure 8.7 illustrates one example of the process whereby packets enter and leave the 2x2 switch. In general, buffers are required to avoid contention arising when two packets require simultaneous access to a router port or routing element. This 2x2 router design uses 1x2 routing elements, so there can be no contention at an input port (e.g. 2 packets entering the switch simultaneously requiring access to the same switching element).

8.3.1.2 simulation waveforms of the 2x2 router

Simulate the optical 2x2 router with the 1x2 router model presented in Chapter 5 using Matlab. The simulated input and output waveforms of the 2x2 router are shown in Figure 8.8. The same OTDM packet signals are simultaneously fed to the two inputs of the router. Packet 1 to 3 formats are 20100, 20110 and 21011, respectively. Observe that the packet consists of a frame signal, distinguishable by its higher amplitude, a bit address and payload information, which is in accordance to the format illustrated in Figure 8.2. Thus according to the routing convention established before packets one and two should be routed to port 2 whereas packet 3 should be routed to port 1. Figure 8.8 shows the waveforms at output port 1 and port 2 of the 2x2 router. The crosstalk has been observed in output of the router due to router A and router B. Notice that the delay–line optical buffers in the router are a much effective way of solving contention, and optical buffers increase the accumulation of intraband crosstalk and amplified spontaneous emission noise.

159
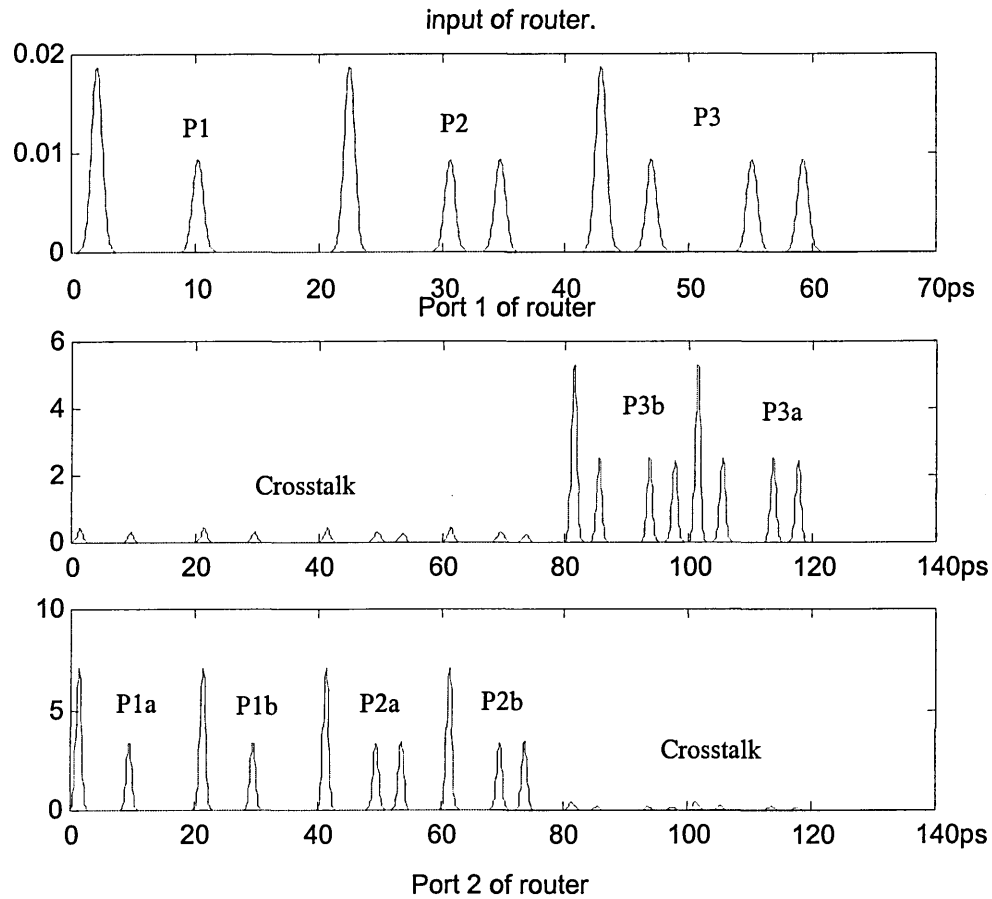
Figure 8.8 Waveforms of input and outputs of 2x2 router with input and output buffers

8.3.2 2x2 router with output buffers only

8.3.2.1 design of 2x2 router with output buffers only

An alternative proposed 2x2 routing element is now described. Now the buffering arrangement is input buffers are removed and output buffers are included in both output branches of the 1x2 routing elements. The idea is as shown in Figure 8.9. The router is constructed from two 1x2 routers and four buffers. The optical buffers are now used to

eliminate contention at the outputs. Data can be stored in the buffers or passed straight through without delay. The number of buffer stages needed at the output is determined by the packet arrival statistics.
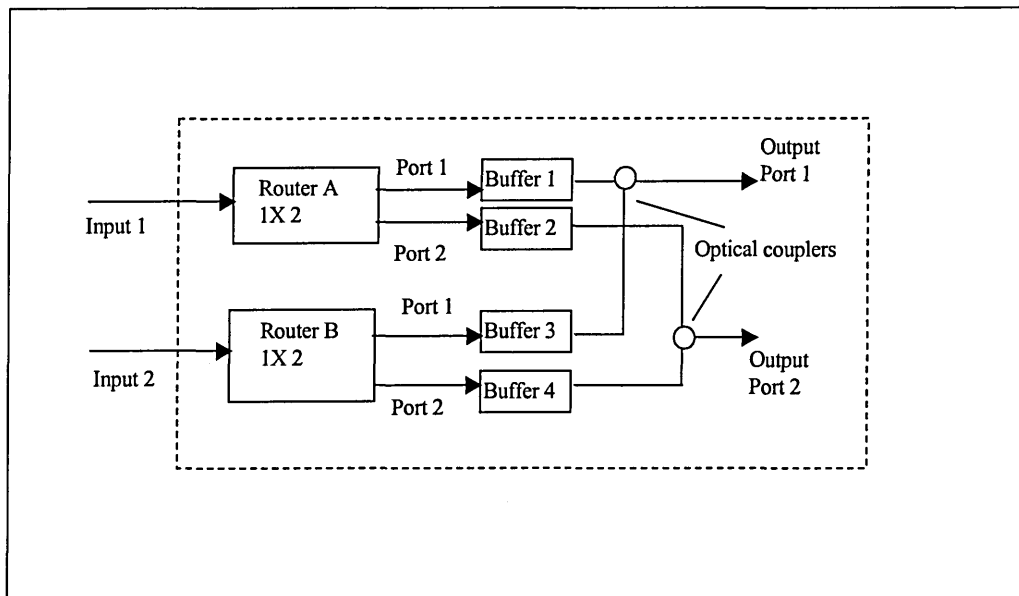
Figure 8.9 2x2 router design using output buffers

Figure 8.10 shows a compact optical buffer design described by Hunter et al [143] suitable for use in conjunction with the 2x2 router previously described.
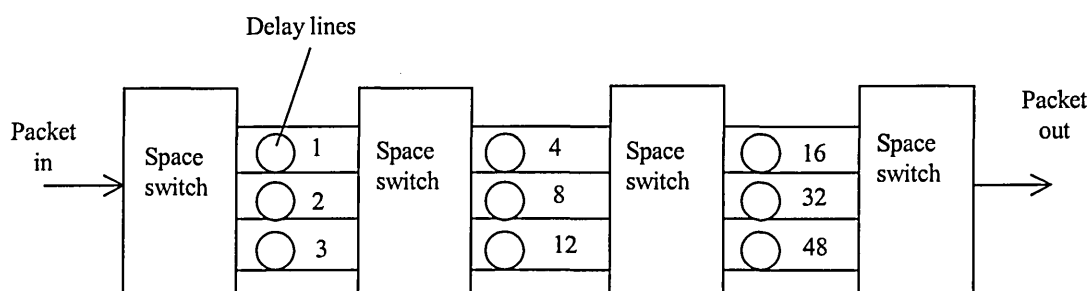
Note: The numbers represent the delay in units of packet length

Figure 8.10 Optical buffer design

161

Figure 8.11 depicts an example of how the buffers are used with this arrangement. In this example three packets arrive simultaneously at input ports 1 and 2. Packets 1a, 1b, 2a, 2b are set to exit at output port 2, and packets 3a and 3b at output port 1.

At Stage 1, packets 1a and 1b both arrive at their respective inputs. One packet can be switched by one of the 1x2 router elements and sent directly to the output port, here it is assumed that packet 1a is switched to the output first. The second packet can only be switched to output port 2 after one packet delay, thus it must be stored in the output buffer to avoid contention. The buffering of packet 1b is shown at the output port 2 as shown in Stage 2.

At Stage 3 packet 1b exits output port 2 and packets 2a and 2b enter the switch. Both these packets are to be switched to output port 2 so both enter the buffer section to output port 2 in their respective 1x2 switches.

At Stage 4, packet 2a exits to output port 2 and packet 2b uses the buffer at output port 2 for a packet period. At the input, packets 3a and 3b enter the switch and both are required to exit at the output port 1. As there are no packets in the path to output 1, then one packet can move directly to output port 1. It is assumed that this is packet 3b. Packet 3a is stored in the buffer at output port 1.

At Stage 5, packet 3a is able to exit to output port 1.
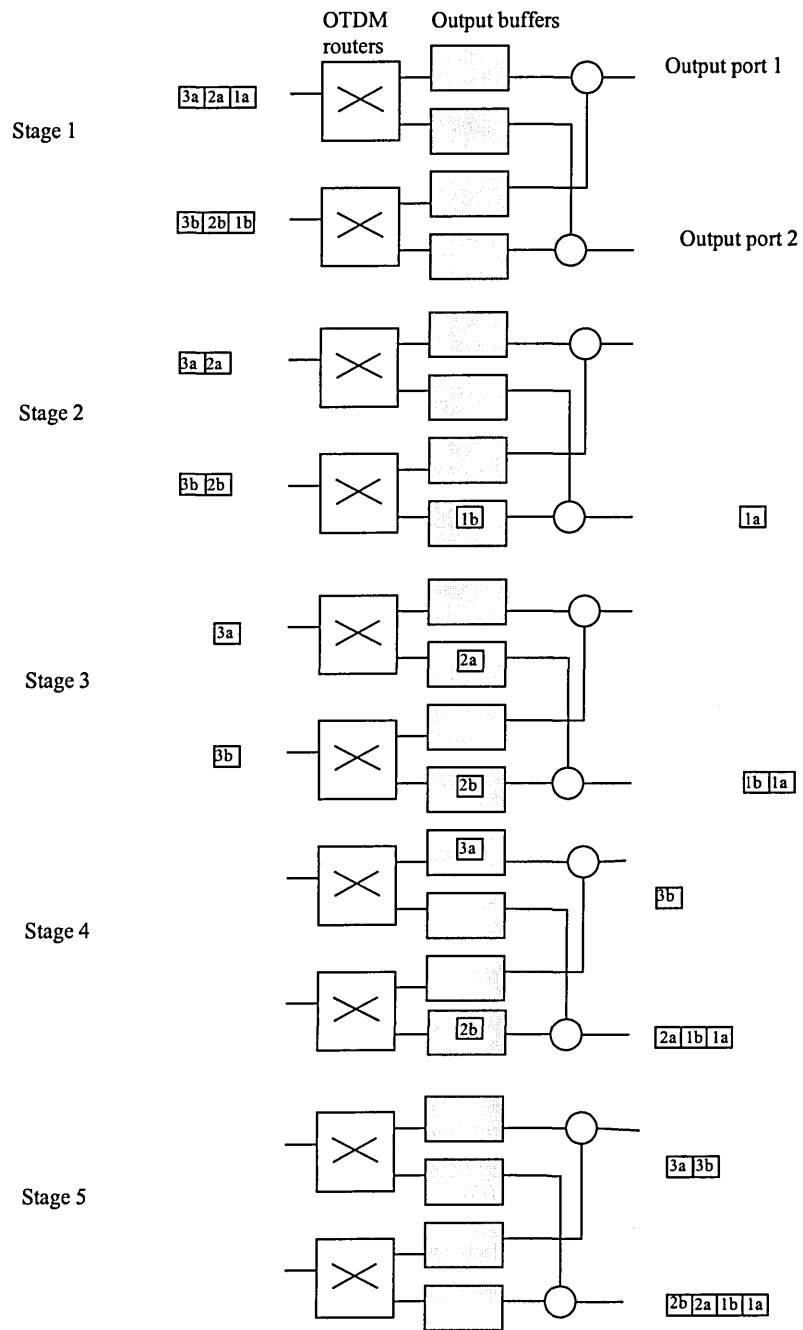
Figure 8.11 Operation of 2x2 OTDM router with output buffering
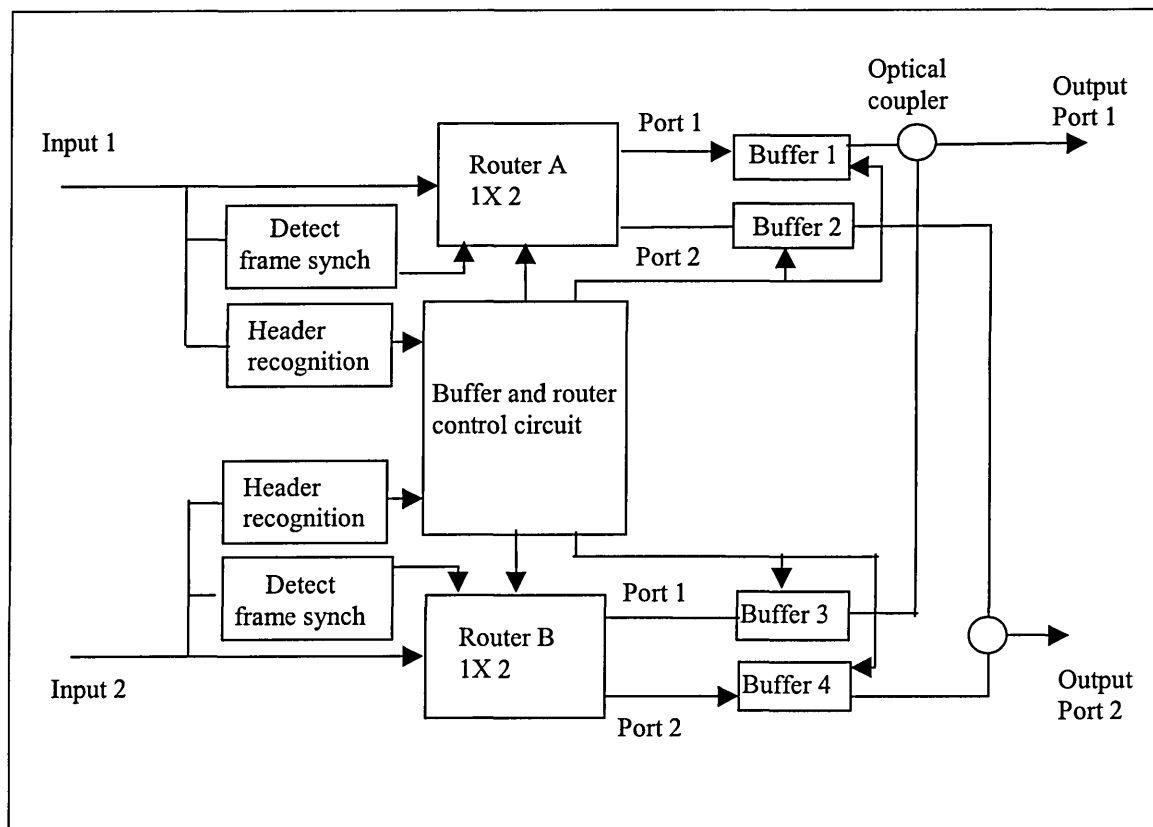
Figure 8.12 2x2 OTDM router with header recognition

Packet routing information is usually carried in a header that is transmitted with data. A number of header detection schemes have been described by Hunter et al [143]. Figure 8.12 shows the proposed architecture of the 2x2 router including header detection circuitry. It uses a buffer and router-control circuit that calculate all the buffering and switching requirements and ensure packet integrity while maximising throughput.
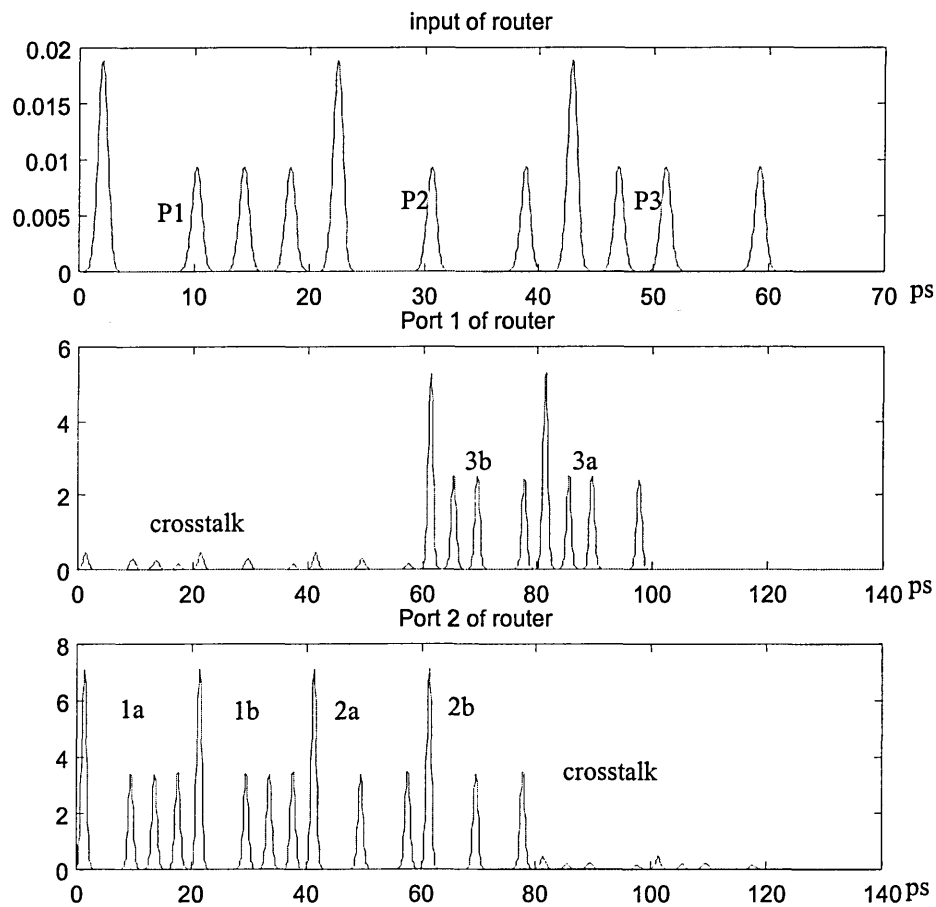
Figure 8.13 Waveforms of input and outputs of the router with output buffers

Simulate the optical 2x2 router with output buffers only using Matlab. Figure 8.13 shows the input and output waveforms of the 2x2 router. The same OTDM packet signals are simultaneously fed to the two inputs of the router. Packet 1 to 3 formats are 20111, 20101 and 21101, respectively. Observe that the packet consists of a frame signal, distinguishable by its higher amplitude, a bit address and payload information, which is in accordance to the format illustrated in Figure 8.2. Thus according to the routing convention established before packets one and two should be routed to port 2 whereas packet 3 should be routed to

165

port 1 as shown in Figure 8.13. The crosstalk has been observed in the outputs of the router. The number of buffers needed at the output is determined by the packet arrival statistics. It can be seen that optical buffers in the router are a much effective way of solving contention. But optical buffers increase the accumulation of intraband crosstalk and amplified spontaneous emission noise.

8.4 Multi-port Routers

8.4.1 Multi-port routers

A key advantage of 2x2 switching element is that it can be used to form larger routers. One example of a multiport packet switching network comprised of 2x2 switches is the Banyan network [145].
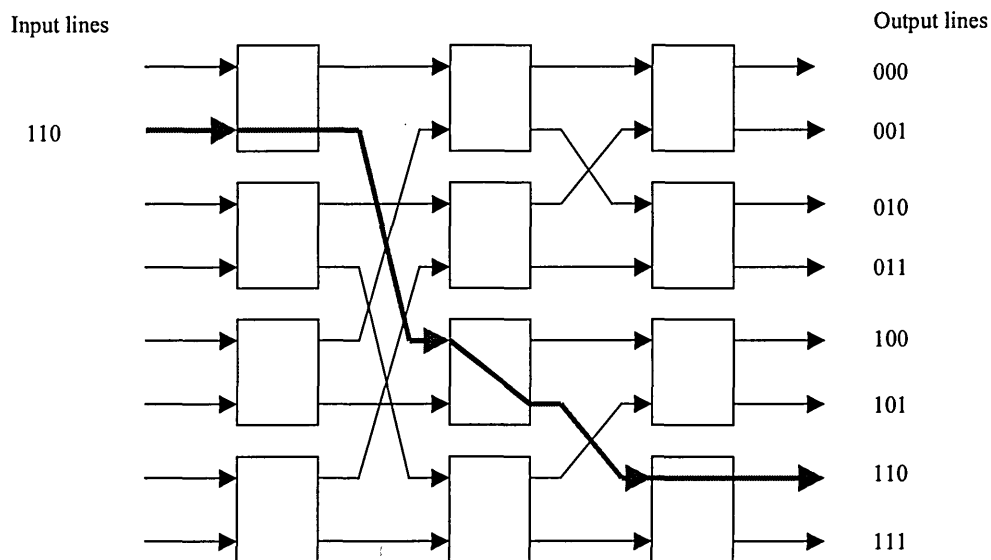
Figure 8.14 8x8 packet switch using a Banyan network architecture

An 8x8 Banyan design is shown in Figure 8.14. The 2x2 switches are connected in 3 column stages. The self-routing property of this network is best illustrated by an example. An input packet with address, say 110, is incident at one of the input ports. The first address bit determines the position of the first column stage switch, the second address bit the second column stage switch and likewise the third. With this addressing system, the packet is routed to output 110. The network design is such that this address will take the packet through to the same output as determined by the address label regardless of the input by which these packets enter the network.

The technique is scalable to larger switch arrays, e.g. a 16x16 network requires 4 column stages each with 8 2x2 switches.

Note that the Banyan network is not a non-blocking switch. To avoid collisions of packets having to traverse the same element, buffers can be used, or collisions can be avoided by using a sorting network such as a Batcher sorting network [147], so that routing paths do not cross.

The 2x2 switch described in this chapter could be used as a switching element in a Banyan network. The packet format shown in Figure 8.2 would then need to be modified to include 'N' address bits for a switch with 2^N ports. Each address bit identifies the state of the switch in one stage of the multistage switch.

One proposed way of physically selecting address bits is to select the relevant pulses at each stage using a TOAD that demultiplexes the relevant address bit in the time domain.

This has the advantage that it keeps all the processing on a single wavelength, i.e. OTDM. A schematic diagram of a 3 stage switch using such a TOAD to select the address bit for each switching stage is shown in Figure 8.15. This corresponds to the upper half of the switch architecture shown in Figure 8.12. $TOAD_1$ is used to identify the switch position for switch stage 1, $TOAD_2$ for switch stage 2 and $TOAD_3$ for switch stage 3. Different address bits can be selected at each stage by delaying the window function for each TOAD so as to be centred on the relevant address bit.
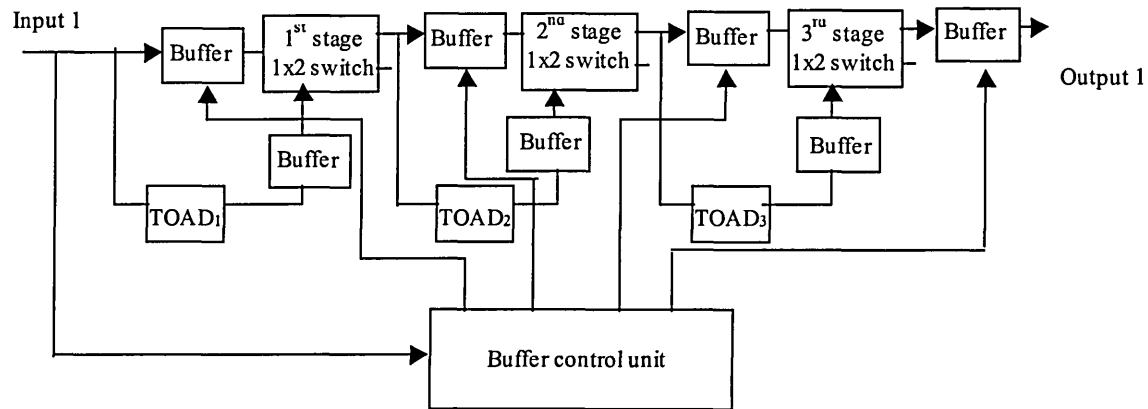
Figure 8.15 Three-stage switch using TOADs to identify each address bit

Note: An alternative approach is to use a separate wavelength for each address bit. So at each stage in the switch, the relevant address bit can be optically filtered and used to control that stage of the switch.

168

8.4.2 Throughput

The proposed optical router is efficient in terms of throughput. In this proposed optical router design, the throughput is determined from the proportion of header bits in the overall frame, and the size of the guard band. The maximum capacity is therefore given when:

Throughput efficiency (η) $= [P/(P+F+N+G)] \times 100\%$ (8.8)

where P is total number of bits in the payload, N is number of bits in the address field, F is number of bits in the frame field, and G is time interval of the Guard band (in bits).

For example, for a frame with a payload of 200 bytes (=1600 bits), an 8 bits address field, an 8 bits frame field and a guard band of 16 bits, then the throughput efficiency is:

$\eta = [1600/(1600+8+8+16)] \times 100\% = 98\%$

For a router with 2^N ports, the maximum throughput is given by:

$$H_{max} = \left(\frac{2^N}{T}\right)\eta \qquad \text{(bits/sec)} \qquad (8.9)$$

where T is the bit period.

So for a bit period of 10 ps the maximum throughput of the router is ($2^N \times 100 \times 0.98$) Gbit/s. The maximum throughput scales exponentially with the number of ports on the router, thus for a 16 port router the maximum throughput is approximately 1.568 Tbit/s.

169

The advantage of this OTDM router design is that it is capable of very high speed routing as shown in the previous derivation. The header processing, which is electronic, will be at a much lower speed, and must be completed within the length of a packet. So for a packet with 1600 bits and a bit period of 10 ps, the processing must be completed in 16 ns. This is achievable with standard silicon processing circuits [148].

8.5 Crosstalk Analysis of Multiport Router

With the advent of advanced optical technology and devices, a new class of all optical routing systems is emerging [149-152]. Such systems generate optical crosstalk, which can lead to a significant degradation in network performance. Here crosstalk of an all-optical router for routing optical data packets is determined from an analysis that uses a mathematical model developed by the author. There are two routing configurations to be considered, i.e. series and parallel. Such configurations generate two types of crosstalk, inter-channel crosstalk *CXT* and residual crosstalk *RXT*. The former is caused by non-target channels appearing within the switching window, the latter is due to the slight difference in CW and CCW gain/phase during the recovery period within the router. Details of an analysis to determine the residual and inter-channel crosstalk in router can be found in [71]. Using this technique the crosstalk of an 8x8 Banyan network architecture based on series and parallel router configurations is investigated. Predicted and simulated (for one specific path) results are presented.

8.5.1 Series configuration
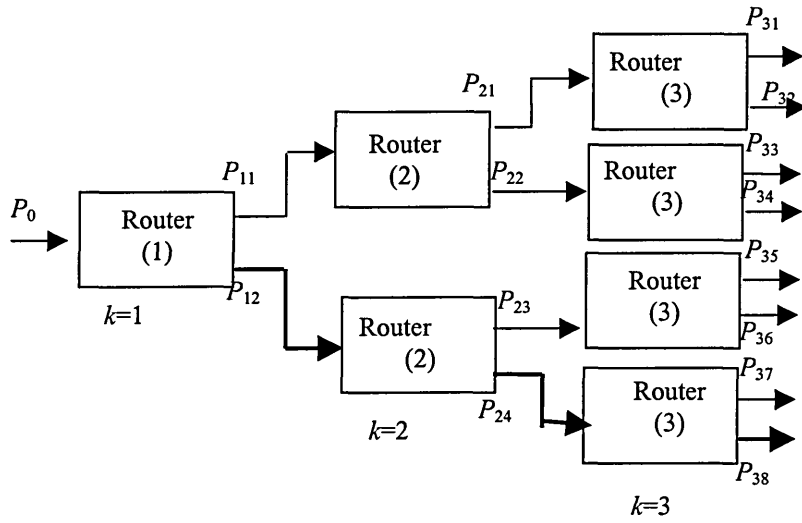
Figure 8.16 Series router configuration

Figure 8.16 is a block diagram of a three-stage 1 x N series router. All of the router is based on the TOADs as described in Section 5.5. Here consider the crosstalk at each stage, for the worst path, which is shown as solid arrows in Figure 8.16.

The signal power at the output port 2 of the first stage router is given by:

$$p_{12} = p_0 \cdot (1 + CXT_1 + RXT_1) \qquad (8.10)$$

where p_0 is the input signal power, and RXT_1 and CXT_1 are the respective residual and inter-channel crosstalk at port 2 (reflection port), respectively.

Similarly at the output of the 2nd and 3rd stages, the respective signal power is given as:

$$p_{24} = p_{12} \cdot (1 + RXT_2 + CXT_2) \qquad (8.11)$$

$$p_{38} = p_{24} \cdot (1 + RXT_3 + CXT_3) \qquad (8.12)$$

In general, the signal power at the output of the kth stage is defined as:

$$
\begin{aligned}
p_k &= p_{k-1}[1 + RXT_k + CXT_k] \\
&= p_0[1 + RXT_1 + CXT_1][1 + RXT_2 + CXT_2] \\
&\quad \cdots\cdots \quad \cdot [1 + RXT_k + CXT_k]
\end{aligned}
\qquad (8.13)
$$

For a series configuration, the normalised crosstalk at any stage is defined as:

$$X_{ct} = \frac{p_k - p_0}{p_0} \qquad (8.14)$$

Here, it is assumed that both RXT_k and CXT_k are the same for each individual 1x2 router as determined from the component parameters. The total router crosstalk is then $XT_T = RXT + CXT$.

Substituting for p_k in (8.14) results in:

$$
\begin{aligned}
X_{ct} &= (1 + XT_T)^k - 1 \\
&= kXT_T + \frac{k(k-1)}{2!}XT_T^2 + \cdots\cdots \frac{k!}{j!}XT_T^j
\end{aligned}
\qquad (8.15)
$$

From (8.15) it can be seen that the crosstalk X_{ct} depends on the network size k, RXT and CXT, but is independent of the input signal power.

172

8.5.2 Parallel configuration
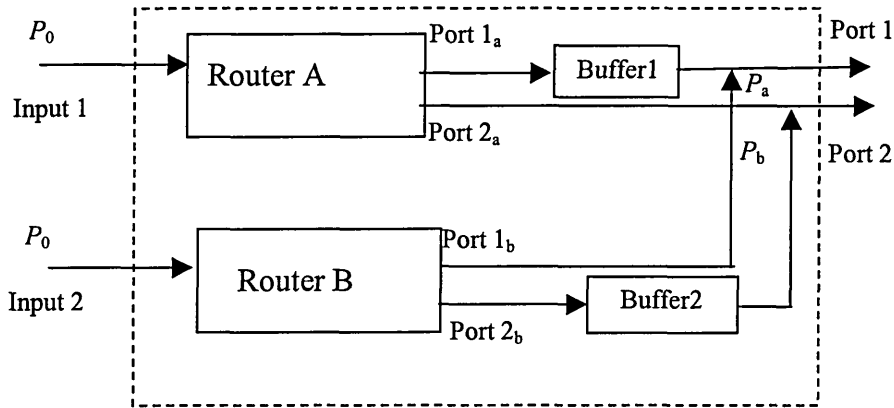
Figure 8.17 Parallel router configuration

Figure 8.17 shows the block diagram of a 2x2 parallel router configuration. It is configured from two 1x2 routers (A and B) and two buffers (buffer 1 and buffer 2). Optical buffers are used to eliminate contention at the outputs. Data can be stored in the buffers or passed straight through without delay. When two optical packets are received simultaneously at the inputs and are required to be routed simultaneously to the same output port via switching elements, only one can exit at the output port at any one time and the other is stored in the buffer. In this example it is assumed that a packet from router A is switched first, whereas the packet from router B is stored in buffer to avoid a contention at output port 2.

The signal powers at the output port 2 of router A and router B are given respectively as:

$$p_a = p_0 \cdot [0(1) + RXT_a + CXT_a] \tag{8.16}$$

173

$$p_b = p_0 \cdot [1(0) + RXT_b + CXT_b] \tag{8.17}$$

The output power at port 2 of the composite router can be expressed as:

$$
\begin{aligned}
p(2) &= p_a + p_b \\
&= p_0 \cdot [0(1) + RXT_a + CXT_a] \\
&\quad + p_0 \cdot [1(0) + RXT_b + CXT_b] \\
&= p_0 \cdot (1 + RXT_a + CXT_a \\
&\quad + RXT_b + CXT_b)
\end{aligned}
\tag{8.18}
$$

Similarly, the output power at port 1 can be determined in a similar manner to the procedure used to derive (8.18). In this case the crosstalk RXT and CXT are with smaller values compared to these at port 2. Here the signal at output port 2 is only considered, which is the worst case crosstalk optical path for this configuration.

For simplicity, it is assumed that RXT and CXT for both A and B are the same. Then the signal power at output port 2 of the router is given by:

$$p(2) = p_0 \cdot (1 + 2XT_T) \tag{8.19}$$

Similarly, the output power of n parallel routers can be expressed by

$$p(2) = p_0 \cdot (1 + nXT_T) \tag{8.20}$$

Again the normalised crosstalk of the parallel configuration is defined by

$$
\begin{aligned}
X_{ct} &= \frac{p(2) - p_0}{p_0} \\
&= nXT_T
\end{aligned}
\tag{8.21}
$$

8.5.3 Case study
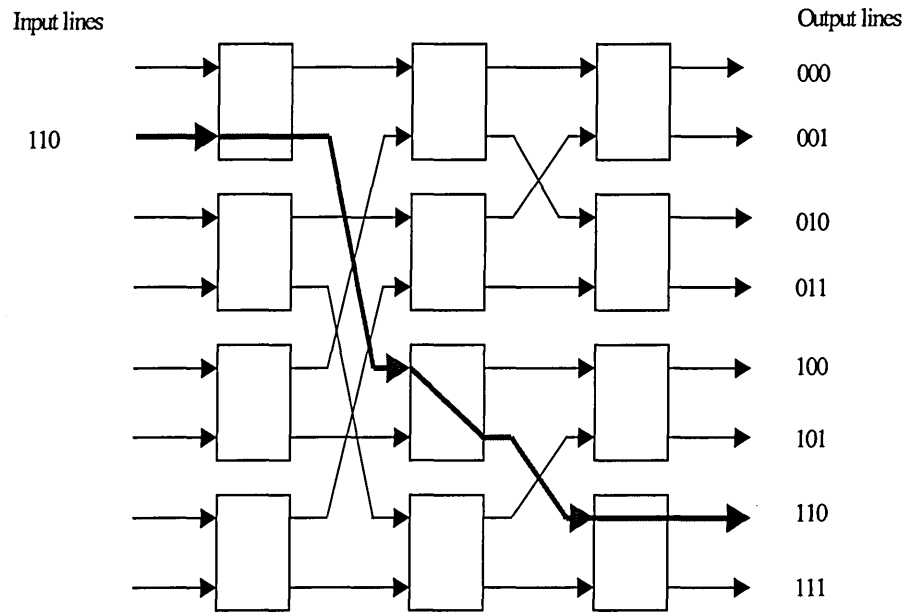
Figure 8.18 8x8 Banyan network architecture

Figure 8.18 shows an 8x8 Banyan router design composed of parallel router elements connected in series. Each router element is basically a 2x2 parallel configuration as shown in Figure 8.17. A signal will pass through three stages, before reaching the output. At each stage, the crosstalk is due to two parallel router, and for this network the crosstalk at any output port following the approach given in Section 8.5.1 is given by:

$$X_{ct} = \left(1 + XT'_T\right)^k - 1, \tag{8.22}$$

where, $k = 1, 2, \ldots n$ represents the number of series stages and $XT'_T = RXT'' + CXT''$.

RXT'' and CXT'' are the residual and inter channel crosstalks of an individual 2x2 router, respectively, defined as:

$$RXT' = n \cdot RXT \qquad (8.23)$$

$$CXT' = n \cdot CXT \qquad (8.24)$$

where n is the number of the parallel routers. In this case $n = 2$.

For an 8x8 Banyan network, the number of series stage $k = 3$, and substituting (8.23) and (8.24) into (8.22) gives the output crosstalk as:

$$X_{ct} = (1 + 2RXT + 2CXT)^3 - 1 \qquad (8.24)$$

8.5.4 Simulation results

The crosstalk of a cascaded 2x2 router network is calculated using equation 8.22 for the best and worst case values of XT_T, and the results are shown in Figure 8.19. For a 2x2 router, the best and worst cases refer to the crosstalk at port 1 (transmission) and port 2 (reflection), respectively. Parameters used in the simulation and subsequent calculation are those given in [71] with additional are given in Table 8.2. The solid line in Figure 8.19 represents the crosstalk for the worst case where $XT_T = -26.58$ dB, and the dotted line represents the best case crosstalk where $XT_T = -30.68$ dB. The values of XT_T were obtained from [71]. Based on a mathematical model of the all-optical router employing TOAD [71],

simulated crosstalk for 8x8 Banyan network for a particular path as highlighted path is also shown in Figure 8.19. As expected, the crosstalk increases with the number of router stages. Simulation results show that the crosstalk induced power penalty depends on the crosstalk contributed by the individual 2x2 switches as well as on the size and architecture of the switching fabric.

Table 8.2. Packet parameters for crosstalk simulation in Banyan network

Parameters	Values
Framing bits per packet	1
Address bits per packet	3
Payload bits per packet	2
Guard-band between packets	12 ps
Bit period	4 ps
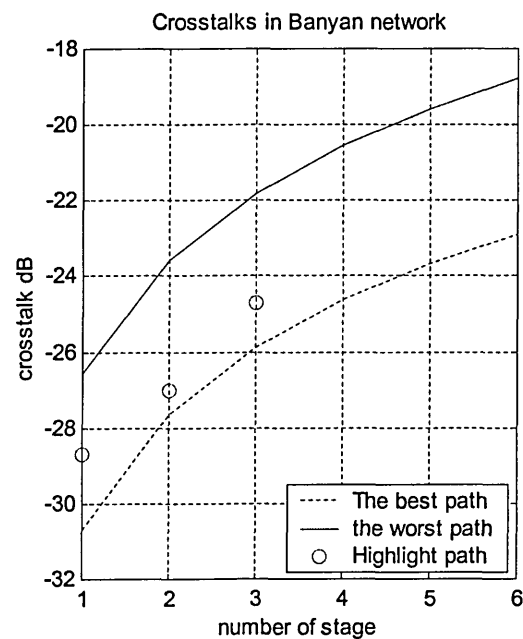
Figure 8.19 Crosstalk of 8x8 router against the number of stage

As experimental work reported shows that at bit rates of 10 Gb/s typical value of optical signal-to-noise ratio is expected to be greater than 25 dB [140] to maintain an acceptably low bit error rate, which corresponds to crosstalk values of less than -18.24 dB, and crosstalk calculations for an 8x8 Banyan network employing the proposed router show that the performance is better than -21 dB for the worst case scenario. Therefore, the crosstalk of the proposed router does not limit its performance with up to 6 stages.

8.6 Summary

In Chapter 8, new models of all optical router with multi-input and outputs have been further developed, i.e. 1x4 router, 2x2 router, which are based on 1x2 TOAD routers. Crosstalk of all optical routers has been investigated using a mathematical model developed by the author. Simulations show that the models can recognise the address bits and route optical packets for containing data with a bit period of only 4 ps, which corresponds to a 0.25 Tb/s bandwidth optical network.

The crosstalk performance of 1x4 router has been investigated and the results has been compared to a 1x2 router. Results show that threshold switching energy is present at 0. 2 pJ. Higher values result in a decrease in crosstalk by about 0.5 dB at 1.9 pJ energy. Lower values result in negligible switching.

Analysis of residual crosstalk and neighbour channel crosstalk of all optical routers with multi-input and outputs in Banyan networks has also been carried out. It is shown that crosstalk induced penalty depends on the crosstalk level of individual 2x2 switches as well as on the size and architecture of the switching fabric. Crosstalk calculations for 8x8 Banyan network employing the proposed router shows that performance better than – 21 dB can be achieved even at the worst case scenario, which is comparable with practical devices used in routing.

It is believed that the proposed configurations are promising as components for high-speed all optical TDM networks due to its ultrafast switching capability.

Chapter 9

Conclusions and Further Works

9.1 Conclusions

The primary objective of the work presented in this thesis is to design and analyse an all optical router based on TOADs using OTDM in high-speed communication systems. In order to carry out this task, it is first necessary to fully understand the characteristics of optical communication systems. From the review carried out in Chapter 2, it is clear that communication technology has made significant advances with the improvement of semiconductor technology and system development. Traditional communication techniques based on electronics are now being challenged by new optical systems. In new optical system networks, the tardy opto-electrical (O/E) or electro-optical (E/O) conversions that are inherent in common fibre network systems are avoided. Consequently, there is a significant reduction in bandwidth bottlenecks resulting in superior quality of service (QoS) standards. To date most research on optical networking has concentrated on wavelength-division multiplexing (WDM), which routes different packets according to the wavelength of the optical carrier. Optical time-division multiplexing (OTDM) is considered as an alternative to WDM for future networks which utilise a single wavelength at high (> 100 Gbit/s) data rates. In OTDM networks many signals are combined before being transmitted using a single wavelength. Each signal from a lower bit-rate source is broken up into many segments (slots), each having very short duration and multiplexed in a rotating repeating

sequence (i.e. round robin fashion) onto a high bit-rate transmission line. The use of short duration (soliton) pulses allows information to be transmitted at very high bit rates (>100 Gb/s). An asset of OTDM is its flexibility, the scheme allows for variation in the number of signals being sent along the line, and constantly adjusts the time intervals to make optimum use of the available bandwidth. Consequently, it is believed that OTDM networks are excellent candidates for meeting the future system requirements for massive ultrafast networks. To realise all optical communication systems, the all-optical router is potentially a key device. Therefore this work has focused on the investigating the potential of the all optical router in high-speed lightwave systems.

When evaluating all optical routers used in high speed lightwave systems, the important criteria are switching time, repetition rate, control pulse energy, and practicality. From the review of current optical routing techniques presented in Chapter 3, it may be concluded that the most likely candidate for an optical router is TOAD. Its low control energy requirement, reasonable noise figure, integratability, and overall practicality distinguish it among other similar all optical routers. Therefore TOAD has been adopted to investigate the performance of all optical routers in this work.

The operational principle of the all-optical TOAD router is based on the nonlinear properties of the semiconductor laser amplifier. The theoretical backgrounds of the SLA were described in Chapter 4. There are two fundamentally different types of optical amplifiers, semiconductor laser amplifiers (SLAs) and fibre amplifiers. Semiconductor laser amplifiers have a distinct advantage over fibre amplifiers in that they can be used for optical switching. A semiconductor laser amplifier is based on a semiconductor laser structure and the interface between the signal is formed from the coupling of an optical

fibre to an area of semiconductor. The efficiency obtainable from this coupling is a main contributor to the coupling loss of these devices. A description of SLAs was given with the accompanying equations that described the characteristics of the device under continuous wave input. The concept of noise and how it originates from amplified spontaneous emission were described and its contribution to receiver generated noise was shown with the introduction of noise equations. Pulse amplification in TWSLAs was reviewed and the special case of ultrashort pulse amplification was discussed. Models of the SLA were described in this Chapter.

Based on mathematical models of SLAs given in Chapter 4, Chapter 5 described the models developed by the author to simulate the routing action of all optical router based on terahertz optical asymmetric demultiplexer (TOAD). For modelling purposes the TOAD was divided into three components: fibre coupler, fibre loop and non-linear element (SLA). The first functional component to be modelled is the input-output coupler. The fibre loop is assumed initially to consist of a simple time delay until a later section when the polarisation and briefringence effects are considered. Fundamental to loop operation is the asymmetry of the SLA and its effect on the router performance was investigated. Equations to describe the special case of small asymmetry were developed in Section 5.4 and loop performance was investigated by looking at the switching resolution of the system and adjacent pulse crosstalk were taken into account. To investigate the performance of the router, the mathematical model of router was developed for evaluating the switching window. The mathematical models were also used for optimisation of the device parameters for maximising peak transmittance of the switching window. A new analytical expression was developed to calculate the width of the all-optical switching window. Using a new convolution approach, the profile of the switching window can be determined. In the router

model, the switching energy of control pulse is optimised for maximising the transmission gain of the switching window.

To simulate the all optical router, the Matlab engineering software package has been used to produce a complex software tool, which was found to be very useful in implementing the system in hardware. The simulation package incorporates a graphical user interface through which the user can look at all aspect-functions of the all optical router. Furthermore, simulation results indicate that the system measurements were carried out effectively and accurately.

In Chapter 6 mathematical expressions for evaluating the crosstalks of the all optical router have been developed, which were used to analyse the relative intensity noise, the residual crosstalk and the neighbour channel crosstalk characteristics of the router. The noise and crosstalk analyses of the router were discussed. It was found that noise and crosstalk are largely independent of the initial gain of the SLA located asymmetrically with the fibre loop. Apart from that, the dependence of the noise and crosstalk on the other parameters displayed complex characteristics.

In an OTDM based network employing all optical routers, system bit error rate (BER) performance is limited by a number of additional noise sources due to the router. This work, described in Chapter 7, investigated the theoretical BER performance of OTDM systems. In this study it has been shown that the two factors, the channel crosstalk, and the relative timing jitter associated with the non-linear switching element play a major role in determining the overall system performance. The analysis reported in the thesis describes a system comprising an all optical router, OTDM demultiplexer, optical pre-amplifier and

optical receiver. To fully evaluate the OTDM system performance, a number of noise sources such as: bit pattern noise of the router due to crosstalk; the intensity noise of the router due to timing jitter between the control and signal pulses; interferometer noise and other noise sources were taken into consideration. This chapter also investigated the characteristics of these noise sources at data rate exceeding 100Gb/s, and an expression was developed for the overall system BER. For BER analysis, the switching window within the router is treated as a rectangular shape. Calculations based on the real switching window shapes enabled estimation of the timing tolerance width for combining control and signal pulses at the input of the router.

The power penalty, defined as the difference between the minimum average received optical power levels at BER of 10^{-9} of the signal at the output of the transmitter and the router, was also studied. The mathematical models developed in this thesis can be used to evaluate the BER performances of OTDM systems for various system parameters. BER analysis of packet based high-speed OTDM system employing all optical routers has been studied using a mathematical model considering the time jitter, crosstalk due to the router and demultiplexer, and the noises due to the receiver. The OTDM channels used in the analysis are 10 and 100 for the 100 Gb/s signal, 30 and 300 for the 300 Gb/s signal.

Section 7.4 predicted power penalties from BER simulation results based on the proposed optical receiver model. The simulation results showed that the router intensity noise plays a critical role in the system performance, which needs to be kept at $< 10^{-3}$. To achieve a power penalty of 1.5 dB at 100 Gb/s, it is essential that the crosstalk is less than -20 dB. The simulation results can be considered as an example of BER analysis using the mathematical models developed by the author. Using the same procedures of BER

calculation, power penalties for different values of system parameters can be evaluated and compared.

Bit-error-rate comparisons of all optical routers at different bit rates from 100 Gb/s to 300 Gb/s bit rates have been carried out. The bit-error-rate performance can be maximised by plotting the power penalty against different values of the TOAD parameters. SLA length and SLA asymmetry are the two key parameters which affect the power penalty of the router. The device parameters of the all optical router have been optimised for minimising the power penalty at the bit rates from 100 Gb/s to 300 Gb/s.

In Chapter 8, new models of all optical router with multi-inputs and multi-outputs have been developed further, i.e. 1x4 router, 2x2 router. Analyses of the residual crosstalk and the neighbour channel crosstalk of all optical routers with multi-inputs and multi-outputs in Banyan networks have been carried out. It was shown that the crosstalk induced penalty depends on the crosstalk level of individual 2x2 switches as well as on the size and architecture of the switching fabric. Crosstalk calculations for an 8x8 Banyan network employing the proposed router showed that performances better than − 21 dB can be achieved even in the worst case scenario, which is comparable with practical devices used in routing.

In summary, this thesis has presented the design, analysis, simulation and results of all optical routers based on TOADs using OTDM scheme. The primary objective of this study was to investigate the potential of the all optical router based on TOADs in high-speed lightwave systems. The noise and crosstalk characteristics of router have been addressed.

9.2 Further work

So far the theoretical analysis of the performance of all optical routers based on TOADs has been investigated. A practical test bed should be set up to test performance issues including, but not limited to: network throughput; latency; packet loss; scalability; crosstalk and dispersion. The performance of the all optical router can be improved experimentally by using the practical test bed.

As described in Chapter 5, in the all optical router based on TOADs, the target channels are routed by control pulses, which periodically change the carrier dynamics of the SLA. The carrier density of the SLA is firstly depleted by a control pulse, which then recovers back to the equilibrium level for the next cycle of the carrier dynamics to begin. Two problems arise. One is the highest bit rate of the individual OTDM channel, which is restricted by the recovery time of the SLA. In the router model, the recovery time of the SLA is assumed to be 100 ps, which is equivalent to the baseband bit rate of 10 Gb/s. For a further increase of baseband bit rate, the recovery time of the SLA needs to be decreased for stable operation. The shortest recovery time of the current state-of-the-art SLA is about 100 ps, which limits the highest baseband bit rate to 10 Gb/s. R.J.Manning and D.A.O Davies demonstrated that the recovery time of an SLA can be shortened to less than 10 ps, provided that a continuous light beam passes through the SLA [153][154]. If the bit rate of the OTDM channels is increased to greater than 10 Gb/s, the router model in Chapter 5 needs to be modified to incorporate the effect of the continuous light beam into the routing mechanism. On the other hand, a problem arises when the length of the packet is longer than 100 ps. To route the whole packet to the destination port, a series control pulse will be required to keep the

SLA saturated until a whole packet passes through the router. How the periods of control signals affect the packet routing needs to be investigated.

As components used to construct multi-node architectures are expensive, simulating these architectures has significant advantages for investigating nodes of any size and with different configurations. Based on the single node of all optical router, the multi-node architectures should be further simulated. Various characteristics should be investigated against different system parameters such as: packet size, node size, bit-rate, and so on.

During the routing processing, more attention should be paid to the header detection, synchronisation, packet width and the width of switching window.

It was not a requirement of this PhD project to implement the all-optical communication system in hardware. However, it is recommended that further research work should carry out a hardware design so that measurements may be taken. However, it is expected that measurement results will agree closely with the theoretical and simulation results.

Reference:

[1] D. Cotter, "High-speed digital optical networking", *Lasers and Electro-Optics Society Annual Meeting, LEOS '98. IEEE*, Vol. 1, 1-4, pp. 231 –232, Dec 1998.

[2] P. Green, "Progress in optical networking" *IEEE communications Magazine*, pp. 54-61, Jan 2001.

[3] V. Chan, L. Hall, E. Modiano, K. Rauschenbach, "Architectures and technologies for high-speed optical data networks", *Journal of Lightwave Technology*, Vol. 16, No. 12, pp. 2146-2168, December 1998.

[4] A.H, Gnauck, "High-speed lightwave systems", *Communications, 1992. ICC 92, Conference record, SUPERCOMM/ICC '92, Discovering a New World of Communications. IEEE International Conference on*, vol. 2, 14-18, pp. 733 –737, Jun 1992.

[5] Y. Lu, J. Lin, "Future all-optical networks", *Info-tech and Info-net, 2001. Proceedings. ICII 2001 - Beijing. 2001 International Conferences on*, Vol. 2, pp. 193 –198, 2001.

[6] "IEE colloquium 'Towards terabit transmission' (Digest No.1995/110)" *Towards Terabit Transmission, IEE Colloquium on*, 19 May 1995.

[7] G. Eisenstein, R.S. Tucker, S.K. Korotky, "Multi-gigabit per second optical time-division multiplexed systems", *Optical Communication, 1988. ECOC 88. Fourteenth European Conference on* (Conf. Publ. No.292), vol.1. 11-15 pp. 461-462, Sep 1988.

[8] K.Uchiyama, T. Morioka, "All-optical signal processing for 160 Gbit/s/channel OTDM/WDM systems", *Optical Fibre Communication Conference and Exhibit*, vol. 4, pp. ThH2 -T1-3, 2001.

[9] A.G. bell, "Selenium and the photophone", *The Electrician*, pp. 214,215,220,221, 1880.

[10] D. Hondros, P. Debye, "Elektromagnetische Wellen An Dielektrischen Draehten", *Annal Physik.*, 4 Folge, 32, pp. 465-476.

[11] K.C. Kao, and G.A. Hockamm, "Dielectric fibre surface waveguides for optical frequencies", *Proc. IEE*, 113, (7), pp. 1151-1158, 1996.

[12]   J.K. Lucek, R.J. Manning, K. Smith, "Recent advances in photonic processing", Lasers and Electro-Optics Society Annual Meeting, IEEE, Vol. 1, 31, pp. 37 – 38,1994.

[13]   K. Kikuchi, "Wideband and flat supercontinuum generation from optical fibres and its applications", *Lasers and Electro-Optics, 1999. CLEO/Pacific Rim '99. The Pacific Rim Conference on*, Vol. 1, pp. 17-18, 1999.

[14]   A. R. Chraplyvy, "New fibres for long-haul transmission", *Lasers and Electro-Optics Society Annual Meeting, 1995. 8th Annual Meeting Conference Proceedings*, Vol. 2, 30, pp. 46, Oct. 1995.

[15]   T. Sakurai, "Femtosecond technology: a new industrial technology platform", *Lasers and Electro-Optics Society*, Vol. 1, pp. 3–4, 2001.

[16]   H. Takara, K. Uchiyama, I.   Shake, T. Morioka, "Ultra-high speed OTDM transmission systems and sub-systems", *Lasers and Electro-Optics, Technical Digest. Summaries of papers presented at the Conference on*, pp. 526 –527, 2001.

[17]   H.G. Weber, R. Ludwig, U. Feiste, C. Schmidt, C. Schubert, J. Berger, E. Hilliger, M. Kroh, T. Yamamoto, "High-speed all-optical signal processing in optical communication systems", *Lasers and Electro-Optics, 2002. CLEO '02. Technical Digest. Summaries of Papers Presented at the Conference on*, Vol. 1, pp. 610, 2002.

[18]   J. Zhang; "Very-high-speed fibre-optic networks for broadband communications", *Electronics & Communication Engineering Journal*, Vol. 8, Issue 6, pp. 257 –268, Dec. 1996.

[19]   R.S. Tucker, G. Eisenstein, S.K. Korotky, "Optical time-division multiplexing for very high bit-rate transmission", *Journal of Lightwave Technology*, Vol. 6 Issue, 11, pp. 1737 –1749, Nov 1988,

[20]   D.M. Spirit, A.D. Ellis, P.E. Barnsley, "Optical time division multiplexing: systems and networks", *IEEE Communications Magazine*, Vol. 32 Issue, 12, pp. 56 –62, Dec. 1994.

[21]   D. Cotter, J.K. Lucek, D.D. Marcenac, "Ultra-high-bit-rate networking: from the transcontinental backbone to the desktop", *IEEE Communications Magazine*, Vol.. 35 Issue, 4, pp. 90 –95, Apr. 1997.

[22]   http://www.cisco.com/univercd/cc/td/doc/product/mels/dwdm/dwdm_fns.htm

[23]   M. Saruwatari, "All-optical signal processing for terabit/second optical transmission", *IEEE Journal on Selected Topics in Quantum Electronics*, Vol. 6, Issue 6, pp. 1363 –1374, Nov. 2000.

[24]   J. Zhang, "Very high speed fibre optic networks for broadband communications", *Journal of IEE Electron. & Comm. Eng.*, pp.257-268, December 1996.

[25]   P. Prucnal, "Advances in ultra-high speed optical TDM networking", *Lasers and Electro-Optics Society IEEE*, Vol. 2, pp. 590, 1999.

[26]   I.Y. Khrushchev, I.H. White, R.V. Penty, "High-quality pulse compressor for WDM/OTDM applications", *IEE Colloquium on High Speed and Long Distance Transmission (Ref. No. 1999/022)*, pp. 8/1 -8/4, 1999.

[27]   M.Saruwatari, "Ultrafast photonic devices for tera-bit/s optical TDM/WDM communications", *Lasers and Electro-Optics, 1999. Conference on CLEO/Pacific Rim '99*, Vol. 1, pp. 114 –115, 1999.

[28]   I.H. White, M. Owen, M.F.C. Stephens, P. Vasil'ev, J.D. Bainbridge, R.V. Pentry, "WDM and hybrid WDM/OTDM applications of the multi-wavelength grating cavity (MGC) laser", *Fifth Asia-Pacific Conference on Communications, APCC/OECC '99*. Vol. 2, pp. 1429 –1431, 1999.

[29]   K. Seppanen, "Shared OTDM packet compressor and decompressor", *Electronics Letters*, Vol. 36 Issue 25, pp. 2090 –2092, Dec. 2000.

[30]   I. Glesk, J. P.Sokoloff, and P.R. Prucnal, "Demonstration of all-optical demultiplexing of TDM data at 250 Gbit/s," *Electron. Letter*, 30, pp.339-341, 1994.

[31]   I. Morita, N. Edagawa, "Study on optimum OTDM signals for long-distance 40 Gbit/s transmission", *Optical Fibre Communication Conference and Exhibit*, pp. 5 –6, Mar. 2002.

[32]   A.D. Ellis, M.C. Tatham, D.M. Spirit, D.A.O. Davies, D. Nesset, D.G. Moodie, G. Sherlock, "Ultra high speed OTDM over standard fibre", *IEE Colloquium on Towards Terabit Transmission*, pp. 9/1 -9/4, May 1995.

[33]   H.N. Poulsen, K.S. Jepsen, A.T. Clausen, A. Buxens, K.E. Stubkjaer, R. Hess, M. Dulk, G. Melchior, "Fast optical signal processing in high bit rate OTDM systems", *Lasers and Electro-Optics Society Annual Meeting, IEEE*, Vol.1, 1-4, pp. 67 –68, Dec 1998.

[34]   P.J. Delfyett, "Hybrid WDM - OTDM technologies using semiconductor optical amplifiers for networking, instrumentation and signal processing", *Semiconductor Device Research Symposium*, pp.589, 2001.

[35]   M. Nakazawa, T. Yamamoto, K. Tamura, "Ultra high speed OTDM transmission using femtosecond pulses", *The 4th Pacific Rim Conference on Lasers and Electro-Optics, 2001*, Vol. 1, pp. I-618 -I-619, 2001.

[36]   K. Rauschenbach, S. Finn, R. Barry, K. Hall, J. Moores, N. Patel, "100-Gbit/s time-division multiplexed multi-access networks", *Conference on Optical Fibre Communication*, Vol. 16, pp. 86 –87, Feb 1997.

[37]   P.R. Prucnal, K. Bergman, "TDM optical networks", *Conference Proceedings of Lasers and Electro-Optics Society Annual Meeting*, Vol. 1, 30-31 pp. 216 –217, 1995.

[38]   N.S.Patel, K.L.Hall, and K.A. Rauschenbach, "40 –Gb/s demultiplexing using an ultrafast nonlinear interferometer (UNI), " *IEEE Photo. Technol. Letter*, 8, pp.1695-1697, 1996.

[39]   B.K. Mathason, H. Shi, I. Nitta, G. A. Alphonse, J. Abeles, J. C. Connolly, and P.J. Delfyett, "Multiwavelength all-optical TDM switching using a semiconductor optical amplifier in a loop mirror," *IEEE Photo. Technol. Letter*, 11, pp.331-333, 1999.

[40]   S. Nakamura, Y. Ueno, K. Tajima, J. Sasaki, T. sugimoto, T. Kato, T. Shimoda, M. Itoh, H. Hatakeyama, T. Tamanuki, and T. Sasaki, " Demultiplexing of 168-Gb.s data pulses with a hybird-integrated symmetric Mach-Zehnder all-optical switch", *IEEE Photon. Technol. Letter*, 12, pp. 425-427, 2000.

[41]   K.J. Blow, N. J. Doran, and B.K. Nayar, " Experimental demonstration of optical soliton switching in an all-optical nonlinear Sagnac interferometer," *Optics Letters*, 14, pp. 754-756, 1989.

[42]   M. Kane, I. Glesk, J. Sokoloff, and P. Prucnal, "Asymmetric optical loop mirror: analysis of an all-optical switch", *Applied Optics*, 33 (29), pp. 6833-6842, Oct. 1994.

[43]   K.S. Jepson, B. Middelsen, A.T. Clausen, H.N. Poulsen, K.E. Stubkjaer, M. Vaa, "High-speed OTDM switching", *Technical Digest. Summaries of papers presented at the Conference on Lasers and Electro-Optics,* pp. 1, May 1998.

[44]   H. Takara, "High-speed optical time-division-multiplexed signal generation" *Conference on Lasers and Electro-Optics*, pp. 234 –235, 2000.

[45]   S.P. Shipley, G.Gergious and A. C. Boucouvalas, " Compact all-fibre Mach Zender Devices", *IEE Proc. J.*, 134 (3), pp. 203-207, June 1987.

[46]   K.L. Kang, I. Glesk, T. G. Chang, P.R. Prucnal and R.K. Boncek, "Demonstration of all optical Mach-Zender Demultiplexer", *Electron Letter*, 31,(9), pp. 749-750, April 1995.

[47]   A. Strass, " OTDM switch on a chip blazes at 20 Gbit/s", *Lightwave*, pp. 14 June 1996.

[48]   J. Leuthold, J. Eckner, C. Holtmann, R. Hess and H. Melchior, "All optical 2x2 switches with 20 dB extinction ratios", *Electron. Letter*, Vol. 32, pp. 2235-2236, November 1996.

[49]   B. Y. Yu, P. Tollver, R.J. Runser, K. Deng; D. Zhou; I. Glesk, P.R Prucnal, "Packet-switched optical networks", *Micro IEEE*, Vol. 18 Issue 1, pp. 28 –38, Jan. 1998.

[50]   R.J. Manning, D.A.O. Davies, D. Cotter, and J.K. Lucek, "Enhanced recovery rates in semiconductor laser amplifiers using optical pumping", *Electron. Letter,* 30, pp.787-788, 1994.

[51]   B.S. Robinson, S.A.Hamilton, E.P. Ippen, "Multiple wavelength demultiplexing using an ultrafast nonlinear interferometer", *Technical Digest. Summaries of papers presented at the Conference on Lasers and Electro-Optics*, pp. 528, 2001.

[52]   K.L. Hall and K.A. Rauschenbach, "100-Gbit/s bitwise logic", *Optics Letters*, 23, pp. 1271-1273, 1998.

[53]   P.A. Andrekson, N.A. Olsson, J.R. Simpson, T. Tanbun-ek, R.A. Logan and M. haner, " 16 Gbit/s all optical demultiplexing using four wave mixing", *Electron, Letter*, 27, (11), pp. 922-924, May 1991.

[54]   T. Takiguchui, S. Kawanishi, H. Takara, O. Kamatani, K. Uchiyama, A. Himeno and K. Jinguji, "Dispersion slope equalising experiment using planar lightwave circuit for 200 Gbit/s time-division-multiplexed transmission", *Electron. Letter*, 32, (22), pp. 2083-3085, October 1996.

[55]   T. Morioka, S. kawanishi, H. Takara and M. Sarawatari, " Multiple-output 100 Gbit/s all optical demultiplexer based on multichannel four-wave mixing pumped by a linearly-chirped square pulse", *Electron. Letter*, 30, (23), pp.1959-1960, November 1994.

[56]   A. Buxens, H.N. Poulsen, A.T. Clausen, P. Jeppesen, "All-optical OTDM-to-WDM signal-format translation and OTDM add-drop functionality using bidirectional four wave mixing in semiconductor optical amplifier", *Electronics Letters*, Vol. 36 Issue 2, pp.156 –158, Jan. 2000.

[57]   S.Nakamura, Y.Ueno, and K. Tajima, "Ultrafast (200-fs switching, 1.5 Tb/s demultiplexing) and high repetition (10 GHz) operations of a polarization discriminating symmetric Mach-Zehnder all –optical switch," *IEEE Photo. Technology Letter*, 10, pp.1575-1577, 1998.

[58]   D.G. Moodie, M.J. Guy, M.J. Harlow, A.D. Ellis, C.W. Ford, S.D. Perrin, "High modulation depth electroabsorption modulator modules for OTDM systems", *IEE Colloquium on High Speed and Long Distance Optical Transmission*, pp. 5/1 -5/6, Apr 1996.

[59]   H. Takara, S. Kawanishi, T. Morioka, K. Mori, and M. Saruwatari, "100 Gbit/s optical waveform measurement with 0.6 ps resolution optical sampling using subpicosecond supercontinuum pulses," *Electron. Letter*, 30, pp. 1152-1153, 1994.

[60]   K. L. Deng, R.J. Runser, P. Toliver, C. Coldwell, D. Zhou, I. Glesk, P.R. Prucnal, "Demonstration of a highly scalable 100-Gbps OTDM computer interconnect with rapid inter-channel switching capability", *Electron. Letter*, 34, pp. 2418-2419, 1999.

[61]   J. Leuthold, P. A. Besse, E. Gamper, M. Dulk, S. Fischer, G. Guekos, and H. Melchior, "All-optical Mach-Zehnder interferometer wavelength converters and switches with integrated data and control signal separation scheme", *J. of Lightwave Technol.*, 17, pp. 1056-1066, 1999.

[62]   D. Lee; H. Yoon; N. Park; "Extension of dispersion decreasing fibre-pulse shaping method for the optical time division multiplexing system source applications", *The Pacific Rim Conference on Lasers and Electro-Optics*, Vol. 4, pp. 1071 –1072, 1999.

[63]   R.J. Runser, P. Toliver, I. Glesk, and P.R. Prucnal, "Expermental demonstration of 1.5 ps demultiplexing window for high speed optical networks using a forward–pumped mach-Zehnder TOAD", *Conference on Information Sciences and Systems*, pp.FP6-17, March, 2000.

[64]   S. Kawanishi, H. Takara, K. Ulchiyama, I. Shake, and K. Mori, "3 Tbit/s (160 Gbit/s x 10 ch) OTDM_WDM transmission experiment", *OFC/IOC '99 Postdeadline Papers*, pp. PD1-1, Feb. 1999.

[65]   J.P. Sokoloff, P.R. Prucnal, I. Glesk, and M. Kane, " A Terahertz Optical Asymmetric Demultiplexer (TOAD)", *IEEE Photon. Technol. Letter*, 5, pp. 787-790, 1993.

[66]   K. Uchiyama, T. Morioka, "All-optical time-division demultiplexing experiment with simultaneous output of all constituent channels from 100 Gbit/s OTDM signal", *Electronics Letters*, Vol. 37 Issue 10, pp. 642 –643, May 2001.

[67]   K. Uchiyama, H. Takara, K, Mori, T. Morioka, "160 Gbit/s all-optical time-division demultiplexing utilising modified multiple-output OTDM demultiplexer (MOXIC)", *Electronics Letters*, Vol. 38 Issue 20, pp. 1190-1191, Sep 2002.

[68]   C. Cheung, " Noise and Crosstalk Analysis of All Optical Time Division Demultiplexers", *Thesis of the degree of Doctor of Philophy*, pp.189, 2001.

[69]   D. Zhou, K. Kang, I. Glesk, and P.R. Prucnal, " An analysis of signal-to noise ratio and design parameters of a terahertz optical asymmetric demultiplexer", *Journal of Lightwave Technology*, Vol. 17, No 2, pp. 298-307, February 1999.

[70] K. Kang, I. Glesk, and P.R. Prucnal, "Ultrafast optical time demultiplexers using semiconductor optical amplifier2, *Int., J. high Speed Electron. System*, Vol. 7, No. 1, pp. 125-151, 1996.

[71] R. Gao, Z. Ghassemlooy, G. Swift, and P. Ball, "Simulation of all optical time division multiplexed router", *Proceedings of Photonics West 2001*, Vol. 4292, pp.214-223, Jan. 2001.

[72] H. Shi; "Performance analysis on semiconductor laser amplifier loop mirrors", *Journal of Lightwave Technology*, Vol. 20, Issue 4, pp. 682-688, Apr 2002.

[73] H. Sotobayashi, W. Chujo, "Inter-wavelength-band conversions and demultiplexings of 640 Gbit/s OTDM signals", *Optical Fibre Communication Conference and Exhibit*, Vol. 17, pp. 261 –262, Mar 2002.

[74] S. Seung-Woo; P.R. Prucnal, "Transparent optical networks for high-performance distributed computing", *Proceedings of the Fifth IEEE Computer Society Workshop on Future Trends of Distributed Computing Systems*, Vol. 28, pp. 178 –184, Aug 1995.

[75] A.G. Nowatzyk, P.R. Prucnal, "Are crossbars really dead? The case for optical multiprocessor interconnect systems", *Proceedings. 22nd Annual International Symposium on Computer Architecture*, Vol. 22, pp.106 –115. Jun. 1995.

[76] K. Rauschenbach, E. Modiano, K. Hall, K. S Finn, J. Moores, "Broadband optical network technology for next generation LAN and access systems", *Lasers and Electro-Optics Society Annual Meeting, IEEE*, Vol. 2, 3-4, pp. 230 –231, Dec. 1998.

[77] D. Cotter, "Asynchronous digital optical networks", *Broadband Optical Networks and Technologies: An Emerging Reality/Optical MEMS/Smart Pixels/Organic Optics and Optoelectronics. IEEE/LEOS Summer Topical Meetings*, pp. I/21 -I/22, Jul 1998.

[78] I.Y. Khrushchev, I.D. Philips, A.D. Ellis, R.J. Manning, D. Nesset, D.G. Moodie, R.V. Penty, I.H. White, "OTDM applications of dispersion-imbalanced fibre loop mirror", *Electronics Letters*, Vol. 35, Issue 14, pp. 1183 –1185, Aug 1999.

[79] V. Kaman, J.E. Bowers, "120 Gbit/s OTDM system using electroabsorption transmitter and demultiplexer operating at 30 GHz", *Electronics Letters*, Vol. 36, Issue17, pp. 1477 –1479, Aug 2000.

[80] www.lucent.com

[81] J. Barthel and T. Chuh, " Optical switches enable dynamic optical add/drop models", *Laser Focus World WDM solution*, pp.93-96, August 2001.

[82] www.nortel.com

[83]   I. Nakamura, S. Nishikawa, S. Kohmoto, K. Asakawa, "Saturation intensity in InAs quantum dot and its application to all-optical switches", *Lasers and Electro-Optics Society, The 14th Annual Meeting of the IEEE*, Vol. 2, pp. 562 –563, 2001.

[84]   L. Boivin, A.R. Chraplyvy, "Testing optical time-division multiplexed transmission systems with interleaved bit sequences", *Optical Fibre Communication Conference*, Vol. 2, pp. 314 –316, 2000.

[85]   H. Tanaka, T. Otani, M. Hayashi, M. Suzuki, "Optical signal processing with electroabsorption modulators", *Optical Fibre Communication Conference and Exhibit, 2002*, pp. 262 –264, Mar 2002.

[86]   G. Toptchiyski, K. Obermann, K. Petermann, E. Hilliger, S. Diez, H.G. Weber, "Modeling of semiconductor optical amplifiers for interferometric switching applications", *Summaries of Papers Presented at the Conference on Lasers and Electro-Optics*, pp. 215 –216, May 1999.

[87]   F. Romstad, P. Borri, J. Mork, J. Hvam, F. Heinrichsdorff, M.H. Mao, D. Bimberg, "Pulse distortion in a quantum dot optical amplifier", *Conference on Lasers and Electro-Optics*, pp. 471, 2000.

[88]   I. D. Henning, M. J. Adams, J.V. Collins, "Performance predictions from a new optical amplifier model", *IEEE Journal of Quantum Electronics*, Vol. QE-21, no. 6, pp.609-613, 1985.

[89]   T.G. Ulmer, W.S. Astar, P.W. Juodawlkis, S.E. Ralph, R.P. Kenan, C.M. Verber, A.J. SpringThorpe, "Optical time-division demultiplexing with surface-emitted second-harmonic generation", *Summaries of Papers Presented at the Conference on Lasers and Electro-Optics*, pp. 377, May 1999.

[90]   P.J. Delfyett, B. Mathason, S. Gee, C. DePriest, "Novel modelocked semiconductor lasers for networking, instrumentation and signal processing", *Lasers and Electro-Optics Society 1999 12th Annual Meeting, IEEE*, Vol. 2, pp. 699 –700, 1999.

[91]   D. Zhou; K. Kang; G. C. Tian, I. Giesk, P.R. Prucnal, "A simple method to characterize dynamic parameters of semiconductor waveguide amplifiers", *Lasers and Electro-Optics Society Annual Meeting, IEEE*, Vol. 1, pp. 198 –199, Dec. 1998.

[92]   G.P. Agrawal, "Fibre-optic Communication system", 2nd Edition, Wiley 1997.

[93]   J. Hansryd, P.A. Andrekson, P.O. Hedekvist, L Jie, M. Westlund, "Optical parametric amplifiers and their applications", *Optical Fibre Communication Conference and Exhibit*, pp. 123 –125, Mar 2002.

[94]   M..J.Adams, J.V.Collins, I.D. Henning, "analysis of semiconductor Laser optical amplifiers", *IEE Proceeding*, Vol. 132, Pt. J, No. 1, pp.58-63, 1985.

[95]   H.K. Dong, H.K. Sang, C.J. Jae, S.C. Sang, "A fibre-integrated semiconductor ring laser for 10 GHz optical timing extraction", *The Pacific Rim Conference on Lasers and Electro-Optics*, Vol. 2, pp. 521 –522, 1999.

[96]   E. Desurvire, " Erbium-doped fibre amplifier", *Wiley Inter-Science*, 1994

[97]   X. Chen; M. Yao, M. Chen, J. Zhang, L. Xu, Y. Gao, C. Chen; "Demonstration of optical switch operation of an ultrafast nonlinear interferometer (UNI) with counter-propagating control pulse", *Fifth Asia-Pacific Conference on Communications, APCC/OECC '99*, Vol. 1, pp. 475 –476, 1999.

[98]   J. Wilson, J.F.B. Hawkes, "Optoelectronics: An Introduction", *Prentice-Hall International Series in Optoelectronic*, 3rd Edition 1998.

[99]   T. Inoue, H. Sugahara, A. Maruta, Y. Kodama, "Interactions between dispersion managed solitons in optical-time-division-multiplexed system", *Fifth Asia-Pacific Conference on Communications*, Vol. 1, pp. 375 –377, 1999.

[100] www. Alcatel.com

[101] K.S. Jepsen, B. Mihkelsen, M. Vaa, H.N. Poulsen, A.T. Clausen, K.E. Stubkjaer, R. Hess, M. Duelk, W. Vogt, E. Gamper, E. Gini, P.A. Besse, H. Melchior, S. Bouchoule, "Simultaneous all-optical add and drop multiplexing of 40-Gbit/s OTDM signals using monolithically integrated Mach-Zehnder interferometer", *Technical Digest of Optical Fibre Communication Conference and Exhibit*, pp. 310 –311, Feb 1998.

[102] D.T. Cassidy, C.Derwyn, C. Johnson and K. O. Hill, " Wavelength dependence transmission of monomode fibre tapers", *Appl. Opt.*, 24, (7), pp. 945-950, April 1985.

[103] K. Nonaka, H. Takara, K. Uchiyama, A. Takada, "Bit rate flexible, all-optical RZ/NRZ transformation with saturable absorption laser diode", *Technical Digest. Summaries of papers presented at the Conference on Lasers and Electro-Optics*, pp. 5 –6, May 1998.

[104] G. Swift, Z. Ghassemlooy, and A.K. Ray, J.R. Travis, " Modelling of semiconductor laser amplifier for the terahertz optical asymmetric demultiplexer", *IEE Proc.-circuits Devices Syst.*, Vol. 145, No.2, pp. 61-65, 1998.

[105] G. Raybon, B. Mikkelsen, R. J. Essiambre, "High speed, 40 to 100 Gbit/s OTDM transmission over nonzero dispersion fibre", *Lasers and Electro-Optics Society 12th Annual Meeting 1999, IEEE*, Vol. 1, pp. 341 –342, 1999.

[106] J.P. Sokolloff, I. Glesk, P.R. Prucnal, and R.K.Boncek, " Performance of a 50 Gbit/s optical time domain multiplexed signal using a terahertz optical asymmetric demultiplexer", *IEEE Photon Technol. Lett.*, 6, (1), pp.98-100, January 1994.

[107] I. Morita, T. Tsuritani, N. Edagawa, "Experimental study on optically band-limited 40-Gb/s RZ signals with optically time-division demultiplexing receiver", *Journal of Lightwave Technology*, Vol. 20, Issue 12, pp. 2182 –2188, Dec 2002.

[108] M.G. Kane, I. Glesk, J.P. Sokoloff and P.R. Prucnal, " Asymmetric optical loop mirror: analysis of an all optical switch", *Appl. Opt.,* 33, (29), pp. 6833-6842, October 1994.

[109] M. Eiselt, W. Pieper and H. G. Weber, "All optical high speed demultiplexing with a semiconductor laser amplifier in a loop mirror configuration", *Electron. Lett.*, 29, (13), pp. 1167-1168, June 1993.

[110] W. Weiershausen, H. Scholl, F. Kuppers, R. Leppla, B. Hein, H. Burkhard, E. Lach, G. Veith, "40 Gb/s field test on an installed fibre link with high PMD and investigation of differential group delay impact on the transmission performance", *Technical Digest of Optical Fibre Communication Conference*, Vol. 3 , pp. 125 – 127, 1999.

[111] N.Olsson, "Lihgtwave System With Optical Amplifers", *Journal of Lightwave Technology*, 7(7), pp. 1071-1082, July 1989.

[112] B. Olsson, P. Andrekson "Noise Filtering with the Nonlinear Optical Loop Mirror". *Journal of Lightwave Technology*, 13(2), pp. 213-215, February 1995.

[113] T. Akiyama, A. Neogi, H. Yoshida, O. Wada, "Enhancement of optical nonlinearity for short wavelength (~1.5 μm) intersubband transitions by n-doped InGaAs/AlAsSb MQW", *Summaries of Papers Presented at the Conference on Lasers and Electro-Optics,* pp. 257, May 1999.

[114] M. Jinno, "Effects of crosstalk and timing jitter on all –opitcal time-dvision demultiplexing using a nonlinear fibre sagnac interferometer switch*" IEEE J. Quantum Electron*. 30, pp. 2842-2853, Dec. 1994.

[115] W. Wong, P. Hansen, "In-Band Amplified Spontaneous Emission Noise Filtering with a Dispersion-Imbalanced Nonlinear Loop", *Journal of Lightwave Technology*, 16(10), pp. 1768-1771, October 1998.

[116] D.G. Moodie, A.D. Ellis, A.R. Thurlow, I.F. Lealman, C.W. Ford, M.J. Robertson, "Electroabsorption modulators for ultra high speed OTDM systems", *IEE Colloquium on Towards Terabit Transmission*, pp. 3/1 -3/5, May 1995.

[117] K. Uchiyama, T. Morioka, S. Kawanishi, H. Takara, and M. Saruwatari, "Signal-to noise ratio analysis of 100 Gb/s demultiplexing using nonlinear optical loop mirror", *Journal of Lightwave Technology*, 15, pp. 194-201, February 1997.

[118] M. Owen, V. Saxena, R.V. Penty, I.H. White, "10-Gbits/s all-optical 3R regeneration and format conversion using a gain-switched DFB laser", *Conference on Lasers and Electro-Optics*, pp. 472 –473, 2000.

[119] J. Zhang; M. Yao; X. Chen; L. Xu; M. Chen; Y. Gao; "Bit error rate analysis of OTDM system based on moment generation function", *Journal of Lightwave Technology*, Vol. 18, Issue 11, pp. 1513 –1518, Nov 2000.

[120] Y.J. Chai, R.V. Penty, I.H. White, "Interferometric noise suppression for WDM applications using a dispersion-imbalanced loop mirror", *Technical Digest. Summaries of papers presented at the Conference on Lasers and Electro-Optics*, pp. 381 –382, 2001.

[121] K.L. Deng, K. I. Kang, I. Glesk, P.R. Prucnal, "Influence of cross talk on the scalability of large OTDM interconnects using a novel fast time-slot tuner", *Technical Digest. Summaries of papers presented at the Conference on Lasers and Electro-Optics*, pp. 4 –5, May 1998.

[122] J. Hansryd, P.A. Andrekson, B. Bakhshi, "A simple, low timing jitter, sub-multiple clock recovery technique", *24th European Conference on Optical Communication*, Vol. 1, pp. 471 –472, Sep 1998.

[123] A. Buxens, A.T. Clausen, H.N. Poulsen, P. Jeppesen, S. Fischer, M. Dulk, E. Gamper, W. Vogt, W. Hunziker, E. Gini, H. Melchior, "All-optical regenerative OTDM add/drop multiplexing at 40 Gbit/s using monolithic InP Mach-Zehnder interferometer", *Conference on Lasers and Electro-Optics*, pp.255, 2000.

[124] W. Wong, P. Hansen, "In-Band Amplified Spontaneous Emission Noise Filtering with a Dispersion-Imbalanced Nonlinear Loop", *Journal of Lightwave Technology*, 16(10), pp.178-183, Feb. 1999.

[125] M. Jinno, "Effects of crosstalk and timing jitter on all –opitcal time-dvision demultiplexing using a nonlinear fibre sagnac interferometer switch" *IEEE J. Quantum Electron.* 30, pp. 2842-2853, Dec. 1994.

[126] B. Olsson, P. Andrekson "Noise Filtering with the Nonlinear Optical Loop Mirror". *Journal of Lightwave Technology*, 13(2), pp. 213-215, February 1995.

[127] B.E. Olsson, D.J. Blumenthal, "80 to 10 Gbit/s demultiplexing using fibre cross-phase modulation and optical filtering", *Lasers and Electro-Optics Society 2000 Annual Meeting, 13th Annual Meeting. IEEE*, Vol. 1, pp. 159 –160, 2000.

[128] Y.M. Yang; H.F. Liu; Y. Matsui, "A new scheme of all-optical clock division for optical time division multiplexing networks", *IEEE Lasers and Electro-Optics Society 2000 Annual Meeting. 13th Annual Meeting.* Vol. 2, pp. 623 –624, 2000.

[129] H. Murai, H.T. Yamada, K. Fujii, Y. Ozeki, "Carrier-suppressed dispersion-managed RZ transmissions using novel OTDM techniques with phase alternation", *Digest of the LEOS Summer Topical Meetings on Advanced Semiconductor Lasers and Applications/Ultraviolet and Blue Lasers and Their Applications/Ultralong Haul DWDM Transmission and Networking/WDM Components*, pp. 2, 2001.

[130] V. Mikhailov, P. Bayvel, R. Wyatt, I. Lealman, "Fibre grating laser-based RZ pulse source for 40 Gbit/s OTDM transmission systems", *Electronics Letters*, Vol. 37, Issue 14, pp. 909 –910, Jul 2001.

[131] C.D. Chen, I. Kim, O. Mizuhara, T.V. Nguyen, K. Ogawa, R.E. Tench, L.D. Tzeng, P.D. Yeates, "40 Gbit/s×25 ch (1 Tbit/s aggregate capacity) WDM transmission over 342 km of fibre", *Electronics Letters*, Vol. 35, Issue 8, pp. 648 –649, Apr 1999.

[132] A.D. Ellis, R.J.Manning, I.D. Phillips, D. Nesset, "1.6 ps pulse generation at 40 GHz in phaselocked ring laser incorporating highly nonlinear fibre for application to 160 Gbit/s OTDM networks", *Electronics Letters*, Vol. 35, Issue 8, pp. 645 –646, Apr 1999.

[133] A.M. Weiner, "Optical information processing and waveform shaping with femtosecond pulses", *The 4th Pacific Rim Conference on Lasers and Electro-Optics*, Vol.1, pp. I-246 -I-247, 2001.

[134] H. Sotobayashi, W. Chujo, T. Ozeki, "80 Gbit/s simultaneous photonic demultiplexing based on OTDM-to-WDM conversion by four-wave mixing with supercontinuum light source", *Electronics Letters*, Vol. 37, Issue 10, pp. 640 –642, May 2001.

[135] K. Deng; R.J. Runser, P. Toliver, I. Glesk, P.R. Prucnal, "A highly-scalable, rapidly-reconfigurable, multicasting-capable, 100-Gb/s photonic switched interconnect based upon OTDM technology", *Journal of Lightwave Technology*, Vol. 18, Issue 12, pp. 1892 –1904, Dec. 2000.

[136] P.J. Legg, D.K. Hunter, P.E. Barnsley, I. Andonovic, "Crosstalk effects in optical time division multiplexed switching networks", *IEE Colloquium on Optical Switching*, pp. 11/1 -11/4, Jun 1993.

[137] S.A. Hamilton, B.S. Robinson, "100 Gbit/s synchronous all-optical time-division multiplexing multi-access network testbed", *Optical Fibre Communication Conference and Exhibit*, pp. 603 –605, Mar 2002.

[138] K.S. Jepsen, H.N. Poulsen, A.T. Clausen, A. Buxens, K.E. Stubkjaer, "Investigation of cascadability of add-drop multiplexers in OTDM systems", *24th European Conference on Optical Communication*, Vol. 1, pp. 619 –620, Sep 1998.

[139] R.J. Runser, K.L. Deng, P. Toliver, I. Glesk, P.R. Prucnal, P.R.; "Highly scalable OTDM router using computer controlled time slot tuner with picosecond resolution", *Electronics Letters*, Vol. 35, Issue 13, pp. 1097 –1099, Jun 1999.

[140] L. Tangjun, P. Cuizhu, and Z. Yucheng, "Study on improving the performance of OTDM device", *IEEE Photonics Technology Letters*, 11 (1), pp. 60-62, Jan.1999.

[141] M.M. Mosso, W.R. Ruziscka, D. Souto, F. Silva, D. Castanheira, C.F.Silva, "OTDM quasi-all-optical demultiplexing techniques comparative analysis", *Proceeding of Microwave and Optoelectronics Conference, 1997. 'Linking to the Next Century'*, Vol. 2, pp. 692 –697, Aug 1997.

[142] G. Hanke, "Electronics for an experimental 40 Gbit/s OTDM-system", *Proceedings of Microwave and Optoelectronics Conference, 1997. 'Linking to the Next Century'*, Vol. 1, pp. 363 –367, Aug 1997.

[143] D. Hunter et al, "WASPNET: A wavelength switched packet network", *IEEE Communications Magazine*, pp. 120-129, March 1999.

[144] K. Lee; C. Shu, "Terabit-per-second time division multiplexer", *12th Annual Meeting on Lasers and Electro-Optics Society 1999. IEEE*, Vol. 1, pp. 210 –211, 1999.

[145] G.Einarsson, " Principles of lightwave communications", *John Wiley*, 1996

[146] V. Mikhailov, R.I. Killey, S. Appathurai, P. Bayvel, "Investigation of intra-channel nonlinear distortion in 40 Gbit/s transmission over standard fibre", 27th European Conference on Optical Communication, Vol. 1, pp. 92 –93, 2001.

[147] S.A. Hamilton, B.S. Robinson, T.E. Murphy, S.J. Savage, E.P. Ippen, "100 Gb/s optical time-division multiplexed networks", *Journal of Lightwave Technology*, Vol. 20, Issue 12, pp. 2086 –2100, Dec 2002.

[148] H.K. Dong, H.K. Sang, C.J. Jae, S.C. Sang, "Harmonically mode-locked fibre-integrated semiconductor ring laser for a transform-limited pulse generation at 10 GHz", *Summaries of Papers Presented at the Conference on Lasers and Electro-Optics*, pp. 152 –153, May 1999.

[149] R. Calvani, F. Cisternino, R. Girardi, E. Griseri, M. Puleo, E. Riccardi, "40 Gbit/s OTDM transmission over 150 km of SMF using an optimised all-optical demultiplexer", *Electronics Letters*, Vol. 35, Issue 15, pp. 1261 –1263, Jul 1999.

[150] Y. Ueno, S. Nakamura, J. Sasaki, T. Shimoda, A. Furukawa, T. Tamanuki, T. Sasaki, K. Tajima, "Ultrahigh-speed all-optical data regeneration and wavelength conversion for OTDM systems", *27th European Conference on Optical Communication*, Vol. 4, pp. 566 –569, 2001.

[151] S. Nakamura, Y. Ueno, K. Tajima, "Ultrafast all-optical switching using a frequency shift accompanied by cross-phase modulation in a semiconductor optical amplifier", *Technical Digest. Summaries of papers presented at the Conference on Lasers and Electro-Optics*, pp. 348 –349, 2001.

[152] C. Schmidt, E. Dietrich, S. Diez, H.J. Ehrke, U. Feiste, L. Kuller, R. Ludwig, H.G. Weber, "Mode-locked semiconductor lasers and their applications for optical signal processing", *Summaries of Papers Presented at the Conference on Lasers and Electro-Optics*, pp. 348 –349, May 1999.

[153] R. Ngah, Z. ghassemlooy, and G. swift, "Simulation of an all optical time division multiplexing router employing symmetric Mach-Zehnder (SMZ)", 7th *IEEE High Frequency Postgraduate Student Colloquium*, pp.133-139, Sept. 2002.

Appendix A

Buffer control process

The following flow diagrams show the process for determining the buffer assignment for incoming packets in the OTDM router with output buffers only as shown in Figure 8.

Figure A1 shows the process of buffer control for packets entering at Input 1 of the switch and leaving at Output port 1. Figure A2 shows the process of buffer control for packets entering at Input 1 and leaving at Output 2.

Figure A2 shows the process of buffer control for packets entering at Input 1 and leaving at Output 2.

Figure A3 shows the process for packets entering at Input 2 and leaving at Output 1.

Figure A4 shows the process for packets entering at Input 2 and leaving at Output 1.

The Buffer Status table keeps a record of the occupancy of each buffer. This is updated at each clock cycle. Dotted lines indicate communication to/from the buffer.

Output buffer depth selected as follows:

Required output buffer depth = n + ym

  Where:
   n = number of buffer stages already occupied at required output port
   m = 1 (if there is a packet at the other input destined for the same output)
       = 0 (if no packet at other input destined for same output)
   y = 0 (if input 1 has priority)

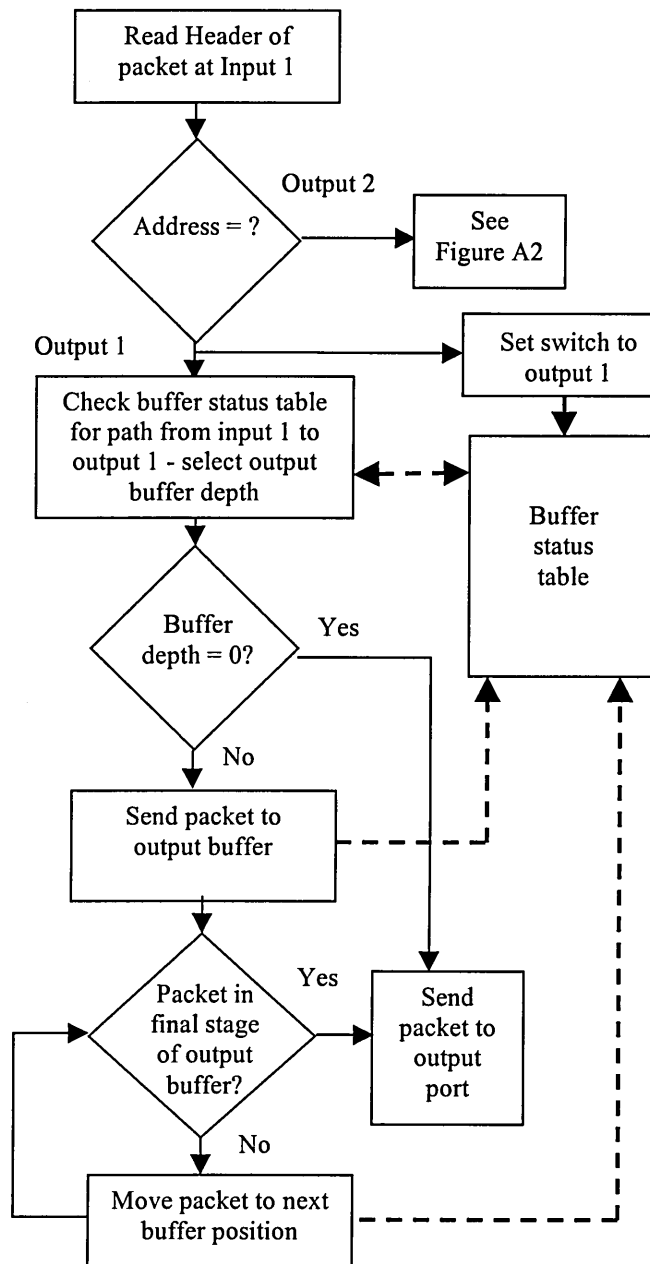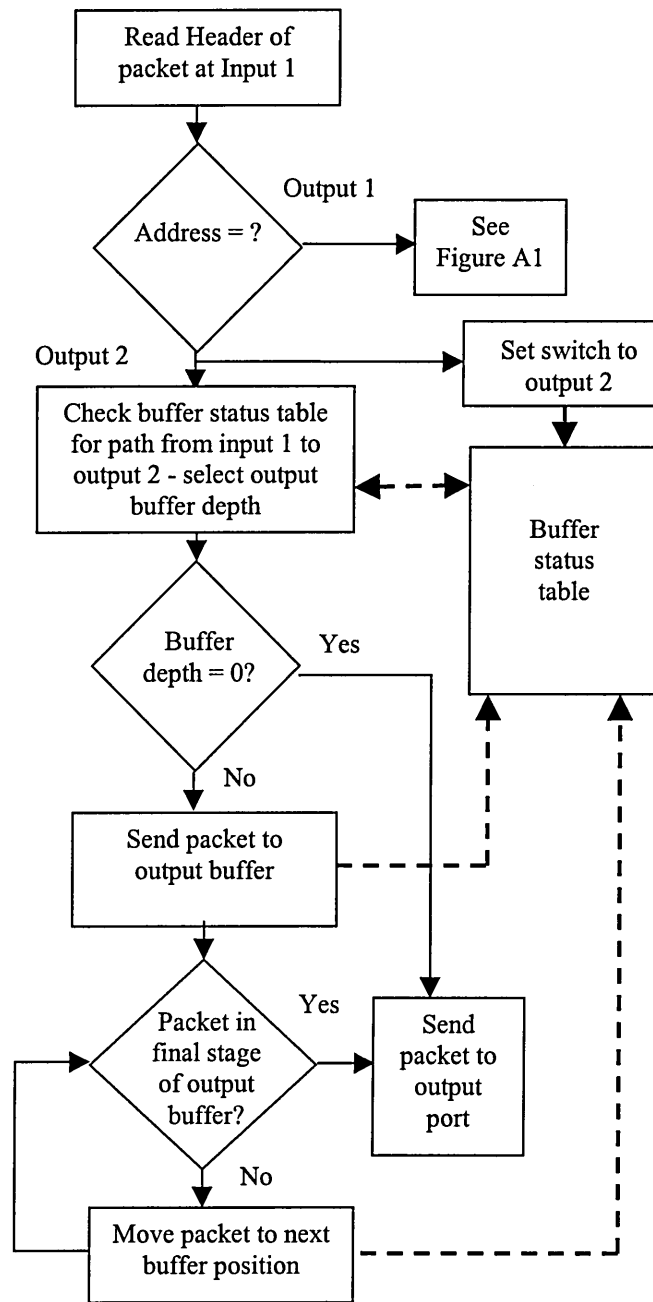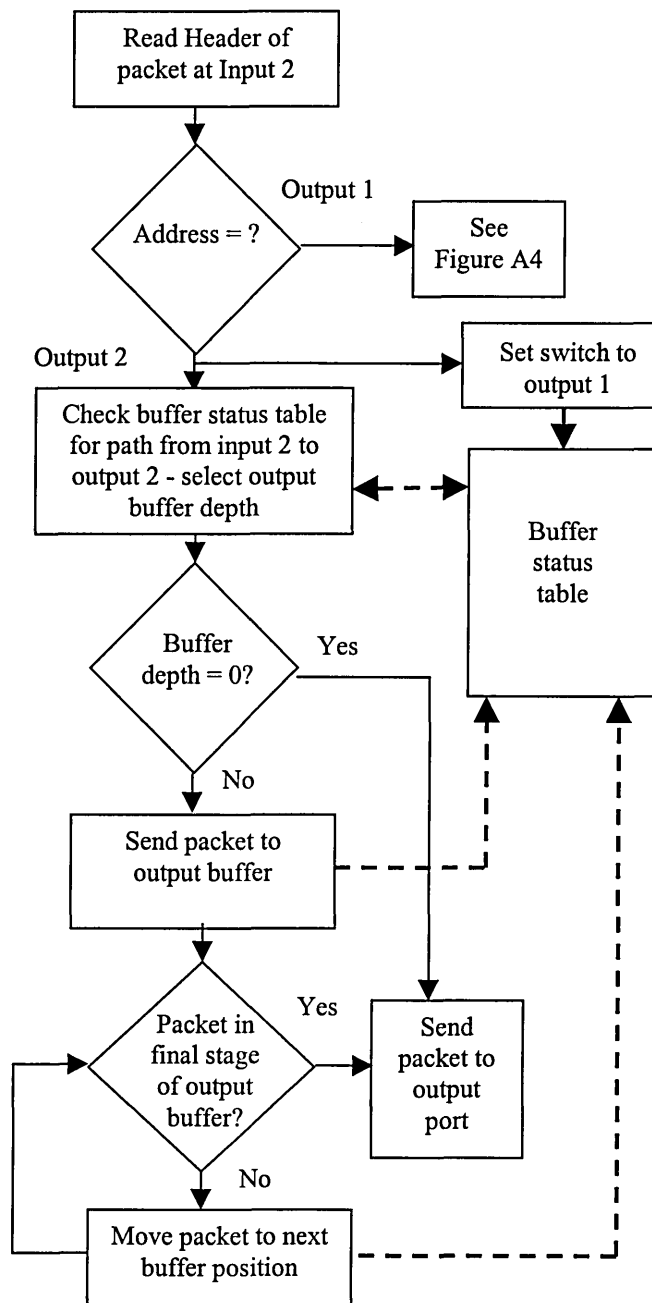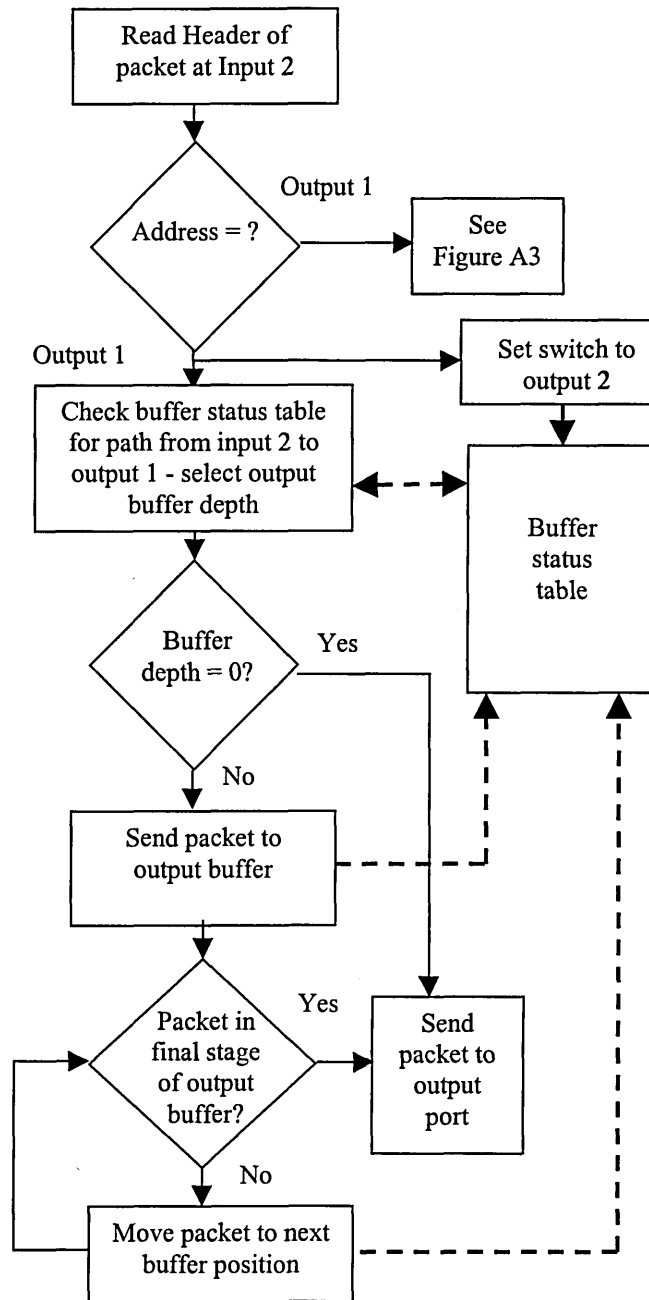   = 1 (if input 2 has priority)

Appendix B

Figure A1 Buffer control process for packets entering at Input1 leaving at Output 1

Figure A2 Buffer control process for packets entering at Input1 leaving at Output 2

204

Figure A3 Buffer control process for packets entering at Input 2 and leaving at Output 2

Figure A4 Buffer control process for packets entering at Input 2 and leaving at Output 1